FINAL PROGRESS REPORT

Principal Investigator Information:
Kurt E. Beschorner, Ph.D.
University of Pittsburgh
Swanson School of Engineering
4420 Bayard St #306
Pittsburgh, PA 15213
412-624-7577
beschorn@pitt.edu

Institution to which award was made:
University of Pittsburgh
Office of Research
123 University Place
Pittsburgh, PA 15213-2303

Project Information:

Title: Impact of Worn Shoes on Slipping
Project Director: Kurt Beschorner, Ph.D.
Co-Investigators: Mark Redfern, Ph.D., Joel Haight, Ph.D., Brian Moyer, Ph.D.
Sponsor: National Institute of Occupational Safety and Health
Grant number: R01OH010940
Start date: 9/30/2015; End date: 9/29/2020

Final Progress Report Submitted in December 16, 2020.

Final report number 1

A.Table of Contents

B.List of Terms and Abbreviations

ACOF: Available coefficient of friction (synonymous with coefficient of friction)
γ: Correction factor for leakage
η: Fluid viscosity
λ: Dimensionless film thickness
μ_i: Coefficient of friction for the frame, i
Δh_i: Change in height of node, i, due to wear
Δh_{imax}: Maximum change in node height during a single finite element analysis wear iteration
Δt: Time between samples of the fluid pressure sensor
Δx: Distance between fluid pressure scans, in the direction transverse to sliding
Δy: Distance between fluid pressure samples, in the sliding direction
b: width of worn region
h_0: minimum film thickness
k: Wear constant
l: length of the worn region
p_i: Fluid pressure at the frame, i
s: Sliding distance
v: Sliding velocity
AICc: Akaike information criterion, corrected for small sample size
E: Elastic modulus
F_{fluid}: Load supported by the fluid
F_{xi}: Shear force in the direction transverse to the sliding direction for the frame, i
F_{yi}: Shear force in the sliding direction for the frame, i
F_{zi}: Normal force for the frame, i
F: Normal load
K_p: Shape constant
NSR: Shoes that are not labeled as slip-resistant
PFT: Predicted film thickness (identical to h_0)
P_i: Contact pressure at the node, i
R_a: Average roughness of a surface profile
RCOF: Required coefficient of friction
R_q: Root-mean-square deviation of a surface profile
R_z: Mean peak to valley height of surface profile
S: Shore A hardness
SR: Shoes labeled as slip-resistant
SWR: Size of the worn region (product of the width and length of the worn region)

C.Abstract

Title: Impact of Worn Shoes on Slipping
Principal investigator: Kurt E. Beschorner, Ph.D.
Contact information:
4420 Bayard St #306
Pittsburgh, PA 15213
412-624-7577
beschorn@pitt.edu

Slip and fall accidents are a major source of occupational injuries. Heavy wear of shoes is associated with reduced coefficient of friction (COF) increased slipping risk. Worn tread loses the capacity to drain fluid from beneath the shoe, which causes the fluid to become pressurized and the friction to decrease. We have generated new knowledge on the impact of shoe wear on tread friction performance and slipping risk. Experiments were conducted to determine the contribution of footwear design to the shoe's friction response to wear (Aim 1), thresholds for when worn shoes should be replaced (Aim 2), physics-based models that explain wear progression and its impact on friction (Aim 3), validated the wear progression findings of Aims 1 and 3 using a prospective study on natural shoe wear (Aim 4), and validate the thresholds of Aim 2 using human slip data (Aim 5).

Aim 1: Using controlled wear experiments in the lab, we characterized the friction response of shoes to progressive wear. Shoes experienced an initial increase followed by a steady decrease in friction performance. The decrease in friction aligned with an increase in fluid pressures, which indicate that a lack of fluid drainage explains this change in performance. Tread design influenced the shoe's response to wear and drainage capacity. In particular, shoes with increased tread coverage in the heel and with smaller tread lugs were associated with improved performance.

Aim 2: The size of the worn region emerged as a critical factor for predicting the loss in friction performance for slip-resistant shoes. The study identified a size threshold (the base of a AAA or AA battery) that was associated with a reduced friction performance. This provides a basis for inspecting and monitoring shoes.

Aim 3: Physics-based models were used to predict tread geometric changes of the tread in response to wear and the effect of wear on under-shoe fluid drainage. Both of these models demonstrated strong agreement with experimental results.

Aim 4: Shoes were prospectively tracked in the workplace to monitor their change in friction performance due to natural wear. The wear progression trends observed in Aim 1 and modeled in Aim 3 were similarly observed for naturally worn shoes in workplaces. The model of under-shoe fluid drainage (Aim 3) predicted the friction progression of naturally worn shoes.

Aim 5: Participants were exposed to a slippery contaminant, while wearing shoes of varying level of worn condition. The mechanistic model developed in Aims 2 and 3 was validated using this data. The developed battery test for inspecting shoes (Aim 2) was found to predict slipping risk.

This study led to numerous outputs and outcomes. The work was disseminated by 12 published peer-reviewed papers and over 30 presentations that targeted the scientific, footwear industry, and safety professional communities. A direct translational product (intermediate outcome) resulting from the study was a quick and useful method to evaluate tread wear, termed the battery test. This test formed the basis for a NORA poster to communicate the test to restaurant and hospital employees.

D.Section 1 of the Final Progress Report

D.1. Significant or Key Findings.

This study led to important key findings for each of the five aims that were proposed.

Aim 1: Identify the effects of tread design and material properties on wear progression.

We developed a process of generating mechanical wear under controlled conditions. Shoe friction testing was performed. The friction response to wear was quantified across tread designs.

Key Finding 1: The most common response of friction performance to wear progression was an initial increase in friction followed by a steady decrease in friction. This decrease in friction performance was associated with increased fluid pressures, an indicator that poor fluid drainage was the causal factor.

Key finding 2: The amount of tread on the shoe surface (e.g., proportion of the shoe covered in tread) but not the tread hardness influenced the friction response. A higher proportion of the heel region covered in tread material was associated with a slower impact of wear on friction performance.

Key finding 3: Shoe designs responded differently to wear. Treads with large lug patterns had low performance (low friction and poor drainage) in their new condition and experienced improving performance with wear, which was the opposite effect that most shoes experienced. Notably, shoes with large lugs had lower friction performance and worse drainage compared to shoes with smaller lugs through most of the wear progression experiment.

Aim 2: Identify shoe tread depth limits where COF begins to significantly decrease. Quantify the effects of tread pattern on this threshold.

Experiments from Aim 1 also enabled quantifying of wear thresholds associated with a reduction in friction performance.

Key finding 4: A critical observation was that changes in shoe friction performance (lower friction and higher fluid pressures) were associated with the size of the worn region. This represented an important paradigm shift from previous research that focused on tread depth. A continuous measure of worn region size was developed and measured as: the product of the maximum width and length of the worn region. This value was found to correlate with an increase in fluid pressures and a reduction in friction performance.

Key finding 5: A threshold for worn shoes was developed by comparing the size of the worn region to the size of a AAA or AA battery. This test was found to differentiate between shoes with poor versus good friction performance. Shoes that passed the test had lower fluid pressures (indicating better drainage) than shoes that failed the test. Shoes that failed the battery test were associated with a ~30% reduction in friction performance. See Key Finding 12 for a product resulting from this research.

Aim 3: Develop a computational model of shoe wear progression and predict a shoe's slip-resistant life

Key finding 6: A finite element analysis model was developed to predict geometric changes in tread pattern as a shoe became worn. The finite element model predicted the order in which treads became worn that was consistent with experimentally-measured wear progression.

Key finding 7: A fluid-film model was developed that predicted the impact of the size of the worn region on fluid dynamics underneath the shoe (i.e., drainage capacity). The fluid-film model determined that the film thickness predicted by the model was strongly correlated with experimentally-measured under-shoe fluid dynamics and a loss in friction.

Aim 4: Validate the ability of experimental (Aim 1) and modeling (Aim 3) methods for predicting actual shoe wear in occupational settings.

Workers were provided shoes, wore those shoes in their workplace, and then returned the shoes to the research team each month for testing.

Key finding 8: This study revealed that naturally worn shoes responded similarly as mechanically worn shoes. Specifically, shoes commonly experienced a slight increase in friction performance after initial wear followed by a steady decline in friction performance.

Key finding 9: The fluid model that was developed predicted under-shoe fluid pressures for naturally worn shoes.

Key finding 10: Variation in wear rate was dominated by individual biomechanics more than shoe design. Wear rates across participants varied by a fully order of magnitude. The kinetics of gait (shear force and required coefficient of friction) explained much of this variation.

Aim 5: Validate the wear threshold levels that lead to increased human slipping risk.

We performed human slipping experiments to validate the mechanistic model for how wear influences slip risk and to validate the wear thresholds from Aim 2. Participants wore their own naturally worn shoes and were exposed to a slippery liquid contaminant. Under-shoe fluid pressures and slipping kinematics were measured.

Key Finding 11: Data from 57 participants were used to validate the mechanistic model. The experimental data showed similar results to the model; specifically, increased worn region size led to an a) increase in fluid pressure, b) a decrease in friction performance, and c) an increase in slipping.

Key Finding 12: The “battery test” predicted the risk of experiencing a slip, slip severity, and under-shoe fluid pressures during slipping. This finding, along with Key Finding 5, led to a major research product, a poster targeting restaurants and hospitals with information on performing shoe inspections (developed and approved by the NORA Traumatic Injury Prevention cross council).

D.2. Translation of findings:

Translation and dissemination efforts have focused on three pathways: 1) disseminating scientific knowledge to the research community, 2) disseminating knowledge on footwear design to footwear designers, and 3) disseminating footwear inspection information to workers and safety professionals.

1: Scientific knowledge to research community: This research has been communicated to the scientific community through 12 peer-reviewed published manuscripts (4 more in review and 2 more in preparation), three students’ PhD published dissertations (1 more in progress), 22 conference presentations (5 of which are accompanied by full conference papers), and 9 invited talks. One talk included a Keynote lecture at the International Slips, Trips, and Falls meeting (Madrid, February, 2020).

2. Dissemination to footwear designers: Research has been communicated to footwear companies involved in designing, manufacturing, and selling footwear via eight presentations. Three presentations were made directly to engineers at footwear companies. One of those presentations was to the F13 committee, which has membership of more than 20 individuals working at footwear companies. Another was to Grainger, which was attended by over 50 employees in the Safety Footwear division.

3. We have disseminated our knowledge to the broader safety communities. A poster has been developed in coordination with the NORA Traumatic Injury Cross-Sector Council (approved but pending 508c compliance review). This poster provides a simple method (battery test) for translating the research to footwear inspection behavior, which is expected to lead to improved footwear maintenance and reduced slips. Website mockups for the NORA website and our personal website have been developed. I have completed eight presentations and contributed to a NIOSH research rounds article targeting safety professionals to disseminate this research.

D.3. Research Outcomes/Impact.

D.3.1. Potential outcomes

The battery test that we developed for footwear inspection and maintenance is expected to lead to behavioral changes that increase shoe replacement. The impact of increased footwear replacement will be a reduction in slip and fall accidents. The knowledge that we have provided to footwear companies is expected to lead to improvements of footwear design by designing smaller treads with larger coverage across the shoe surface.

D.3.2. Intermediate outcomes

The development of the NORA poster is considered an intermediate outcome since it provides a workplace product for reducing slip and fall accidents.

D.3.3. End outcomes:

None

Section 2 of the Final Progress Report: Scientific Report.

E. Background

E.1. Problem Statement and Significance

Slips and falls are among the leading and fastest growing sources of occupational accidents. In 2012, slip, trip and fall events accounted for approximately 24% of all non-fatal occupational accidents [1] and 15% of fatal occupational accidents [2]. Since 1998, same level fall workers' compensation costs have been growing faster than all other events [3]. Approximately 40 to 60% of all falls are initiated by a slipping event [4].

E.2. Previous studies on the contributions of shoe wear to slip risk

Several factors impact slips and falls with friction having the greatest influence. Logistic regression models have consistently demonstrated that the risk of a slip is dependent on the amount of friction between the shoe and floor surface and the required friction for walking [5, 6]. The available friction at the shoe-floor interface is commonly measured using a slip-tester [7-9] although it also can be predicted with computational models as shown in the work of our recently completed NIOSH-funded project[10-13]. Other factors that influence the outcome of a slip include biomechanics of locomotion, the effectiveness of a recovery response, and personal factors such as age [14-18]. While all of these factors are important in evaluating slip risk, enhancing shoe-floor friction through footwear and flooring controls has been shown to be an effective strategy [19-21] and is consistent with traditional ergonomics approaches of fitting the workplace to the individual. The proposed research continues an existing line of investigation to reduce slip and fall accidents by understanding and influencing the critical factors that cause low friction.

The wear condition of shoes has recently emerged as a major risk factor for slipping. Worn shoe outsoles reduce the COF [22, 23], increase the perception of slipperiness [24] and increase slipping risk in occupational settings [25-27]. A recently-published prospective crossover study in the limited-service industry found that slip risk was cut by 56% when subjects replaced their worn slip-resistant shoes with new shoes [27]. Similarly in controlled laboratory experiments using an unexpected slip paradigm, worn shoes dramatically increased slip-severity [28]. The impact of wear on slipperiness is not linear. Slight and moderate wear have not typically been associated with any reduction in shoe-floor friction, while higher levels of wear cause a dramatic drop-off in slip-resistance [23, 29]. During our recently completed grant period, we identified the mechanism causing a drop in shoe-floor-fluid friction with severe shoe wear as being a buildup of fluid pressures beneath the shoe surface [22, 29]. To reduce slip events caused by severe shoe wear, the authors of the aforementioned prospective study suggest that "slip-resistant shoe companies may consider designing shoe soles with a marker to indicate the sole wear and the time to replace shoes" [27]. These authors also acknowledged that "further research may be needed to develop criteria for the replacement of slip-resistant shoes" [27]. The proposed research will identify the criteria for tread replacement that will enable shoe companies to put such an indicator at the correct location and inform employers/employees when they should replace their shoes.

Shoe design influences the rate at which shoes wear although the critical factors that increase or decrease wear are not well understood. Gronqvist demonstrated that one shoe design lost just 56% of its tread and experienced an increase in slip-resistance over the first 8 months that it was worn, while another shoe design lost 85% of its tread and 80% of its slip-resistance over the same time period [23]. Yet this study was not able to determine what factor contributed to wear rate since tread patterns and materials were covariates [23]. Other research examined wear over a very limited number of wear cycles (<200) [30, 31], which is negligible compared to a person's typical daily activity (about 5,000 steps per day [32]). In order to extend these studies, additional research is needed to systematically vary shoe material and tread while measuring wear and COF over the entire life. The proposed research will systematically vary tread design and shoe material, while completely wearing out tread in order to evaluate the factors that influence shoe outsole durability.

Another opportunity to improve understanding of the underlying factors that influence shoe wear is to apply fundamental research on elastomer tribology to shoes. Previous elastomer research has revealed that the material and contact pressure have a large impact on wear [33]. Tribological modeling

offers the potential for understanding the effect of tread design and material on wear since these models are being used to improve design of artificial joints, tires and seals [34-36]. The proposed research will apply state-of-the-art knowledge of elastomer wear to shoe outsoles in order to predict the slip-resistant life of shoes and improve design.

F.Methodology, Results and Discussion

F.1. Study #1: Changes in under-shoe traction and fluid drainage for progressively worn shoe tread [37] (Aims 1 & 2, Key findings 1, 2, and 4)

F.1.1. Methods

A progression of wear-related changes in shoe traction performance was determined via iterations of mechanical testing, mold creation (to capture shoe tread geometry), and abrasion via a simulated wear protocol (Figure 1A). During mechanical shoe testing, ACOF and under-shoe fluid pressures were measured as a robotic device moved the shoe across a contaminated surface (Figure 1B). Molds of the heel tread geometry were generated using an apparatus that allowed the mold material to cure while the shoe was held in a fixed and consistent position (Figure 1D). Shoes were progressively worn using an apparatus with a sliding abrasive belt and a means of adjusting the shoe angle [38] (Figure 1C).

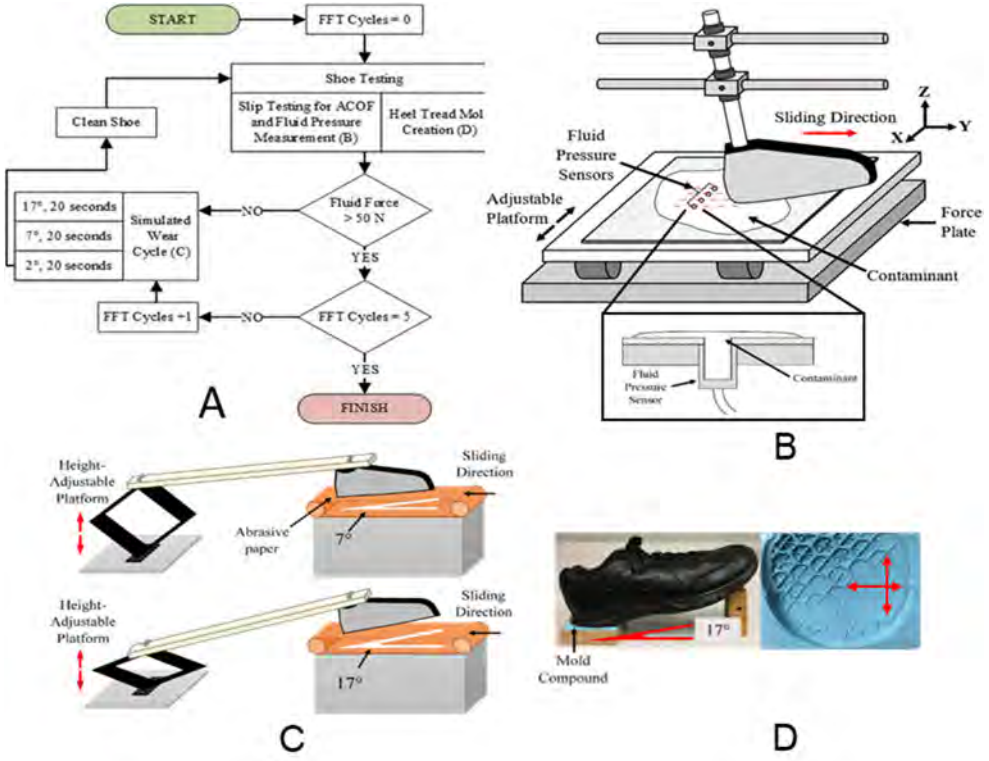

Figure 1: A) Flowchart of mechanical testing and abrasive wear protocol. The Fluid Force Threshold (FFT) is described in Section E.1.2. B) A robotic slip tester used to slide each shoe anteriorly across the contaminated tile along multiple parallel paths. Four fluid pressure sensors mounted above a force plate recorded fluid pressures and shear and normal forces, respectively. Cross-sectional view of contaminant and fluid pressure sensor is shown below the testing apparatus. C) Simulated wear apparatus on which the heel of each shoe was progressively worn at 17°, 7°, and 2°. Examples of wear at 17° and 7° are shown. D) Shoe heel placed in mold frame at 17° (left) and the length and width of the largest wear region indicated with red arrows on the heel tread mold (right).

F.1.1.1.Materials & Procedures:

Simulated Wear Protocol:

The accelerated wear apparatus (Figure 1C), consisting of a linear motion abrasion

device (Ryobi BD4601; One World Technologies, Inc.; Anderson, SC, USA) and an angle-adjustable platform, was used to simulate wear of the right heel of the shoes [38]. The device slid abrasive paper (180 µm diameter particles) at 9.65 m/s across the heel with a normal force of 40 N, similar to abrasion resistance standards for footwear and previous research for abrasively removing shoe tread [28, 39, 40]. A normal force lower than that produced during gait was used to reduce heat generation and due to an inability of the device to overcome friction forces when large normal forces were applied. One wear cycle consisted of abrading each shoe for 20 s at three angles (17° ± 1°, 7° ± 1°, and 2° ± 1°). The angles were chosen to simulate angles experienced from initial heel strike to flat foot [41]. Each wear cycle was equivalent to a total sliding distance of 580 m (193 m at each angle). The angle of the shoe was defined relative to horizontal, which was the orientation of the shoe when it was placed on the floor without an applied external load. Each shoe was abraded until there were five wear cycles for which the fluid force was greater than 50 N (20% of the normal force; described in Section E.1.2). Prior to each accelerated wear iteration, abrasive belt grease (Formax, No. F26) was applied to the abrasive paper to minimize increases in temperature between the shoe and the paper. After each wear cycle, residual grease was cleaned from the heel section of the tread using detergent and water, and then the heel section was rinsed with water and thoroughly dried.

Five pairs of shoes commonly worn in the service industry were included in the study and the right shoe for each pair was tested (Figure 2). All shoes were claimed by their manufacturers to be ‘slip-resistant’ or ‘anti-slip’. Detailed material compound was not available, but shoes were reported as having an outsole composed of ‘rubber’ or ‘rubber compound’. Short-term hardness measurements were recorded at baseline using a Shore A durometer based on ASTM standard D2240 [42] and the proportion of tread surface area to overall heel surface area, “tread proportion”, was recorded (Table 1). To determine tread proportion, 3D models of the heel were created based on measurements of heel and tread geometry (ANSYS Design Modeler, ANSYS Inc., Canonsburg, Pennsylvania, USA). The software was then used to sum the areas on the contact surface of the tread as well as the areas in the tread channels that were parallel to the contact surface. The tread proportion was calculated as the ratio of the contact surface area to the total surface area (sum of contact area and tread channel area parallel to contact surface). The roughness of the continuous sections of each tread block (R_z) was characterized by the maximum peak to valley height measurement which was averaged across five scans each using a sampling scan length of 1.6mm and a cutoff frequency of 0.8mm. Measurements were taken at five different locations on the shoe heels for the baseline tread and the fully worn region (i.e., “untreaded”) at final wear using a 2D contact profilometer (Surtronic S-100, Taylor-Hobson, AMETEK, Leicester, England). Portions of this data set were included in a previous publication that compared a shoe wear model to experimental results [43].

Figure 2: The tread of the five slip-resistant shoes used in the study at baseline (top) and after all wear was completed (bottom).

Table 1: List of shoe code, brand, model, size, short-term hardness, baseline tread depth, initial contact area on the abrasion device at the three angles of wear, proportion of tread surface area to overall heel surface area, and heel edge type.

Shoe Code	Shoe Brand	Shoe Model	Shoe Size US Men's	Short Term Hardness (Shore A)	Baseline Tread Depth [mm]	Initial Contact Area [mm^2] (2°/7°/17°)	Tread Proportion	Heel Edge Type
A	Keuka	Galley 55014	9	56.4	3.7	249/180/145	0.48	Bevel
B	safeTstep	Apollo 140060	8.5	63.5	2.7	191/118/91	0.32	Bevel
C	Shoes for Crews	Falcon 6007	9	56.3	3.4	432/266/85	0.41	Square
D	SR Max	SRM 3500	9	50.1	2.8	271/147/44	0.57	Square
E	Tredsafe	M151044BU	9	60.5	2.4	264/325/160	0.66	Bevel

F.1.1.2.Mechanical Testing of Shoes:

ACOF and fluid pressure measurements were conducted using a robotic slip tester (Figure 1B). The slip tester included three electromagnet motors – one motor to control vertical displacement (Z-direction) and two horizontal motors to control horizontal movement (Y-direction) and foot angle, a force plate measuring shear and normal forces (vertical load capacity = 4450 N; BP400600-1K-Q2046, AMTI, Watertown, MA, 02472), and four fluid pressure sensors (Gems ® 3100R10PG08F002) in a linear array in the X-direction of the device (Figure 1B). A platform was mounted to the top of the force plate, which could be moved in the X-direction (medial-lateral); the platform and the force plate were fully constrained during testing procedures while the horizontal and vertical motors allowed for the shoe to translate in the Y and Z directions and rotate about the X-axis (3 degrees of freedom) (See Figure 1B for axes of the testing device). The fluid pressure sensors, each with an inlet diameter of 3.2 mm, were installed in the top of this platform, spaced 25 mm apart. Forces and hydrodynamic pressures were recorded at 500 Hz. The device is conceptually similar to the Portable Slip Simulator device [44-46] but has 2 horizontal motors that can operate independently to permit active shoe-floor angle control (Figure 1B).

Shoes were slid across a vinyl composite tile (Armstrong, 51804; R_a = 2.19±0.29 µm, R_z = 16.13±2.74 µm, R_q = 3.13±0.42 µm) which was contaminated with a diluted glycerol solution (90% glycerol, 10% water by volume; 219 cP). Tile roughness was measured in three locations on the tile in four orientations, each 45° apart. Contaminant was spread across the tile prior to each test to ensure that the entire region interacting with the shoe was covered with contaminant. Measurements occurred using a shoe angle of 17°± 1°, a speed of 0.3 m/s, and an average force of 250 N ± 10 N. These conditions were intended to approximate the angle [45, 47], speed [45, 47, 48], and normal force [49, 50] at the onset of slipping. These tests were performed at baseline (i.e., prior to any wear cycles) and after each wear cycle as ACOF data using this method has been demonstrated to predict slips [45]. Furthermore, as previous research has shown that fluid pressures may vary across the shoe surface [28, 51], the slip tester platform was moved 5 mm in the X-direction four times for a total of five trials and 20 pressure scans per measurement cycle.

Heel Tread Mold Protocol:

Heel tread at baseline and after each wear cycle was measured by creating a mold of the heel tread using a silicone rubber compound (Smooth-On Inc.; Macungie, PA; Oomoo® 25). To generate the mold, shoes were placed in a frame (92 mm x 76 mm x 28 mm), which was filled with the compound, at a sagittal plane angle of 17° (Figure 1D). Prior to placement in the mold compound, shoe tread was lightly and uniformly coated with a spray petroleum-based oil (WD-40 Company; San Diego, CA, USA) to allow for easy removal of the shoe from the mold. The molds were used to determine the largest region of the heel that lacked any tread as wear progressed for each iteration. For iterations in which the entire heel had tread, the area of one lug from the tread pattern was measured as the largest continuous area of contact between the shoe and the floor. Once a worn region developed, the size of

the region without tread was characterized by the longest length (along the sliding axis) and width (perpendicular to sliding axis) uninterrupted by a tread block (Figure 1D).

F.1.1.3.Data and Statistical Analysis:

The average ACOF for each shoe, wear iteration, and angle was calculated starting 0.1 s before and ending 0.1 s after the shoe crossed the pressure sensors for a total of 0.2 s. ACOF for each frame was determined as the magnitude of the resultant shear force divided by the normal force (Eq. 1) where F_{x_i} and F_{y_i} are the shear forces and F_{z_i} is the vertical ground reaction force for each frame (*i*). ACOF and fluid pressure data from two wear cycles and select trials were excluded because the normal force was outside of the desired range (240-260 N). Experimental complications also caused data from one shoe for one wear cycle to be excluded.

$$\mu_i = \frac{\sqrt{{F_{x_i}}^2 + {F_{y_i}}^2}}{F_{z_i}} \text{ Eq. (1)}$$

The peak fluid pressure was recorded and the force supported by the fluid (fluid force) across the shoe was calculated for each wear cycle. Fluid pressures above five standard deviations from the baseline pressure levels were included in the measurements [28]. The fluid force was determined using numerical integration (Eq. 2), where p_i is the fluid pressure at the *i*th frame, Δx is the distance between scans in the direction perpendicular to sliding (5 mm), v is the sliding velocity (0.3 m/s), andΔt is the time between each frame (0.002 s) [51]. The fluid force was thus summed for all fluid pressure readings across the five trials. Fluid forces were also categorized by percent of normal force during mechanical shoe testing (< 25 N or < 10%; 25-50 N or 10-20%; > 50 N or > 20%). Each shoe was worn until there were five wear cycles – indicated as Fluid Force Threshold (FFT) cycles – for which the fluid force was greater than 50 N (Figure 1A).

$$F_{fluid} = \sum p_i \, \Delta x \, \Delta y = \sum p_i \, \Delta x \, v \, \Delta t \text{ Eq. (2)}$$

Statistical analyses were performed to determine the relationships between ACOF, fluid force (continuous and categorical), the region without tread, tread proportion, and the sliding distance between and within each shoe type. Three generalized linear regression models were used to determine the relationships of each of the dependent variables – ACOF, fluid force, and region without tread – with the independent variables – shoe type (categorical), sliding distance (continuous) as shoes were worn, and their interaction. In the model, a square root transformation was used for fluid force to achieve normally-distributed residuals. Furthermore, a generalized linear regression model was used to determine ACOF differences across fluid force categories and shoe type. Specifically, ACOF was the dependent variable and the independent variables were the fluid force category, shoe type, and their interaction. If an interaction effect was observed between the fluid force category and shoe type, then a Tukey's HSD test was performed to determine significance between the three fluid force categories within each shoe type. Only comparisons across fluid force category within each shoe were analyzed in order to reduce the number of comparisons and maintain sufficient power.

F.1.2. Results

ACOF values ranged from 0.057 to 0.406 with an average ACOF of 0.189. The mean of the standard deviation across a set of ACOF trials within a wear cycle was 0.007 with a maximum standard deviation of 0.025. ACOF increased after the first wear cycle for Shoes A, B, C, and E followed by steady decrease across wear cycles (Figure 3). For Shoe D, an initial ACOF decrease of 0.1 occurred after the first wear cycle followed by a continued steady decrease. ACOF values when a fluid force first exceeded 50 N were 27% to 50% lower than their initial values and 37% to 63% lower than the peak values (Table 2). The regression analysis showed that ACOF was affected by the shoe type ($p < 0.001$), the sliding distance ($p < 0.001$), and their interaction ($p < 0.001$).

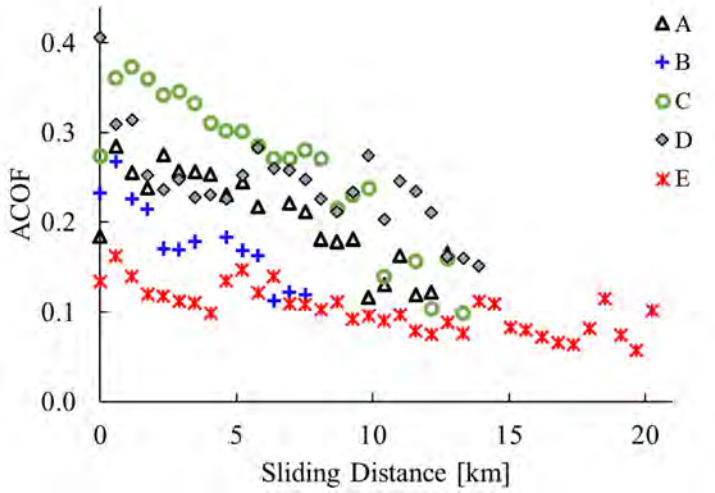

Figure 3: ACOF values plotted against the sliding distance that each shoe was worn on the abrasion device. A sliding distance of 0 represents baseline (prior to wear).

Table 2: Baseline (no wear), maximum, and minimum ACOF values across wear cycles, the ACOF values when the fluid force initially reached 50N, and roughness measurements (R_z) of the tread at baseline (no wear) and of the untreaded region at final wear.

Shoe Code	Total Sliding Distance [km]	Baseline ACOF	Maximum ACOF	Minimum ACOF	ACOF when fluid force first exceeded 50 N	R_z [µm]	
						Baseline	Final
A	12.7	0.183	0.284	0.117	0.117	15.60	13.50
B	7.5	0.232	0.267	0.112	0.168	19.10	14.50
C	13.3	0.269	0.366	0.099	0.136	11.40	14.67
D	13.9	0.406	0.406	0.151	0.202	7.25	12.90
E	20.3	0.134	0.163	0.057	0.066	15.25	12.80

Fluid force values ranged from 0 to 97 N. During the initial wear cycles, when most ACOF values increased relative to baseline, fluid pressures were under 25 N (Figure 4). For shoes A, B, and C, there was a distinct increase of fluid force between 4 and 8 km of wear distance accompanied by a steady decrease of ACOF. Shoe D showed an early increase in fluid force (1.2 km of wear), which was also accompanied by a steady decrease of ACOF. Shoe E showed a steady increase in fluid force across all wear cycles. Fluid force was affected by the shoe type ($p < 0.001$), the sliding distance ($p < 0.001$), and the interaction between shoe type and sliding distance ($p < 0.001$).

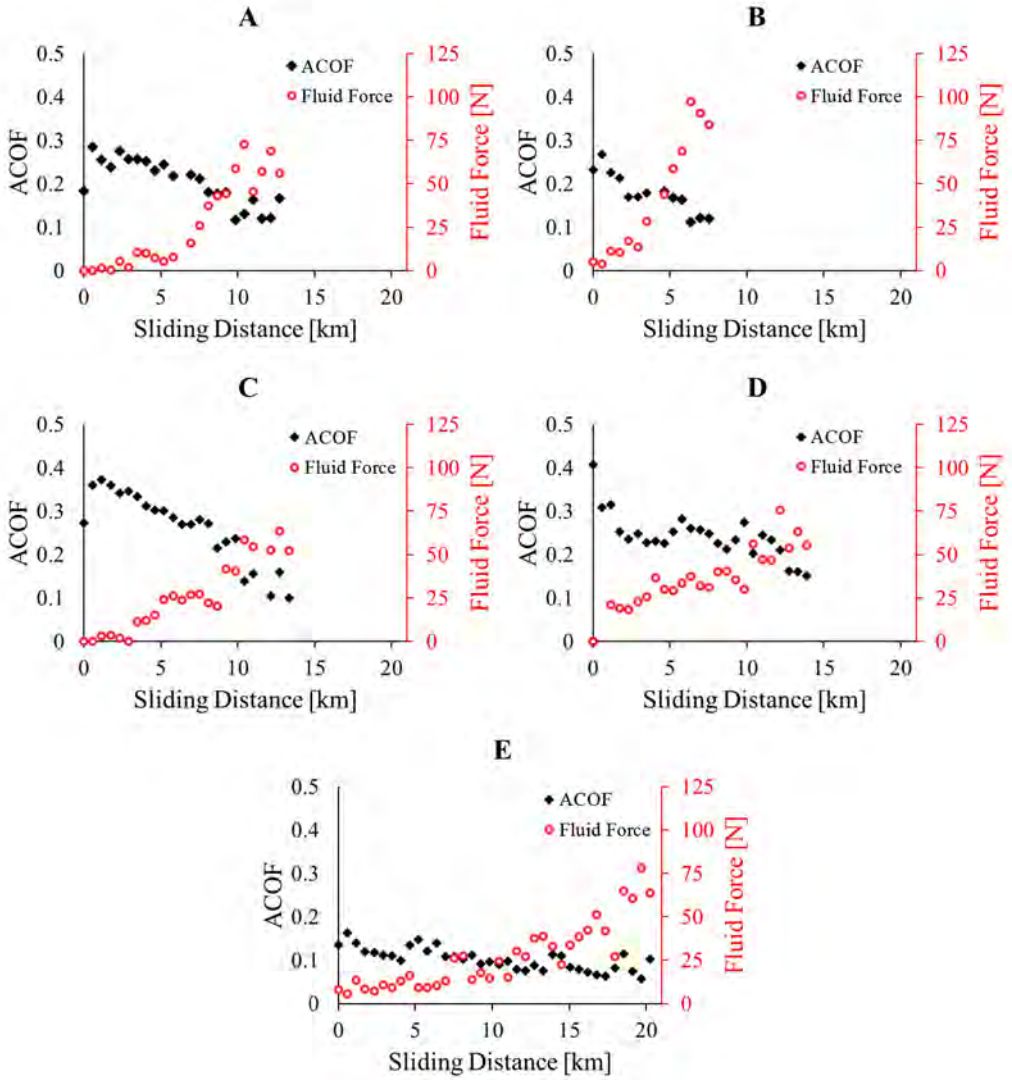

Figure 4: Fluid force and ACOF plotted against the sliding distance that each shoe was worn on the abrasion device. A sliding distance of 0 represents baseline (prior to wear).

Regions of the heel with fully worn tread developed on the lateral side of the heel for shoe A and the medial side of the heel for shoes B, C, D, and E (Figure 2). Within the untreaded region, the length parallel to the sliding axis was greater than the length perpendicular to the sliding axis for shoe A, but smaller for shoes B, C, D, and E. These regions of the untreaded region ranged from 7 mm^2 to 26 mm^2 at baseline and 1192 mm^2 to 1954 mm^2 after the final wear cycle (Figure 5). The region without tread when the fluid force first exceeded 50 N ranged from 840 mm^2 to 1730 mm^2 (mean: 1300 mm^2; standard deviation: 320 mm^2). Subsequently, this region grew at varying rates for each shoe. The region without tread for shoe B and shoe E increased the fastest and slowest, respectively. This region was affected by the shoe type ($p < 0.001$), the sliding distance ($p < 0.001$), and the interaction between shoe type and sliding distance ($p < 0.001$) (Figure 5).

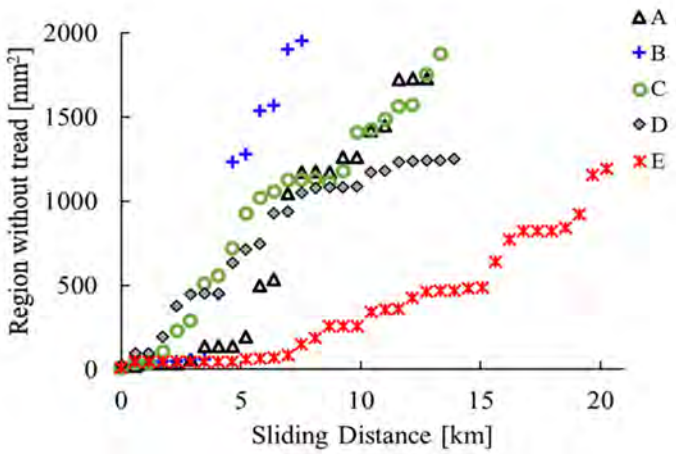

Figure 5: Region without tread (measured at each wear iteration) plotted against wear distance across the wear device.

Increased fluid loading was associated with a reduction in ACOF which was affected by shoe type ($p < 0.001$), fluid force category ($p < 0.001$), and their interaction ($p < 0.001$) (Figure 6). Significant decreases in ACOF between all fluid force categories were seen for two shoes (C and D) and a significant decrease in ACOF between at least two categories was seen in all shoes. The largest decreases in mean ACOF per category were seen in the shoes with the largest ACOF values at baseline (C and D) (Figure 6).

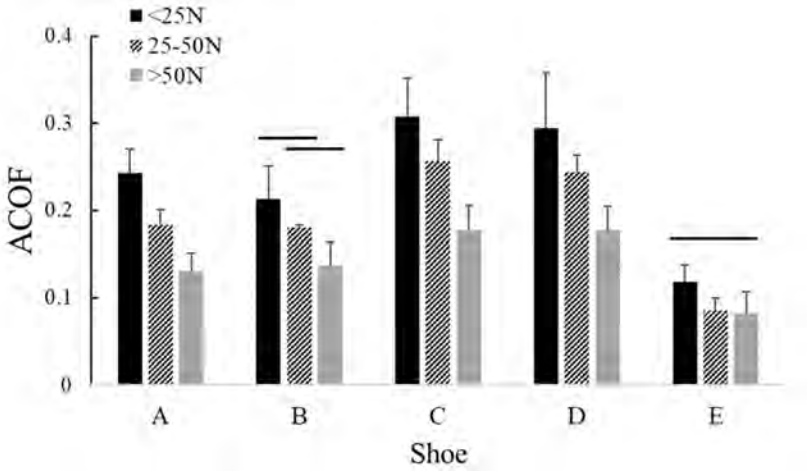

Figure 6: Mean ACOF for each fluid force category (< 25 N, 25-50 N, and > 50 N). Error bars represent standard deviations within fluid force categories. Categories within each shoe connected by a bar are not significantly different.

F.1.3. Discussion

The results confirm that shoe slip-resistance changes as the tread wears. An increase in ACOF and relatively unchanged fluid forces accompanied the initial wear process (< 3 km wear distance) for four of the shoes. After reaching the peak ACOF, fluid forces increased while ACOF values decreased for all shoes. Sudden increases in fluid force occurred at wear distances between 1 and 11 km for four of the shoes indicating that wear thresholds may exist where the shoe performance suddenly changes. The amount of ACOF decrease appeared to scale with the magnitude of the baseline ACOF: the shoes with the highest baseline ACOF tended to have the largest decrease in ACOF among the fluid force categories.

The results were generally consistent with the literature. Slightly worn shoes tended to have an increase in ACOF consistent with Grönqvist [23] who suggested this may be due to an optimum combination of surface roughening and sufficient tread depth. In contrast to Grönqvist's suggestions, there was not a clear effect of the change in surface roughness on ACOF for these shoes. An

alternative explanation is that slightly worn shoes may lead to higher ACOF due to an increase in contact area as the geometry of the shoe conforms to the floor surface [43, 52, 53]. For all shoes, a decrease in ACOF occurred for severe wear, which aligns with previous research findings that highly worn shoes are associated with a higher risk of slipping [23, 54]. Furthermore, this study supports previous research that related higher fluid forces with increased slip risk and lower ACOF [28, 55].

Prior to the sudden increase in fluid force, there was gradual decrease in ACOF. This behavior may be due to the shape factor of the tread which is defined by the loaded area of a rubber block divided by its area of lateral surface that is free to expand [56]. The reduction of tread depth will increase the shape factor of a tread block by decreasing the area of the lateral surface that is free to expand. Consequently, this may result in a higher compression modulus and lower deformability [56] of the tread block. In tire traction applications, the geometry of the tire tread block (given the same volumetric properties and contact area) in contact with a rigid surface affects rubber deformation [57]. On the other hand, tread blocks that have too much height (and subsequently tread channels that are too deep) can reduce the ACOF [58, 59]. Specifically, previous research showed that a large tread depth could lead to lower bending stiffness, which could result in an increase in deflection during sliding. This increase in deflection can reduce the contact area and subsequently decrease the friction force in boundary lubrication. Thus, this research suggests there may be an optimal tread depth that minimizes hydrodynamic pressures, reduces the shape factor, and has increased bending stiffness.

Although ACOF decreased as the shoes were worn, increased fluid forces were more dependent on the size of the region without tread (Figure 5). Faster growth in the untreaded region (e.g. Shoe B) was also associated with faster onset of high fluid pressures, whereas a slower growth in untreaded region (e.g. Shoe E) was associated with slower onset of high fluid pressures. Currently, some footwear providers offer tread gauge meters for tracking the utility of worn shoes [60]. However, this metric may not capture the salient features of the worn shoe condition. The minimum tread depth reached 0 mm as soon as the untreaded region began forming which occurs early in the wear process. Furthermore, the reduction of the minimum tread depth to 0 mm occurred prior to substantial increases in the fluid forces. Specifically, this change occurred prior to fluid forces equal to 10% of the normal load during testing (25N) for all shoe types. Thus, the size of the region without tread may be more relevant to the under-shoe tribology dynamics.

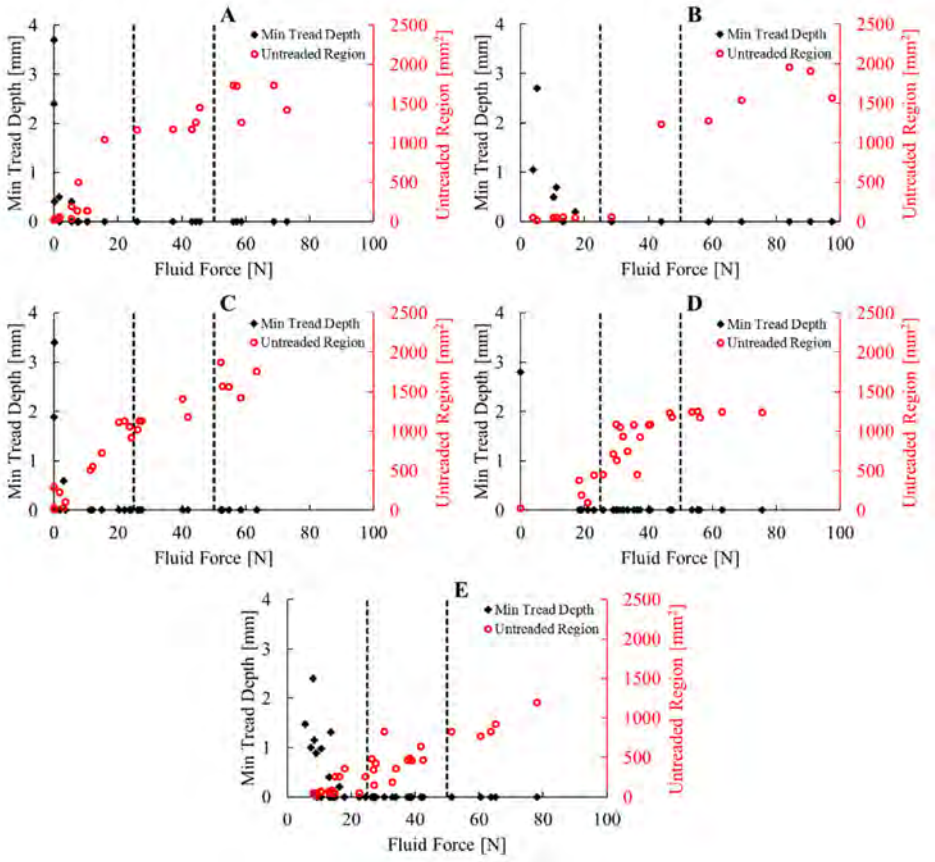

Figure 7: Minimum tread depth and the size of the untreaded region plotted against fluid force for each shoe. Fluid force thresholds of 25N and 50 N are indicated with vertical dashed lines. Minimum tread depth reached 0 when the untreaded region began forming.

Tread may start to be too worn when under-shoe fluid forces rise above 10% of the vertical load (25 N), acting as a first indicator of replacement (Figure 6). A fluid force greater than 20% of the vertical load (50 N) may serve as a replacement threshold since our findings suggest that an ACOF decrease of 25% to 50% of the baseline value may be associated with these fluid forces. Fluid forces exceeded this level when the region without tread exceeded between 840 mm^2 and 1720 mm^2. A conservative estimate might be to replace shoes at the lower limit of this range (approximately 800 mm^2). This information has potential to be used to guide footwear replacement thresholds.

While this study was not designed to determine the tread design parameters that influenced wear progression, notable differences were observed across the footwear designs. For example, Shoe B wore out in the shortest sliding distance whereas Shoe E wore out over the longest distance. The statistical modeling in this study using a nominal code for shoe type has limited predictive ability when extrapolating to other tread patterns and materials. However, a post-hoc analysis was performed to further explore the differences across shoes. Interestingly, the difference in the rate of response to wear might be explained by the proportion of the heel's surface covered in tread (Table 1). A bivariate correlation analysis was used to determine the relationship between tread proportion and total wear distance. Increased tread proportion was associated with an increased number of wear cycles and thus, increased total sliding distance ($p = 0.026$). As such, Shoe E had the largest proportion of tread coverage over the heel (tread proportion). This effect may be associated with Archard's law which describes how the wear rate is proportional to the contact pressure [33, 43]. Thus, a larger tread proportion produces a larger contact area and reduces the contact pressure on the individual tread blocks. However, a more robust study with more shoes and systematically varied tread coverage would need to be conducted to confirm this relationship.

As this is the first research study to examine the association between progressive shoe wear and ACOF, fluid force, and region without tread, certain limitations should be acknowledged. First,

only a limited number of shoes were examined, chosen as industry-marketed slip-resistant shoes. These shoes have significant tread to provide fluid drainage. Other types of shoes may behave differently. Second, the wear device was effective in producing rapid wear that had profiles on the heel similar in appearance to actual wear from walking. However, there may be unforeseen differences between these methods and naturally worn shoes due to varied gait biomechanics. Furthermore, extending this research to additional flooring (roughness, hardness) and contaminants with varying material properties (e.g. viscosity, surface tension) might lead to different wear thresholds. Improvements for future use of this simulated wear protocol could include employing personal gait characteristics (supination/pronation, heel strike angle, etc.) to better approximate natural wear.

These results suggest that a worn region on the heel with a size larger than 800 mm^2 leads to increased fluid forces and a reduction in ACOF. Research has shown that these changes are consistent with an increase in slip risk [6, 28]. Thus, the amount of wear in specific areas on the shoe may be useful in determining a threshold for shoe replacement to prevent slips. The results are promising and useful for the development of future guidelines for shoe evaluation and for further research taking into account the material properties of shoe wear and flooring and also the gait biomechanics.

F.2. Aim #2: Effect of tread design and hardness on interfacial fluid force and friction in artificially worn shoes (Aim 1, Key findings 2 and 3) [confidential]

F.2.1. Methods

An accelerated wear procedure was performed to simulate wear representative of common gait in the lateral-posterior section of the heel [61]. Nine shoes with systematically varied tread design and hardness were tested. This study tracked changes in under-shoe fluid force and ACOF in each shoe at regular intervals as wear progressed.

F.2.1.1. Shoe selection

In this study, three shoe tread designs each with three levels of hardness were utilized. All shoes had rubber composite outsoles and were EU Size 42. Only the right shoe from each pair was included in this analysis. The first shoe tread design was a repeated grid tread pattern (‘Grid’, Table 3). The second tread pattern contained trapezoidal lugs that were radially symmetric around the center of the heel (‘Lug 1’, Table 3). The third shoe tread design had short and wide lugs with sipes (cuts) in the tangential direction and diamond-shaped lugs in the center (‘Lug 2’, Table 3).

Each tread design had three levels of hardness from the manufacturer classified as soft, medium, and hard. Baseline Shore A hardness measurements were collected according to ASTM standard D2240 [62]. Each shoe type and its corresponding baseline Shore A hardness values are shown in Table 3.

Table 3: Shoe tread geometries and hardness levels

Shoe	Image	Hardness Level	Hardness
Grid		Soft	50
		Medium	57
		Hard	66
Lug 1		Soft	54
		Medium	62
		Hard	71
Lug 2		Soft	49
		Medium	61
		Hard	68

F.2.1.2.Accelerated wear procedure

The shoes in this experiment were abraded using an accelerated wear procedure. Each shoe was attached to an adjustable apparatus that controlled the shoe-floor pitch angle (toe up), while a paper belt with abrasive particles slid across the shoe surface at 9.65 m/s (Rikon Power Tools 50-122). A shoe last was inserted into each shoe and attached to the apparatus prior to wearing. The abrasive grit particles were aluminum oxide with a particle size of 165 µm (POWERTEC #110530). A roll angle (medial side up, rotation about sliding axis) of 6^{o} was applied with a bracket (3D printed using a fused deposition modeled polylactic acid, HATCHBOX 3D PLA-1KG 1.75-BLK) to simulate slight inversion during gait. This bracket was inserted between the shoe last and the frame holding the last on the apparatus. The roll angle was found to correspond with center of pressure slightly lateral to the centerline consistent with data from human slip trials [50]. The shoes were worn at pitch angles of $17^{o}\pm1^{o}$, $7^{o}\pm1^{o}$, and $2^{o}\pm1^{o}$ consecutively (Fig. 8) to reflect shoe angle progression during the early stages of stance consistent with previous shoe wear experiments [61]. One wear cycle consisted of wearing down each shoe for 10 seconds at each pitch angle. The duration (10 seconds) was based on observations in pilot testing that led to an observable but not excessive amount of wear. Each wear cycle abraded a shoe's sole for 289.5 m of sliding distance (30 s at 9.65 m/s). Grease (Formax, No. F26) was applied to the abrasive particles prior to each 10 second interval to minimize heat accumulation. After the shoes were worn, the soles were cleaned using detergent, water, and a scrubbing brush to remove abraded particles and grease residue. The abrasive paper was replaced after every shoe was worn for a given wear cycle.

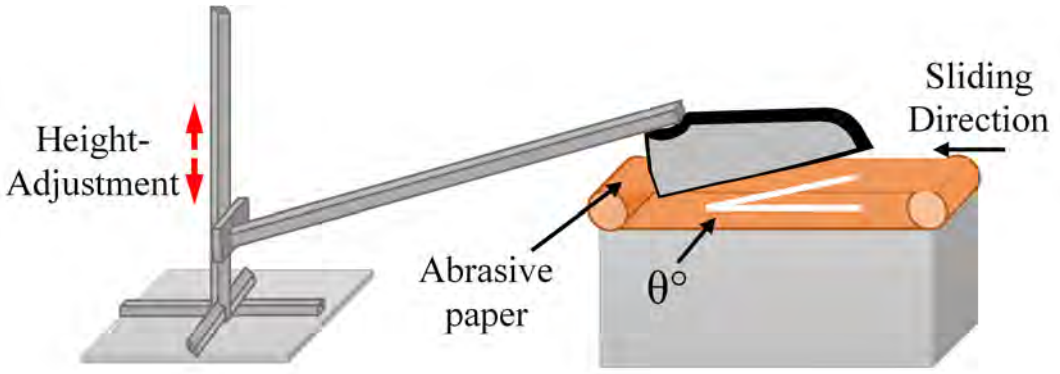

Figure 8: Height adjustable apparatus with shoe resting on abrasive aluminum-oxide paper. θ represents the pitch angle. Roll angle bracket not shown.

F.2.1.3.ACOF and fluid pressure testing

Each shoe underwent testing at baseline (prior to wear) and after every wear cycle. ACOF testing was performed using the Portable Slip Simulator [44, 45, 63], which consists of three vertical linear motors and one horizontal linear motor (LinMot, Elkhorn, WI, USA). The vertical motors controlled the vertical force, while the horizontal motor controlled the speed of the slip. The pitch angle was controlled using an adjustable bracket. The roll angle was controlled using the same polylactic acid wedge at a 6° angle that was used in the wear cycles. The device was instrumented with a force plate (BERTEC Corporation, Columbus, OH, USA) and four fluid pressure sensors (Setra # 3100R100PG089) in a linear configuration spaced 25 mm apart. The fluid pressure sensors were embedded in an elevated platform attached to the force plate. The floor tile contained holes 3.2 mm in diameter that aligned with the inlet of the pressure sensors. The force plate was used to measure friction and vertical forces. The fluid pressure sensors measured interfacial fluid pressures in the shoe-floor interface [51, 61, 64].

ACOF tests were conducted with a normal force of 250 N ± 10 N, a sliding speed (forward) of 0.5 m/s, a pitch angle of 17° ± 0.5°, and a roll angle of 6°. These test conditions reflect the biomechanical state of the shoe during human slips and the force, speed, and pitch angle have been demonstrated as predictive of human slip events [45, 50, 65]. All tests were performed on a vinyl composite tile (Armstrong, 51804). Prior to each trial, the tile was covered with sufficient liquid (90% glycerol/10% water) solution to achieve a natural full film thickness.

In order to characterize the fluid pressure profile across the width of the shoe, five trials were conducted in which the platform on which the shoe slid was moved laterally 5 mm four times [51, 61, 64]. Therefore, 20 total pressure measurements were recorded per shoe for the 5 scans across the four pressures sensors.

F.2.1.4.Data Analysis

ACOF was quantified using the ground reaction force data. ACOF was calculated as the ratio of the resultant friction force to the normal force averaged over 200 milliseconds (ms) starting at the first frame when normal forces reached 250 N. ACOF was averaged across five trials per shoe.

Fluid pressure data was integrated over area to calculate fluid forces under the shoe during ACOF slip testing. Data for each pressure sensor was debiased using the first 0.5 seconds of voltage prior to the start of the trial. Only fluid pressure data five standard deviations above the baseline levels was used to calculate fluid force [28, 61]. The fluid force (F_{fluid}) was calculated using numerical integration using each frame of pressure data (p_i), the lateral distance between scans (Δx), the sliding velocity (v), and the time between samples (Δt) where i is the frame [51, 61], Eq. (3).

$$F_{fluid} = \sum_{i=0}^{n} p_i \times \Delta x \times v \times \Delta t \quad \text{Eq. (3)}$$

F.2.1.5.Statistical analysis

The effect of hardness level, tread design, and their interactions with wear iteration on the ACOF and fluid force was analyzed. Preliminary review of the data revealed that wear cycle 4 was the first set of data that showed notable changes in friction performance and fluid force. As such, although data from all wear cycles is reported, only three wear cycles were used in the statistical analysis: baseline, wear cycle 4, and wear cycle 6. Wear cycle 6 was selected because it was the last cycle in which each shoe was tested. A two-way mixed within-between factors ANOVA was performed for ACOF and fluid force as dependent variables. The independent variables were hardness level (categorical, between factor), shoe tread design (categorical, between factor), wear iteration (categorical, within factor), and all first-order interaction effects. An alpha value of 0.05 was used and Tukey's HSD test was performed on all significant main effects.

F.2.2. Results

Tread geometry but not material hardness influenced ACOF and its response to wear. Grid shoes had a range of ACOF between 0.182-0.383 with an average ACOF of 0.295 across wear cycles (Fig. 9). Lug 1 shoes had a range of ACOF values of 0.064-0.212 with an average ACOF of 0.142 across wear cycles (Fig. 9). Lug 2 shoes saw a range of ACOF values of 0.174-0.338 with an average ACOF of 0.250 across wear cycles (Fig. 9). The influence of wear on ACOF was different across tread designs. The main effect of tread design influenced ACOF ($F_{2,12} = 50.7$, $p < 0.001$). Tukey's HSD test showed that the ACOF for all three tread designs were significantly different from each other with Grid shoes having the highest average ACOF and Lug 1 shoes having the lowest average ACOF. An interaction effect was observed between tread design and wear cycles ($F_{4,12} = 6.24$, $p = 0.006$). Grid and Lug 2 shoes both experienced a steady decline in ACOF while Lug 1 shoes experienced an initial increase followed by a small decrease with subsequent wear (Fig. 9). Hardness had no significant effect on ACOF ($F_{2,12} = 1.7$, $p = 0.223$). The main effect of wear cycle ($F_{2,12} = 3.6$, $p = 0.06$) and the interaction effect between hardness and wear cycle ($F_{4,12} = 6.2$, $p = 0.67$) were not significant.

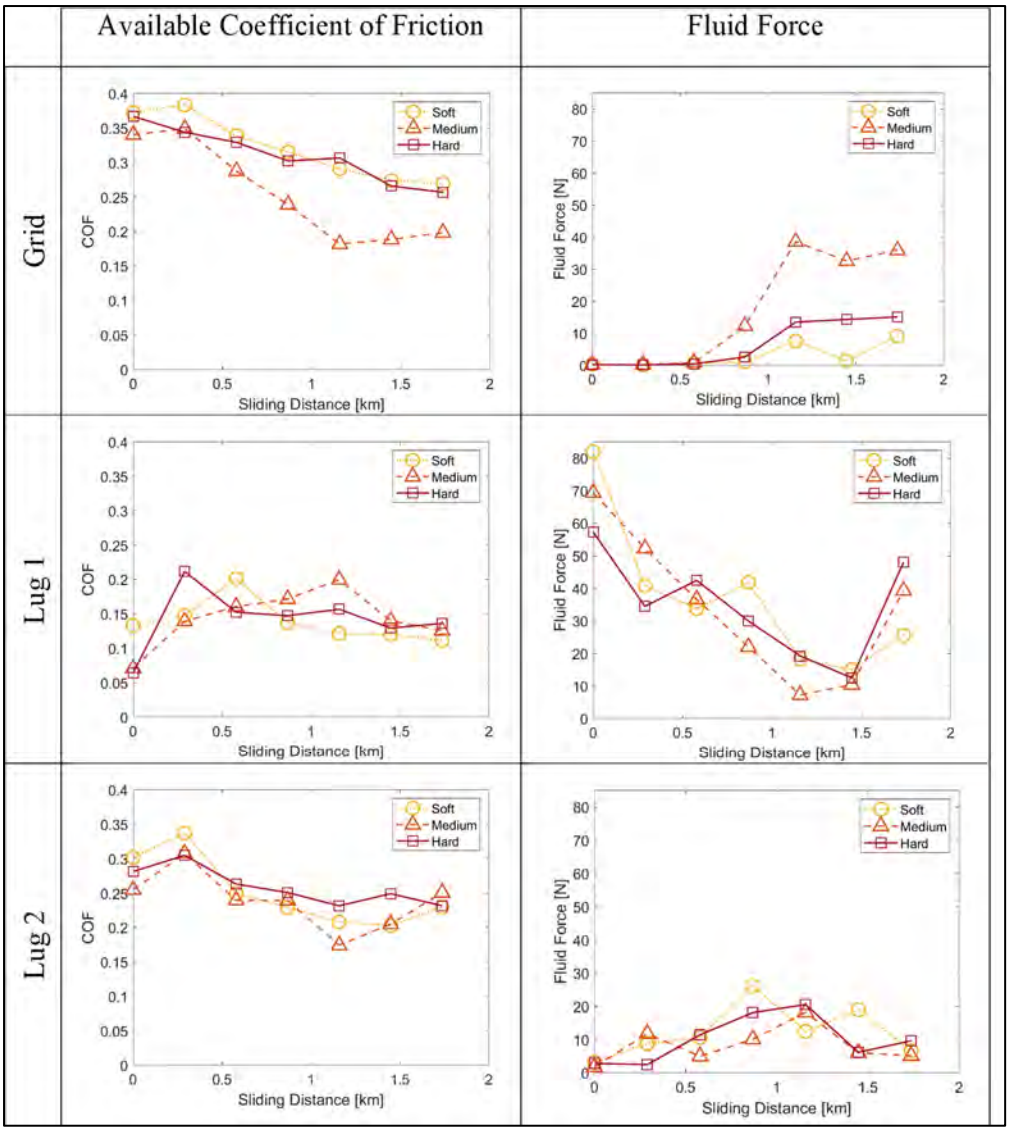

Figure 9: ACOF and fluid force values for each shoe as measured at baseline and after each wear cycle. The x-axis in all plots shows the sliding distance and the y-axis shows ACOF (left column) and fluid force (right column). Each row in the figure corresponds to one of the tread designs. Dotted lines with circle markers represent the softest shoes. Dashed lines with triangle markers represent the medium hardness shoes. Solid lines with square markers represent the hardest shoes.

Tread geometry but not material hardness influenced fluid force and its response to wear. Fluid forces ranged from 0.1-38.6 N for grid shoes, 7.2-82.0 N for Lug 1 shoes and 1.8-26.2 N for Lug 2 shoes (Fig. 9). The influence of wear on fluid force was different across tread designs. The main effect of tread design significantly influenced fluid forces ($F_{2,12} = 28.2$, $p < 0.001$). Tukey's HSD test showed that fluid forces for Lug 1 shoes were higher than the fluid forces for the other two tread designs. The influence of Lug 2 and Grid shoes were not significantly different. An interaction effect was observed between tread design and wear cycles ($F_{4,12} = 14.4$, $p < 0.001$). An increase in fluid forces was observed for Grid and Lug 2 shoes, whereas a high initial force followed by a decrease was observed for Lug 1 shoes. Shoe hardness did not influence fluid force ($F_{2,12} = 0.8$, $p = 0.489$). The main effect of wear cycle ($F_{2,12} = 1.1$, $p = 0.35$) and the interaction effect between hardness and wear cycle ($F_{4,12} = 0.9$, $p = 0.47$) were not significant.

Worn regions in the shoe soles developed differently across shoe types but consistently between hardness levels within each shoe type. Between baseline and the final wear cycle,

Grid shoes had worn regions concentrated in the lateral portion of the heel with a slight tendency to wear towards the posterior (Fig. 10). While wear was similar across the hardness condition, visual inspection appeared to show that the medium hardness shoe had the largest continuous worn region. Lug 1 shoes experienced moderate wear in the lateral-posterior quadrant of the heel and mild wear at all other quadrants but the medial-anterior quadrant where minimal wear was observed (Fig. 10). Qualitatively, the hard Lug 1 shoe had the largest continuous worn region of that tread design. Lug 2 shoes tended to wear most in the lateral-posterior quadrant with notable but reduced wear present in the lateral-anterior quadrant (Fig. 10). No difference was noted in the size of the worn region between these hardness levels of Lug 2 shoes. The arc-shaped sipes across the posterior lugs remained intact after all wear cycles.

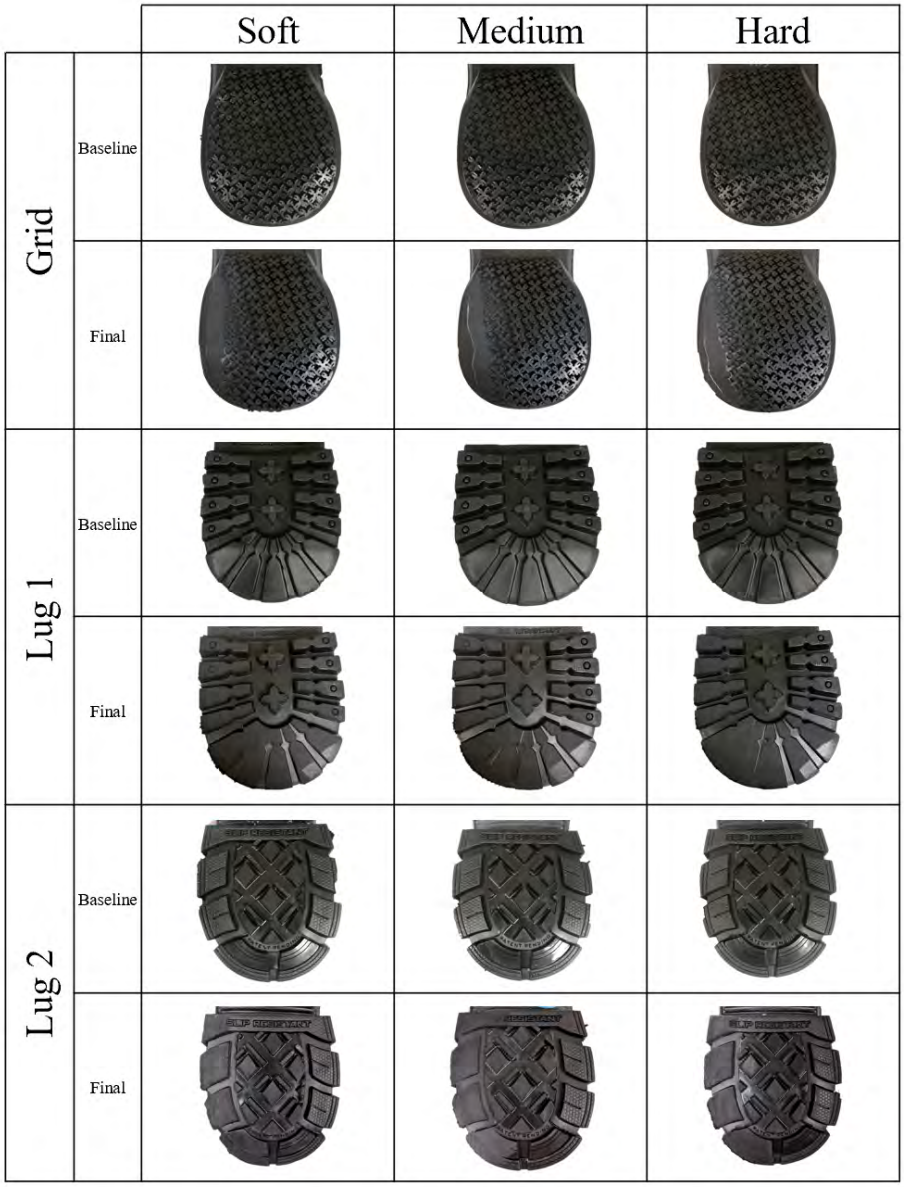

Figure 10: The heel for each shoe at baseline and after final wear cycle 6. Organized in three main columns separating soft, medium, and hard shoes and three main rows representing each tread design. Each main row has two sub-rows distinguishing baseline from final wear cycle.

F.2.3. Discussion

ACOF and fluid forces as tracked as each shoe becomes worn indicate that shoe tread design influences traction performance and its wear progression. The shoe tread design had a substantial impact on ACOF and fluid force as well as how these factors responded to wear. Notably, one tread design experienced an overall increase in ACOF and an overall decrease in fluid force in response to wear, while others experienced a decrease in ACOF and an increase in fluid force. The hardness did not substantively influence fluid force, ACOF, or their response to wear.

The three tread designs were shown to have different trends in both ACOF and fluid force throughout their lifetime. A decrease in ACOF and an increase in fluid force was observed for the Grid and Lug 2 geometries similar to what was observed in both simulated and natural wear progression studies [61, 66]. Because the shoes in the prior research resembled the grid pattern shoe (small treads patterned across the sole surface), the response of the grid shoes to wear are considered consistent with prior research. However, this work indicates that some lug-pattern shoes such as Lug 1 did not have typical trends. This indicates that some lug patterns may benefit from the effects of wear. Thus, the response to wear that has been previously reported may not be universally true, especially for lug designs.

This work is consistent with previous research regarding the size of the worn region. As indicated by Sundaram et al., a larger worn region size negatively affects the shoe's traction performance [65]. The increased worn region in Grid shoes (Fig. 10) may be a key contributor to the increases in fluid force and decreases in ACOF after 1 kilometer of wear (Fig. 9). Lug 1 and Lug 2 shoes still had intact tread channels in the heel strike area after wear cycle 6 (lateral-posterior), minimizing continuous worn region size (Fig. 10). These tread designs, especially Lug 2, were found to have traction performance that was slower to degrade under the accelerated wear protocol.

This study revealed that hardness had a minimal effect on fluid force and ACOF with wear which is consistent with previous work. Soft-soled shoes have previously been connected to higher ACOF values and decreased slip probability compared to harder soles [67-69] which aligns with baseline observations in this study (Fig. 9). Further wear cycles did not show continued influence of hardness on ACOF or fluid force. This finding contradicts theory that links elastomeric wear to hardness [70]. Thus, other material properties of shoe outsoles may be more relevant to friction and wear resistance than hardness.

This research reiterates the complexities of shoe design and its influence on slip risk. Over the shoe's life, material hardness is not necessarily a dominant factor on ACOF or fluid force. Tread design, however, does strongly influence each of those factors. Grid shoes followed previously observed trends of decreasing ACOF and increasing fluid force over increased wear. Lug 1 shoe design, however, responded in the opposite way where increased wear led to a reduction in fluid force and an increase in ACOF. Interestingly, this was the only one of the two lug designs to follow this trend. Lug 2 shoes strongly outperformed Lug 1 shoes in minimizing fluid force, likely due to smaller contiguous tread regions and sipes to disperse contaminant. Thus, the additional tread features (e.g., siping) present in Lug 2 appeared to be advantageous, especially for the shoe's performance at low levels of wear. These observations indicate pathways that shoe companies can follow to better inform tread design for decreased injury risk and longer shoe lifetimes.

Certain limitations should be acknowledged. This study used an accelerated wear procedure where artificial abrasion was the primary mechanism for material removal. This accelerated wear may not fully represent real-world conditions. Further research on naturally worn shoes may confirm whether these results are similarly applicable to other wear mechanisms. Additionally, slip dynamics have been shown to vary with different contaminants and floor types [71, 72] so the use of only glycerol on vinyl tile in this study may not entirely capture different environments.

In conclusion, this study demonstrates the relevance of shoe tread geometry on shoe friction, tread fluid drainage, and the response of these two parameters to wear. Hardness had a small and insignificant contribution and did not influence wear trends. Thus, tread design may be important to prioritize in designing shoes with traction performance that is robust to wear.

F.3. Study #3: An observational ergonomic tool for assessing the worn condition of slip-resistant shoes. [73] (Aims 2 and 5, Key findings 5, 8, and 12)

F.3.1. Methods

F.3.1.1. Selection of an Instrument for Assessing the Worn Region

The instruments chosen to assess the worn region of a shoe for this study were AAA and AA batteries. The criteria were a readily-available object that: 1) is a standardized and stable size over several years; and 2) corresponds with worn region sizes that lead to an increase in fluid pressure and reduction in COF. AAA and AA batteries became popular decades ago and their sizes (diameter of 10.5 mm for AAA and diameter of 14.5 mm for AA) are standardized [74]. Previous research has demonstrated that larger worn regions, especially as multiple treads become completely worn, are associated with increased under-shoe fluid pressures and reduction in COF [37]. Given that slip-resistant shoes tend to have treads that are 2-10 mm in size [43, 69], selecting an object that is 10-15 mm across is appropriate for capturing wear that is larger than typical tread.

The battery tests were applied to shoes by determining whether the worn region was larger than the base of the battery (negative side of the battery terminal). When the worn region was larger than the base of the battery, the tread was labeled as “failing” the test whereas when the worn region was smaller than the base of the battery, the tread was labeled as “passing” the test. (AAA battery: “AAA test” and AA battery: “AA test”) (Figure 11). This test was applied to the tread from shoes used in all three previous experiments.

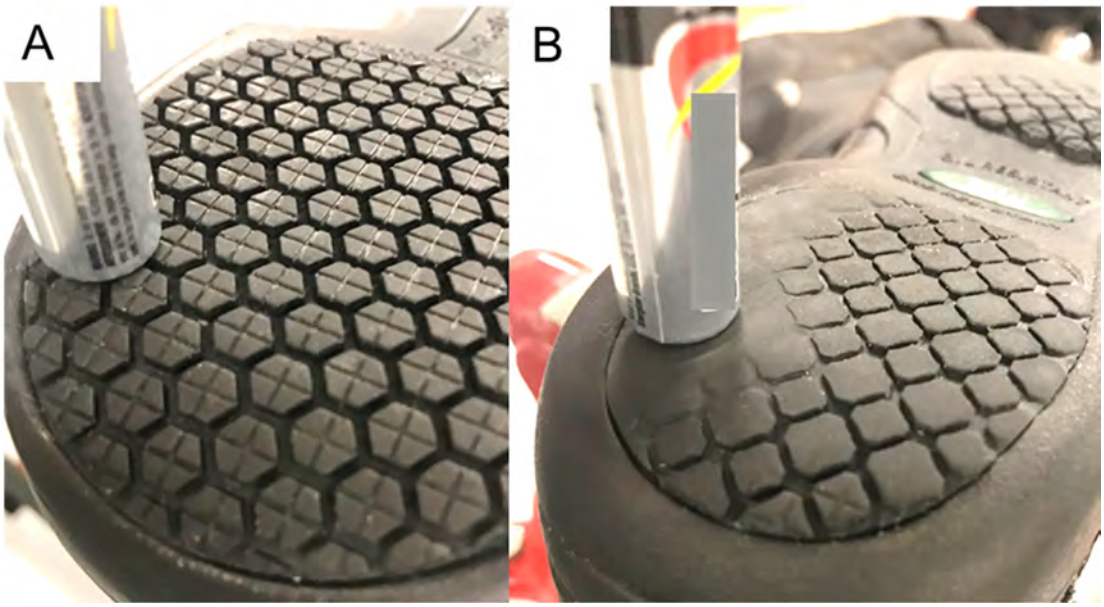

Figure 11: A) The shoe tread passes the battery test because the size of the worn region is smaller than the battery. B) The shoe tread fails the battery test because the worn region fully surrounds the base of the battery. Only the heel region (posterior half of the shoe) is considered in this test.

F.3.1.2. Methodologies of Previous Studies

This current study applied the battery tests to data from three previous studies [37, 75, 76]. These prior studies included similar outcome measures to the present study but did not assess the battery tests. As such, the experimental methodologies from these studies are only briefly described here. Experiment #1 implemented a mechanical accelerated wear protocol that abraded the outsole of the shoe under controlled conditions [37, 77]. Experiment #2 was a longitudinal study where the slip resistance of naturally worn shoes were assessed at monthly intervals throughout their life [75]. Experiment #3 was a cross-sectional study that exposed human participants to a slippery contaminant, while wearing their own shoes [76]. Under-shoe fluid pressures were measured for all three

experiments. COF was measured for Experiments #1 and #2. The slip response was measured for Experiment #3.

F.3.1.2.1.Experiment #1 [37]: Accelerated wear protocol

Five shoes labeled as slip-resistant by their manufacturers were worn through mechanical abrasion. All shoes had a grid-style tread pattern, which is generally representative of slip-resistant shoes [69]. An iterative process of 1) simulating wear and 2) measuring the shoe's COF and under-shoe fluid pressures was performed. Shoes were worn using sliding abrasive paper (180µm diameter particles) moving at 9.65 m/s with a normal force of 40 N at each of three angles (2°, 7°, and 17°, in the sagittal plane of the shoe) between the shoe and the belt. A mold of each shoe's heel tread was created to record the state of the tread at baseline and after each cycle of wear using a silicone rubber compound (Smooth-On Inc.; Macungie, PA; Oomoo® 25). Friction and fluid pressure measurements were collected at each iteration, while each shoe was slid across a contaminated surface using a robotic slip testing device. Shoes were slid across a vinyl composite tile (Armstrong, 51804; Ra = 2.19±0.29 µm, Rz = 16.13±2.74 µm, Rq = 3.13±0.42 µm, cutoff length = 0.8 mm, sampling length = 8.0 mm) contaminated with a diluted glycerol solution (90% glycerol, 10% water by volume; 219 cP) at a speed of 0.3 m/s, angle of 17°, at a normal force of 250 N. Four fluid pressure sensors embedded in the floor tile were separated by 25 mm and each had an inlet diameter of 3.2 mm. The adjustable platform was moved 5 mm lateral in the direction relative to the shoe between each of five trials. This enabled 20 fluid pressure scans (4 scans per trial * 5 trials) each separated by 5 mm.

F.3.1.2.2.Experiment #2 [75]: Natural wear of shoe tread

Twenty-three participants were recruited to wear slip-resistant shoes in their workplace. Three brands (SR Max ®, SafeTStep ®, Shoes for Crews ®) were used in the study. Participants were provided with shoes or boots depending on the footwear requirements of their workplace. Each participant was provided with two different pairs of shoes that they wore on alternating months. These shoes contained grid-style tread, which is representative of slip-resistant shoes [69]. The shoes or boots were returned to the research team on a monthly basis for testing. Twelve participants were excluded due to lack of follow-up (n=6), withdrawal from the study (n=4), and discomfort wearing the shoes (1 of the pairs of shoes were excluded from 2 participants). The included participants worked in the following industry sectors: trade, transportation & utilities; accommodation and food services; and manufacturing. The slip resistance and fluid pressure from the outsoles were tested using the same methods outlined in Experiment #1 at baseline and after each month of wear.

F.3.1.2.3. Experiment #3 [76]: Human slip response

Of the 57 participants that were part of a larger study [76], 32 (13 females, 19 males; mean age: 36±12 years) were included for this analysis. Inclusion criteria were that they: 1) wore shoes labeled as slip resistant by the manufacturer, and 2) stepped on the fluid-pressure plate with contaminate during laboratory slip testing. Of these shoes, 24 (75%) utilized a grid-style tread pattern and 8 (25%) utilized a lug-style tread pattern. Participants completed approximately 15 to 30 walking trials prior to contaminate exposure. The last trial of every assessment was the unexpected exposure to a liquid contaminant. During the unexpected exposure to a slippery contaminant, 100mL of a 90%:10% glycerol: water solution was spread over the fluid sensor array. The outcome measures included the peak fluid pressure and the peak slipping speed that occurred during the human exposure to the liquid contaminant.

F.3.1.3. Data analysis methods for battery tests:

For data from Experiments #1 and 2, the available COF was calculated for each shoe and at each wear time point [37, 45, 46]. The peak fluid pressure across the 20 scans was used to quantify the fluid drainage capabilities of the shoe outsole (higher fluid pressure indicated poorer drainage capability). The median available COF and peak fluid pressure for the cycles preceding and following the shoe's first occurrence of failing the AAA test were included. Similarly, the median COF and fluid

pressure values for the AA test were included. Mixed-model repeated-measures ANOVAs (one for the AAA test and one for the AA test) were then performed with the COF and fluid pressure as the dependent variables and the following independent variables: test outcome (pass, fail), mode of wear (simulated/Experiment #1, natural/Experiment #2), and their interaction. If an interaction was observed, separate paired t-tests were performed for Experiment #1 and #2. A significance level of 0.05 was used for all analyses.

For data from Experiment #3, non-parametric methods (Wilcoxon Rank Sums test) were applied to test fluid pressure and peak slipping speed between shoes that passed versus failed the AAA and AA tests. Non-parametric methods were applied since it was determined that the assumptions of normal residuals and homoscedasticity were not satisfied and could not be corrected using transformations. In addition, relative risk, sensitivity, specificity, and accuracy of the test to identify slips was calculated. Slips were categorized based on a cutoff peak slipping speed of 0.3 m/s consistent with the previous study [76]. A significance level of 0.05 was used.

F.3.2. Results

F.3.2.1. Influence of wear on shoe friction performance (Experiments #1 and #2)

Shoes that failed the AAA test had lower COF values ($F_{1,14}$ = 19.9, p<0.001) and higher fluid pressures ($F_{1,14}$ = 20.9, p<0.001) than those that passed (Table 4, Figure 12). On average, the COF for shoes that failed (mean: 0.158) was 29% lower than shoes that passed (mean: 0.224). Shoes that failed (mean: 81 kPa) had higher fluid pressures than shoes that passed (mean: 37 kPa). Neither the mode of wear nor its interaction with battery test outcome influenced either COF values or fluid pressures for the AAA test (Table 4).

Table 4: Statistical results for the influence of the test outcome, the mode of wear, and their interaction on COF and under-shoe fluid pressure using data from Experiments #1 and #2.

	AAA Test				AA Test			
Dependent variable	COF		Fluid pressure		COF		Fluid pressure	
Independent variable	F(1,14)	p	F(1,14)	p	F(1,8)	p	F(1,8)	p
Test outcome	19.9	<0.001	20.9	<0.001	74.9	<0.001	17.9	0.003
Mode of wear	0.4	0.411	1.8	0.204	0.8	0.402	0.2	0.675
Mode of wear * Test outcome	0	0.874	4.4	0.054	3.1	0.114	13.0	0.007

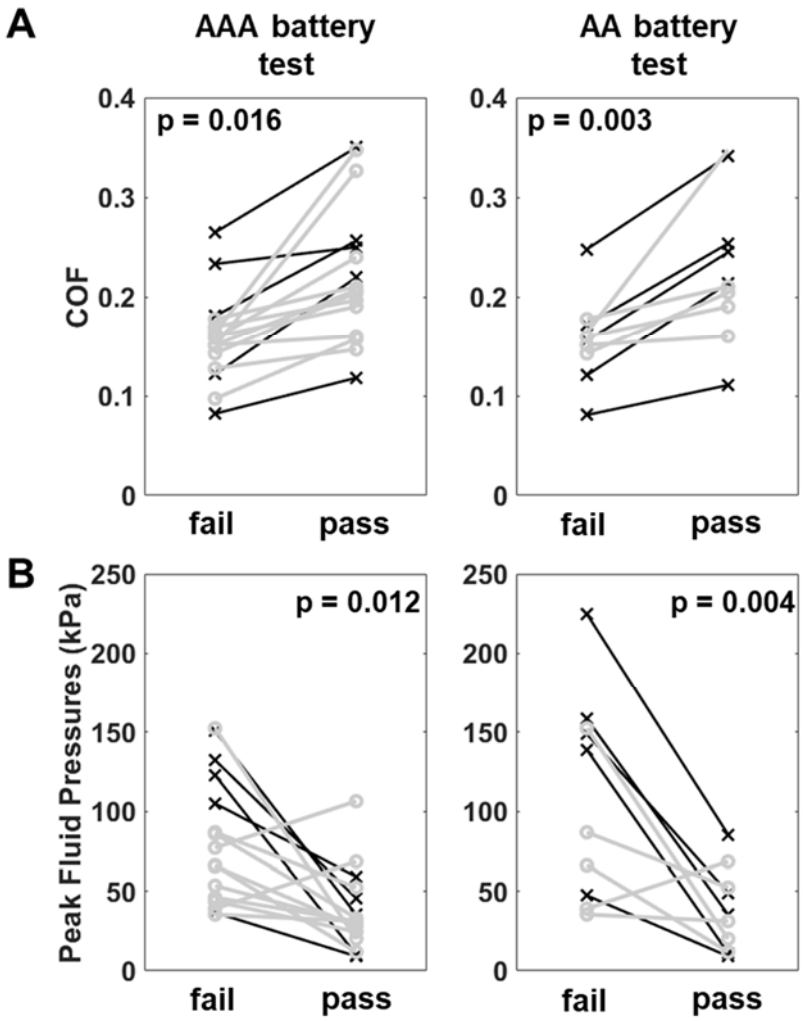

Figure 12: Change in COF (A) and peak fluid pressure values (B) between passing and failing the AAA battery test (left) and the AA battery test (right). The black lines with the “X” markers represent data from the accelerated wear protocol (Experiment 1) and the gray lines with the “O” markers represent data from the human wear experiment (Experiment #2). Each line represents a single shoe before and after failing the test.

Similar to the AAA test, shoes that failed the AA test had lower COF values ($F_{1,8}$ = 74.9, p<0.001) and higher fluid pressures ($F_{1,8}$ = 17.9, p = 0.003) than those that passed (Table 4, Figure 12). Shoes that failed the AA test (mean: 0.147) had COF values that were 30% lower than shoes that passed (mean 0.211). The mode of wear and its interaction with test outcome did not influence either COF. The mode of wear did not influence fluid pressure. However, an interaction effect was observed between the mode of wear and the test outcome on fluid pressure ($F_{1,8}$ = 13.0, p = 0.007). Specifically, a larger difference in pressures between passing and failing shoes was observed for mechanically worn shoes (pass: 40 kPa; fail: 140kPa; t_4 = 5.9; p = 0.004). This effect was smaller and not significant for naturally worn shoes (pass: 70 kPa; fail: 80 kPa; t_4 = 0.4; p = 0.695).

F.3.2.2.Influence of wear on human slipping (Experiment #3)

Fluid pressures ranged from 2 to 696 kPa while peak slipping speeds ranged from 0.07 m/s to 2.63 m/s across the exposures to slippery contaminants in data from Experiment #3. A third of the shoes failed the AA test and 42% of the shoes failed the AAA test. Shoes failing the AA test were associated with a 9-fold increase in fluid pressures ($\chi^2_{(1)}{}^{AA}$ = 12.2, p^{AA} < 0.001) and a 67% increase in peak slipping speed ($\chi^2_{(1)}{}^{AA}$ = 7.6; p^{AA} = 0.006) (Figure 13). Similar trends were observed for shoes failing the AAA tests (330% increase in fluid pressures and 80% increase in peak slipping speed).

These trends reached significance for peak pressure ($\chi^2_{(1)}{}^{AAA} = 6.2$; $p^{AAA} = 0.013$) but not for peak slipping speed ($\chi^2_{(1)}{}^{AAA} = 2.8$, $p^{AAA} = 0.095$). The relative risk (95% confidence interval) was 1.87 (0.82-4.26) for shoes failing the AAA test and 2.67 (1.20 – 5.94) for shoes failing the AA test. The sensitivity/specificity (accuracy) was 57%/68% (64%) for the AAA test and 57%/82% (72%) for the AA test. Thus, the AA test better differentiated human slipping than the AAA test (Figure 13).

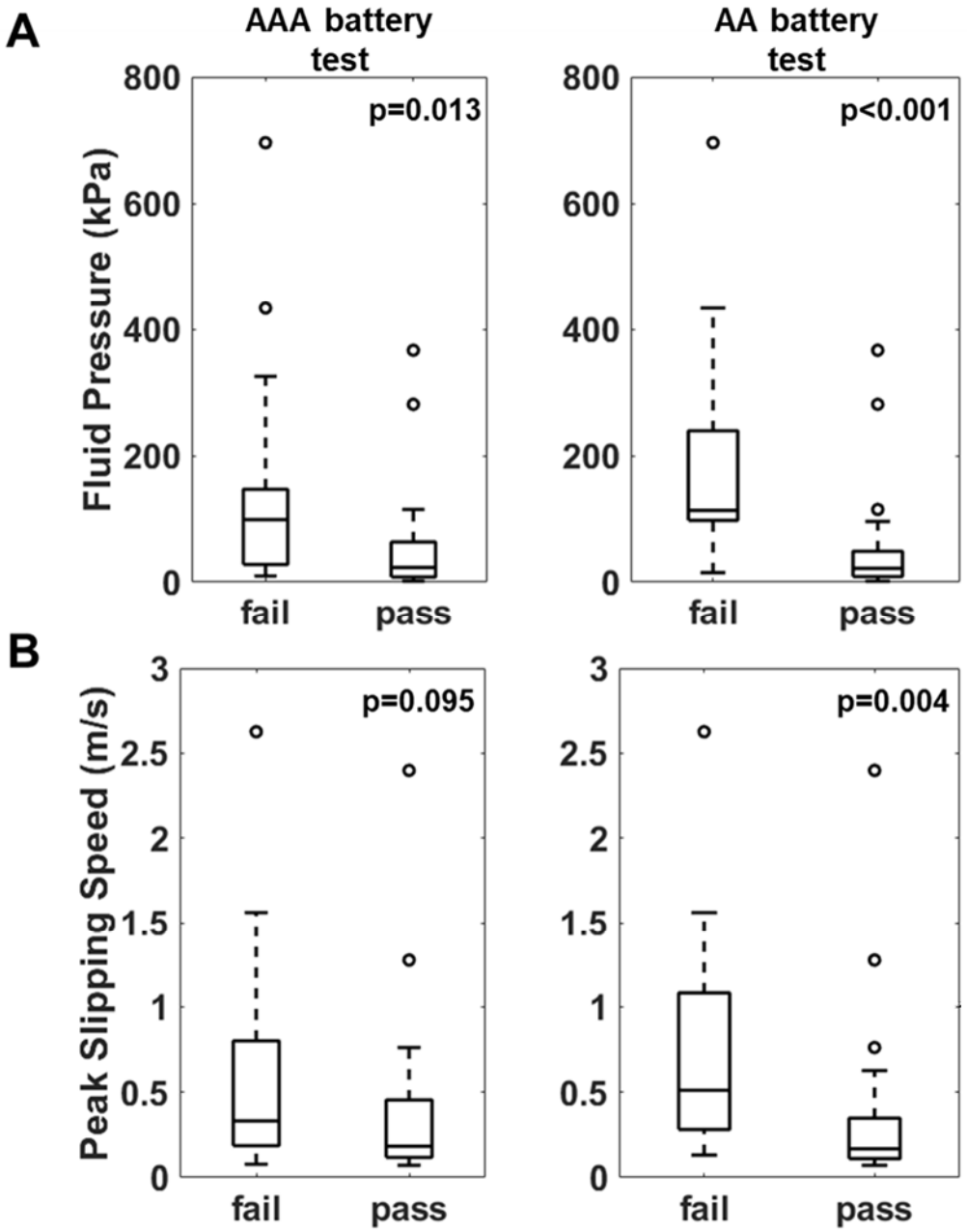

Figure 13: Box plots of peak fluid pressure (A) and peak slipping speed (B) for fail/pass outcomes of the AAA battery test (left) and the AA battery test (right).

F.3.3. Discussion

This study demonstrates that the wear-induced reduction in fluid drainage capacity and friction in slip-resistant shoes can be assessed by comparing the size of the worn region to an object such as a AAA and AA battery. Consistent trends were observed in data from the three different experiments, including: a controlled accelerated wear procedure; a longitudinal study tracking shoe performance throughout its naturally-worn life; and a cross-sectional study examining human exposures to slippery

contaminants, while wearing naturally-worn shoes. Specifically, a reduction of approximately 30% in COF was observed for shoes failing these tests relative to their passing counterparts. Higher fluid pressures were consistently observed in cases where shoes failed the test, however the magnitude of this difference varied across experiments. For the human slip study, increased slipping and slip severity were observed for participants wearing shoes that failed the test compared with participants wearing shoes that passed the test. Although, the battery tests were not fully deterministic of shoe friction performance, they were highly predictive in *loss of friction* performance within the longitudinal experiments. In fact, every shoe that was tracked during wear (shown in Figure 12A) had less friction for the fail condition relative to the pass condition. Furthermore, the tests (particularly the AA test) were moderately sensitive and highly specific predictors of human slipping. The consistency of the results across these three experiments yields robust evidence that applying these tests are an effective way of identifying worn shoes that have degraded performance. However, potential users should be trained to properly apply these tests and understand their scope of applicability. Both tests (AAA and AA) were demonstrated to predict a degradation in friction performance. The AAA test will lead to more frequent replacement of footwear than the AA test. Therefore, the AAA test is an option for more risk-adverse practitioners, while the AA test may be more appropriate to those who are more risk-tolerant.

The proposed battery tests are designed to be a simple and inexpensive solution in assessing the worn condition of slip-resistant shoes. The batteries are a consistent and available product that can lead to wide adoption to assess tread wear and prevent slip-initiated falls. These features are consistent with attributes of an ideal ergonomic tool (i.e., predictive, robust, quick to administer, inexpensive, non-invasive and easy-to-use) [78]. While this test is easy to perform, future research should examine the human factors aspects of this test including inter-rater reliability, usability, and usefulness of the test.

This test assesses the actual worn condition of shoes as opposed to other cutoffs like the age of the shoe. Commonly, shoes are replaced according to a time schedule (e.g., every 6 months) [54]. However, shoe age guidelines do not account for variation in wear due to differences in individual usage or biomechanics. This study found that a substantial portion of shoes with less than 6 months of use failed one of the battery tests (27-36% from Experiment #2) and a substantial portion of shoes older than 6 months passed the test (56-70%). Thus, discrepancies exist between time-based replacement thresholds and worn-condition thresholds. Presumably, replacing shoes on a set time-based schedule may expose high wear individuals (high use or gait pattern that is associated with faster wear [79]) to increased slip and fall risk and may lead to unnecessary cost for low wear individuals (lower use or gait pattern associated with slower wear). Thus, the utilization of this test may enable reallocation of resources to the individuals at greatest slipping risk.

The results of this study are consistent with previous research that demonstrated degraded performance for worn shoes. Our previous research has found that an increase in fluid pressures and a reduction in COF is associated with shoe wear [28, 77, 80-82]. In addition, we also showed a relationship between the size of the worn area and friction [77, 83], which is consistent with assessments targeting the size of the worn region. Thus, the results of these experiments are generally consistent with previously-identified trends of the influence of shoe wear on slip risk.

This study focused on wear in the heel region of the shoe as opposed to the midfoot or forefoot regions. The heel is appropriate for tracking wear since previous research has identified that wear commonly occurs in this region [75]. Furthermore, slips occurring during the heel contact phase of gait are relevant to fall risk since they are 1) capable of generating a backward fall away from the point of contact; 2) occur during the initiation of swing phase for the contralateral limb; and 3) have high frictional requirements [84]. While wear in other regions of the shoe may lead to loss of friction, wear in the heel region is more likely to lead to slips resulting in a fall. Thus, observing wear in the heel region is justified for achieving the goal of reduced slip and fall events.

Certain limitations of this study should be acknowledged regarding the scope of applicability. First, the study focused on shoes that were labeled as “slip-resistant” by the manufacturers and it is unclear if the same test is valid across all shoe types. Second, although this test was effective at predicting loss of friction, it was not fully deterministic of friction performance as indicated by the variability in COF across shoes (Figure 12). Other parameters are known to be relevant to friction performance including tread surface area, material hardness, heel shape, and tread bending stiffness

[46, 58, 69]. Third, while the threshold was tested across data from multiple experiments using a variety of slip-resistant shoes, further efforts are needed to generalize the results to different contaminants and flooring. Tribology theory suggests that the worn regions assessed in this study would lead to greater hydrodynamic pressures and lower COF values when utilized with lower roughness flooring and higher viscosity contaminants [85]. Thus, some correction factor may be warranted when applying these results to smooth floor surfaces with high viscosity contaminants. Lastly, validating these tests using actual workplace slip and fall data would increase confidence in the test.

This study demonstrates that worn shoes, as assessed using a simple test of comparing the worn region to the size of batteries, are associated with a loss in friction. This result was demonstrated consistently across three experiments and is consistent with previous research and theory. The test is expected to offer workers a simple, quick and inexpensive way to assess their shoe wear condition and enable employers to appropriately allocate resources based on the actual worn condition of the shoes. Broader use of shoe wear monitoring through the proposed tests has an opportunity to reduce the burden of slip and fall events in the workplace.

F.4. Study #4: Computational Model of Shoe Wear Progression: Comparison with Experimental Results [43] (Aim 3, Key finding 6)

F.4.1. Methods

F.4.1.1. Computational wear model

Modeling of the contact interface was performed in the explicit finite element package, LS-Dyna® (version R10.0.0, LSTC, Livermore, California, USA). The capability of this software in modeling shoe-floor contact has been previously demonstrated [86]. An automatic, segment-based soft contact was used in which the contact stiffness is determined based on timestep size to ensure stability. The shoe and floor surfaces were designated as slave and master, respectively, for the contact pair given the difference in their elastic moduli. The finite element modeling method simulated the contact pressure distribution at the contact interface of the shoe (Figure 14). The output of the finite element model was the nodal contact pressures at the interface. These pressures were used to calculate the nodal wear depths in each iteration by assuming that the wear depth for each node in each wear iteration was proportional to the interfacial contact pressure based on Archard's equation, Eq. (5). Therefore, the wear process was simulated by moving the respective nodes [87] in a direction perpendicular to the contact interface based on the amount of calculated wear. Specifically, the wear depth at the *i-th* node (Δh_i), was a function of the wear constant (k), the contact pressure at the *i-th* node (P_i), and the sliding distance on the counter-surface (s), Eq (5).

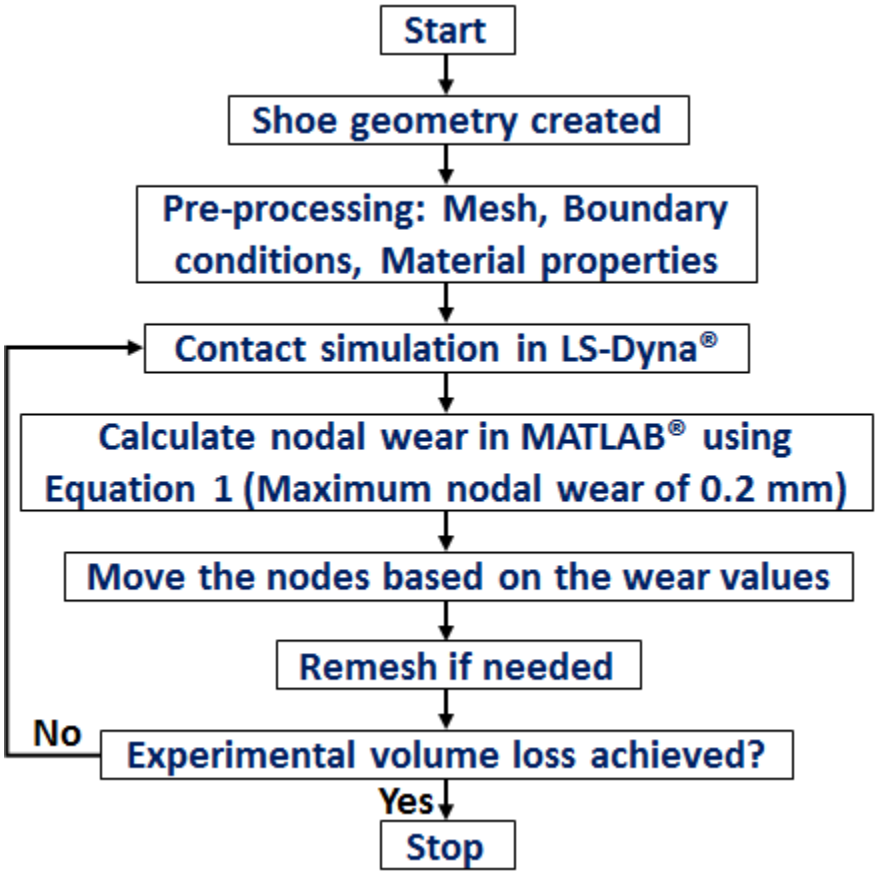

Figure 14. Flowchart of the iterative scheme for modeling wear.

$$\Delta h_i = kP_i s \qquad \text{Eq. (5)}$$

This study was focused on developing a model that predict the locations of the wear as opposed to the overall wear rate. Therefore, the product of the wear constant and sliding distance (*ks* in Eq. (5)), was set for each iteration such that the maximum nodal wear depth (Δh_{imax}) in each iteration was 0.2 mm. This is equivalent to varying the amount of sliding distance in each wear iteration to achieve maximum local wear depth of 0.2 mm. Our preliminary modeling efforts, similar to the observations of Mukras *et al.* [88], determined that limiting the maximum nodal wear in each iteration was needed to achieve stability and convergence in wear progression simulations. Preliminary models also demonstrated that choosing values of less than 0.2 mm for the maximum nodal wear in each iteration, would result in unnecessarily long computational times, given the severity of wear that was expected to occur in shoes (Section E.4.1.2.). A custom script (MATLAB®, MathWorks, Natick, Massachusetts, USA) was developed that calculated wear depths across the contact nodes based upon nodal pressures at each iteration, and moved the contact nodes in the finite element software. The amount of wear during the simulation and subsequent deformations that occurred necessitated the use of global remeshing techniques to discretize the shoe geometry throughout the wear modeling cycles [87]. Meshing software (ANSYS®, ANSYS Inc., Canonsburg, Pennsylvania, USA) was used to perform the global-geometry remeshing when errors in the next wear iteration resulted due to a severely deformed finite element mesh.

The computational models of wear included heel geometries of five shoes that were also examined experimentally (Section E.4.1.2.). Computer Aided Design (CAD) models of the shoes were created in ANSYS DesignModeler® (ANSYS Inc., Canonsburg, Pennsylvania, USA), based on the measurements taken from the shoe outsoles. For shoes with a textured tread, texturing was not included in the CAD models as the preliminary experimental results (Section E.4.1.2.) revealed that texturing quickly wore off. Shoes were modeled as linear elastic for computational efficiency [86]. Linear-elastic material properties for the shoes were obtained using hardness readings of the shoes [86] (Section E.4.1.2.) based on methods described by Giacomin and Mix and Ghent [89, 90], Eq. (6).

In Eq. (6), *S* represents hardness (shore A durometer) and *E* represents the elastic modulus (MPa) of the shoe. Shoe tread was modeled as a nearly incompressible material with a Poisson's ratio of 0.499 [91, 92].

$$\mathrm{E} = \frac{0.0981(56+7.6233S)}{0.1375(254-2.54S)} \qquad \text{Eq. (6)}$$

Finite element models were used to simulate contact between the shoe and a smooth, rigid counter-surface. Key parameters were consistent with the experimental wear protocol, including: shoe-floor angles of 17, 7, and 2 degrees, a sliding velocity of 9.65 m/s, a normal force of 40 N, and a lateral tilt angle that was consistent with the experimental wear protocol (Section E.4.1.2.). Normal force in the finite element models was controlled using the vertical displacement boundary conditions that were applied to nodes at the top surface of the shoe outsole models [86]. The shoe was pressed against the counter-surface until the desired normal force was achieved and then the horizontal sliding velocity boundary condition was applied. Other displacements and rotations of the nodes at the top surface of the shoes were constrained. Shoe models were meshed using tetrahedral elements that are recommended for simulating rubber-like (nearly-incompressible) materials with complex geometries [93]. This type of element overcomes the issue of volumetric locking by defining nodal volumes and representing the nodal pressures in terms of those volumes [94]. Mesh size for the shoes were determined based on the following criteria: (1) Mesh size was reduced until the first occurrence where the difference between the predicted normal force of one model and a subsequent model (with smaller mesh sizes) was less than 4 N. (2) All of the shoe elements had element qualities (the ratio of volume of the element to the edge length [95]) that were greater than 0.1 in the baseline iteration. (3) Mesh refinement was applied only to the elements in the contact region of the shoe to reduce the computational cost without losing accuracy in those regions. (4) The aforementioned mesh settings were used anytime that global remeshing was performed.

F.4.1.2.Experimental shoe wear protocol

Five shoes were worn using a custom-developed accelerated wear apparatus. This apparatus utilized a sliding abrasion belt [38] to wear shoes in angles that approximated the shoe angles of the gait cycle. For each wear trial, the shoe was worn for 193 m (equal to 20 seconds on the abrasion belt) at three different shoe angles of 17, 7, and 2 degrees in the sagittal plane. Sliding speed of 9.65 m/s and a normal load of 40 N were consistent with the modeling conditions (Section E.4.1.1.). These wear angles mimic the variation in shoe-floor angles during gait cycle [84, 96]. The abrasion techniques are similar to previous methods for abrasively removing shoe tread and also measuring abrasion resistance for footwear [38, 97].

After each wear trial, volume loss of the shoes was measured and imprints of the shoe treads were generated using a silicone rubber mold [38]. The cavities in these molds were then filled with water and the mass of the water was weighed to deduce the volume of the water in the tread cavities, and thus the volume loss between the trials. Between wear trials, experimental measurements were made to determine the traction performance of the shoe and record fluid pressures at the shoe-floor interface during shoe sliding experiments [22, 38, 51, 66]. Experimental wear trials were stopped when it was determined that the shoe tread was no longer functional at draining out the fluid contaminant in the shoe-floor interface during lubricated shoe sliding experiments. Increases in the interfacial fluid pressure measurements were used as an indicator that the shoe lacked functional drainage [22, 38, 51, 66]. The method for making this determination is described in more detail in our other publications [38, 51]. The wear coefficient (*k* in Eq. (5)) was defined by the total wear volume (numerator), the sliding distance (denominator), and the normal force (denominator) for each shoe. Material properties were also collected as an input to the finite element models. Shore A hardness values of the shoes [98] were measured using a durometer (Intercomp®, Minneapolis, Minnesota, USA) and durometer readings were used to calculate linear-elastic Young's moduli of the shoe materials [86, 90] for computational models (Section E.4.1.1.). Durometer readings were conducted on nine different portions of the heel for each shoe and the average value was used. Table 5 summarizes the elastic moduli values that were derived from the hardness readings.

Table 5. Elastic modulus of the shoes.

Shoe	S1	S2	S3	S4	S5
Elastic Modulus (MPa)	7.50	9.36	9.27	8.20	11.01

F.4.1.3.Data and statistical analysis

A statistical analysis was performed to evaluate the prediction quality of the model to identify the location of wear. For this analysis, tread blocks on the physical shoe and modeled shoe were ranked according to the order that they became completely worn. Agreement between the model and experiments in predicting regional geometrical wear was then assessed using Spearman's rank-order correlation coefficient (r_s), which quantified how successfully the model predicted the order of tread wear observed in the experiment (Figure 15). The worn region area was approximated by calculating the product of the largest length without tread in the anteroposterior (major axis) and mediolateral (minor axis) directions [38]. Iterations were continued for the model until the total volume loss reached the experimental volume loss observed for each shoe. For each experimental wear trial, the modeling iteration that had the closest volume loss value to that experimental wear trial was picked as that trial's matched modeling counterpart. Afterwards, the volume loss at each modeling iteration was used along with the Archard's wear coefficient (See Section E.4.1.2.) to calculate sliding distance for each modeling iteration. The area of the worn region as a function of sliding distance in experiments and models were then compared. This analysis assessed the accuracy of the model in predicting the worn region area since this area has been demonstrated to be a predictor of the change in shoe-floor coefficient of friction due to wear [38]. Furthermore, a linear regression model quantified the correlation between the area of worn region in the model and experiment. Goodness of fit was assessed using the Pearson correlation coefficient (r) value for each shoe.

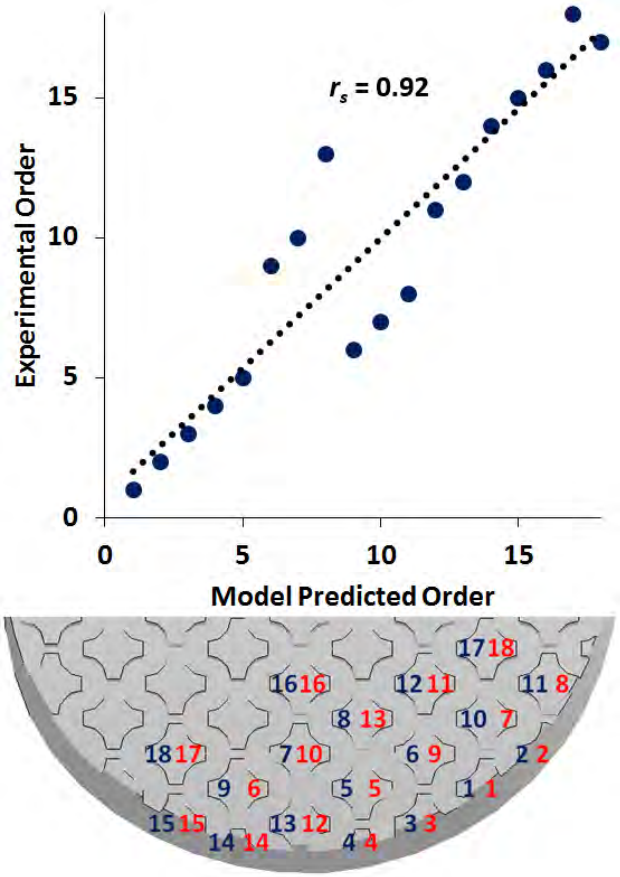

Figure 15. Bottom: representative plot demonstrating the order that shoe (S4) tread wore down in the model (blue) and the experiment (red). Top: the resulting model and experimental wear order and correlation for this shoe.

F.4.2. Results

Table 6 summarizes the distance that each shoe was worn on the experimental wear apparatus, the resulting volume loss, the experimental wear constant, the total number of elements and nodes, and the number of modeling iterations it took to simulate the experimentally-measured volume loss for each shoe. Shoes experienced extensive wear in both the experiments and the models and similar regions wore in the models and experiments (Figure 16). For S1, a majority of the wear occurred in the posterior section of the shoe in both the model and the experiment. For S2, a majority of the wear occurred in the lateral and posterior region of the shoe in the model and in the lateral and medial portion of the shoe in the experiment. For S3, wear in the posterior region of the outsole was observed in both the model and the experiment. For S4, wear was dominant in the posterior and medial portions of the shoe in both the model and the experiment. For S5, the model experienced wear mainly in the posterior region of the shoe and the experimental wear trials resulted in wear of the shoe in the medial region. The progression of wear is demonstrated in videos of the shoe wear progression in shoe models (Supplementary material: S1-S5 (The numbers below the shoes correspond to the distance in kilometers)).

Table 6. Distance on the experimental wear apparatus, the resulting volume loss, wear constant, total number of elements, nodes, and modeling iterations for the shoes.

Shoe	S1	S2	S3	S4	S5
Distance on wear apparatus (km)	9.8	11.6	13.3	8.7	20.3
Total volume loss (mm^3)	3345	7046	3460	3593	3762
k **(mm^3/Nm)**	0.0085	0.0138	0.0065	0.0103	0.0046
Total number of elements (at baseline)	102539	43463	23429	75993	54066
Total number of nodes (at baseline)	24485	12979	5970	16608	12283
Total number of modeling iterations	47	130	30	35	49

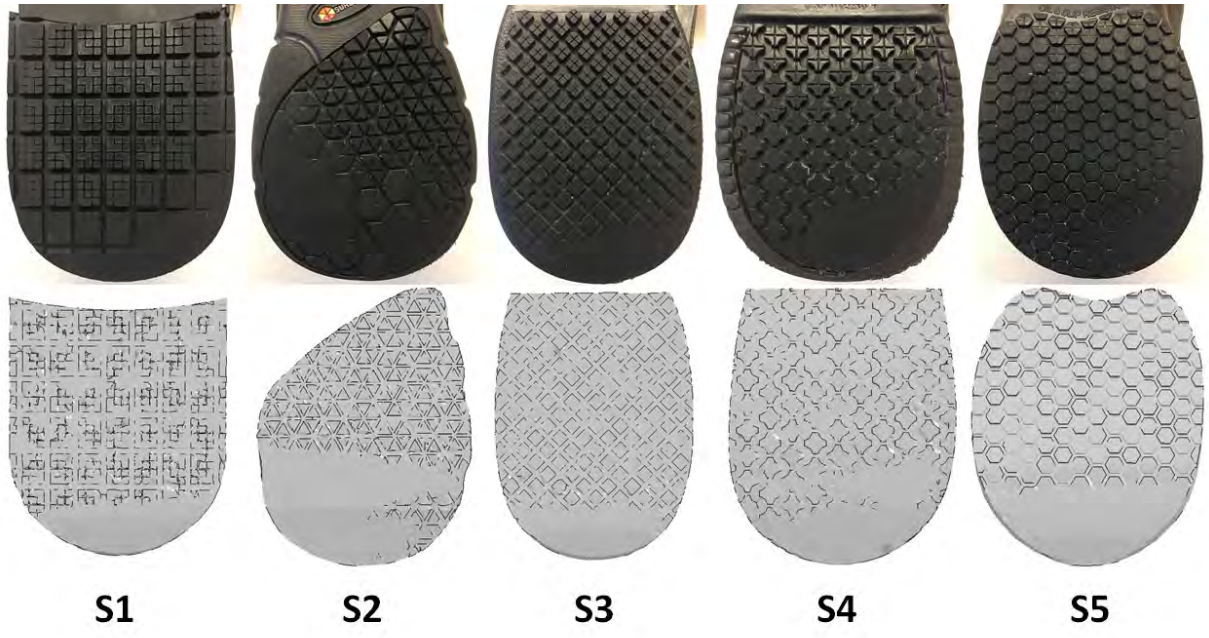

Figure 16. Pictures of the shoes at the end of the experimental wear protocol (top) and final models of wear of the shoes (bottom).

Based on the rank correlation analysis of the order that tread blocks became fully worn, a strong, positive, and monotonic correlation existed between the wear model predictions and the accelerated wear experiment (Table 7, $p < 0.005$ for all of the shoes.). The strongest and weakest rank order correlations were observed in S1 ($r_s = 0.98$) and S5 ($r_s = 0.74$), respectively. The percentage of the tread blocks that wore down in both the model and experiment was greater than the percentage of

the tread blocks that wore down only in the model for all shoes except S5, and greater than the percentage of the tread blocks that wore down only in the experiments for all shoes (Figure 17). For S1, a complete agreement in the number of worn tread blocks between the model prediction and experiment results was observed.

Table 7. Results of the statistical analysis on the order of tread wear.

Shoe	**S1**	**S2**	**S3**	**S4**	**S5**
Number of tread blocks	8	10	17	18	15
Spearman's Rho (r_s)	0.98	0.87	0.94	0.92	0.74
***t*-score**	12.06	4.99	10.67	9.39	3.97
(*p*-value)	(0.000)	(0.001)	(0.000)	(0.000)	(0.002)

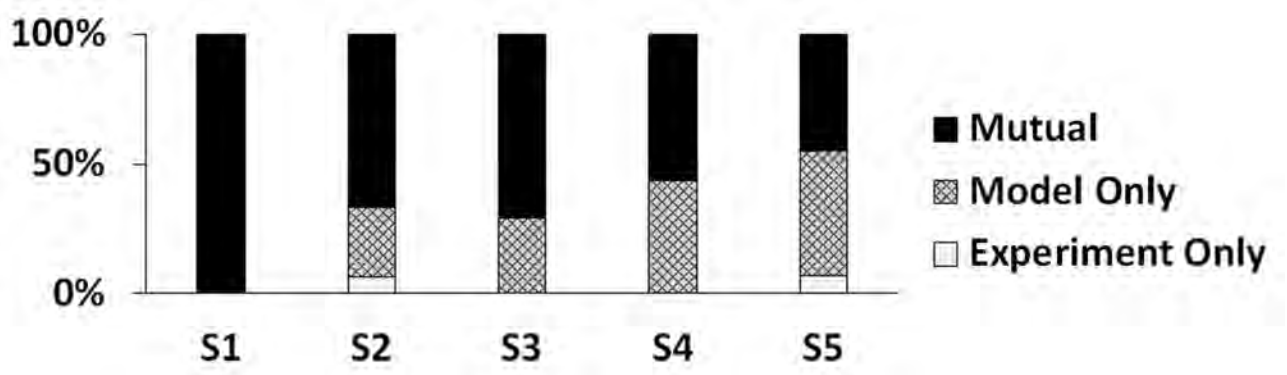

Figure 17. Percentage of the tread blocks that wore down in both models and experiments, only in the model, and only in the experiment

The size of the worn region area observed in the experiments was somewhat predicted by the model (Figure 18). For S1, the model predictions of the worn region area were of similar magnitudes to the experimentally-observed worn region areas (*r=0.76* and with a slope of 0.97). For S2 and S3, the model under-predicted the experimentally-observed worn region areas (*r=0.90* and *0.93* and with slopes of 0.47 and 0.34, respectively). For S4, the model over-predicted the experimentally-observed worn region areas (*r=0.89* and a slope of 1.30). Simulations of S5 appeared not to be particularly successful in predicting the worn region area, as they over predicted the model worn region areas by a factor of 3.4 (*r=0.72*).

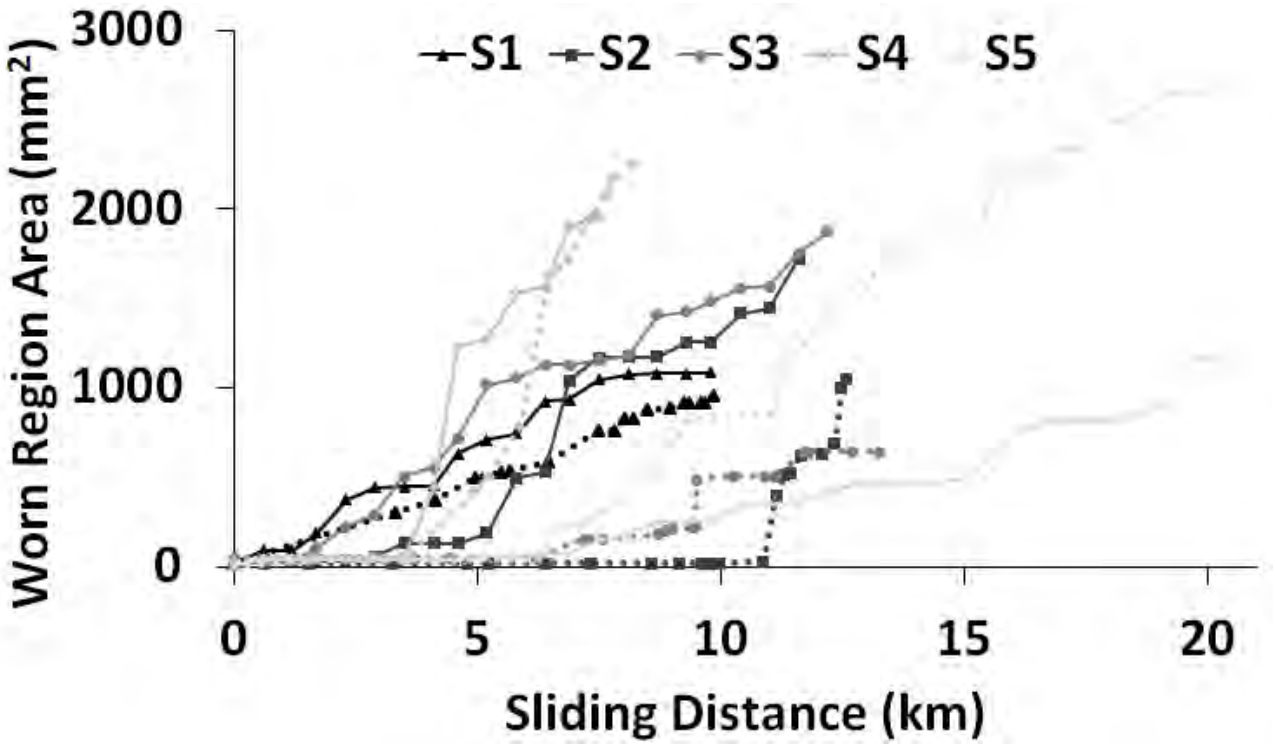

Figure 18. Rectangular worn region areas as a function of sliding distance. Solid and dashed lines demonstrate the experimentally-observed and model worn region areas, respectively.

F.4.3. Discussion

The computational model developed in this paper demonstrates the feasibility of using Archard's equation and finite element analysis in predicting wear progression in footwear. Qualitative and quantitative agreement were observed between the outcomes of the computational model and the results of the experimental wear testing. The findings of this study demonstrate the potential for applying the described modeling framework for shoe wear given its preliminary success in predicting experimentally-observed wear of the outsoles. This modeling approach may offer potential for modeling wear in complex geometries with elastomeric materials.

The results of this study are consistent with the earlier qualitative experimental studies on shoe wear that demonstrate development of worn region areas [23, 54] at the regions of the shoe with higher contact pressures [23, 38, 99]. Findings of the present study are also in agreement with the previously developed computational models of wear in other applications such as disc brakes [100], seals [101], and pin-on-disk wear experiments [102] that use Archard's equation for describing the relationship between wear depth and interfacial pressure. Specifically, the present findings demonstrate that wear of the shoe material can be simulated using Archard's equation, global remeshing, and finite element analysis, similar to the procedures that were developed based on elastomers and metals [87, 100-103]. The Archard's wear coefficients that were calculated for shoes using the experimental volume loss, normal force and sliding distance were within the range of 0.004-0.014 $mm^3/(Nm)$. These values are in line with values available in the literature for the abrasive wear of elastomers on rough surfaces. However, the present values (4×10^{-3} to 1.4×10^{-2} $mm^3/(Nm)$) demonstrate a range that is two orders of magnitude less than prior measurements (5×10^{-4} to 1×10^{-1} $mm^3/(Nm)$) [104-106]. This narrow range is likely to due to the smaller set of test conditions considered in this study, while previous studies considered a variety of elastomers against a variety of rough surfaces. This narrower range may also indicate that elastomer materials that are commonly used in footwear have more consistent durability than the full range of possible elastomers. Once the Archard's wear coefficient of these shoes has been quantified (Table 6), then the sliding distances were extracted from the model data (which previously only enabled the determination of the combined parameter *ks*). With this quantitative measure of the sliding distance, the worn region area across two shoes at a similar point in their life can be compared.

For example, tread design S4 was predicted to have a larger worn area than the others at approximately 7 kilometers. Therefore, these findings demonstrate a strong potential application of the proposed model: the predictive comparison of the worn tread region across different tread designs.

While the outcomes of the model for some shoes were well-described by the model, other shoes were less accurately predicted. These discrepancies included the exact shape and area of the worn region, and the precise order of shoe tread wear in some of the shoes. One possible reason is the use of Archard's equation and its assumption of a linear relationship between the contact pressure and wear depth. While Archard's equation is widely used and has a large body of empirical support, some previous studies have suggested a phenomenological relationship based on power-law equations [107, 108]. Assuming the power-law form for the equation between contact pressure and wear depth would result in a higher difference between the wear depth of the regions with higher and lower contact pressures and would lead to a less uniform wear region in models. The phenomenon of highly localized wear is observed in the wear experiments, but is absent in the model. In our experiments (Figure 16), S1 had a small local wear region in the posterior portion of the shoe, S2 demonstrated local wear regions in the lateral and posteromedial portions of the shoe, S3 had a local wear region in the posterior portion of the shoe, S4 demonstrated a local wear region in the posterolateral region of the shoe, and S5 was locally worn in the medial region of the shoe in the experiments. However, the wear models demonstrated a more uniform wear region (i.e. wear region distributed over a larger portion of the shoe) in comparison to their experimental pairs. Another possible explanation for the differences that were observed between the models and experiments is the method used to define the orientation of the shoe in the model. For the current version of the model, sagittal and frontal plane angles were matched to the experiments based on goniometer measurements of the shoe tilt against the abrasive surface. However, changes in center of pressure can occur with minimal changes in the frontal plane angle [45, 109]. For future versions of this wear model, this approach could be improved by matching the two-dimensional location of the center of pressure [110] to achieve more realistic contact regions. Modifying these biomechanical parameters also offers an opportunity to assess how different gait patterns influence wear patterns. A final possible reason for differences between experimental and model results arises from the discrete nature of wear in the modeling. For example, if one of the tread blocks in the experiment gets worn while the matching tread block in the model is not worn yet, there will be a mismatch between the worn region areas in the model and experiment for a few trials until the matching tread block in the model gets worn down. This mismatch will further intensify in wear distances as this phenomenon is likely to occur multiple times.

A computational model can be particularly useful in guiding the design of durable, slip-resistant shoes by estimating the impact of design modifications (e.g., increasing tread depth in regions that become worn) on the durability of shoes. Furthermore, tread could be designed to spread the contact pressures and wear across a larger region which would increase the coefficient of friction [86, 111, 112] and durability. The computational model for wear can also be used to describe the "running-in" phenomenon [87, 100] that leads to an increase of coefficient of friction for slightly worn shoes [38, 113]. A post-hoc revealed that slightly worn shoes had an increase in contact area relative to the unworn condition both in the models (Figure 19) and experiments [38]. This increase in contact area led to a more distributed contact pressure (Figure 19) over the surface of the shoe [86]. As predicted in previous models [86, 112] and experiments [63], increased contact area and decreased contact pressures led to increased hysteresis friction. This explains the initial increase in shoe-floor coefficient of friction that is common in the early stages of wear [38].

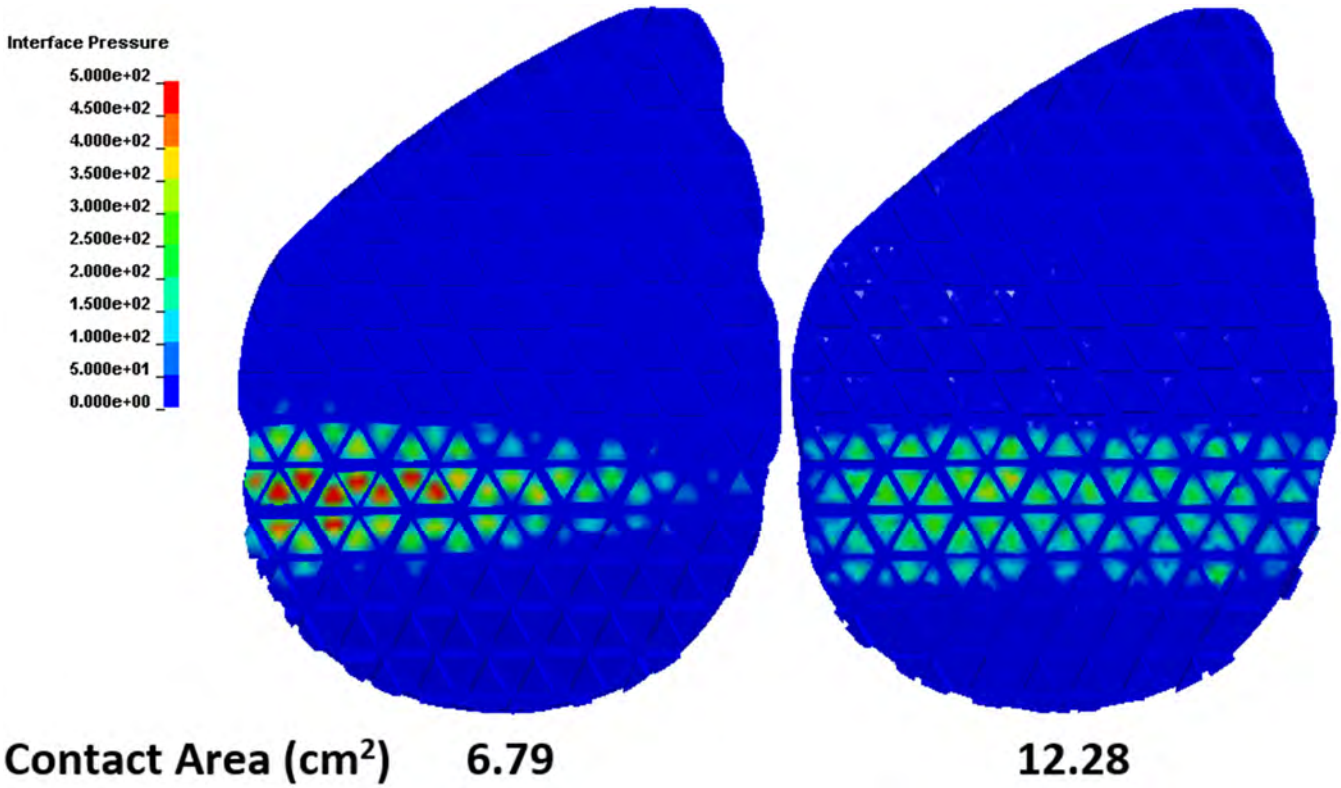

Figure 19. Under-shoe contact pressure in kiloPascals (S2) and contact areas of the shoe at 250 N and 7° shoe angle at the baseline (Left) and after 5.2 kilometers of simulated wear (Right). Total contact area of the shoe in each case is reported below the shoe.

The computational model for wear demonstrates an important first step toward developing more sophisticated models of shoe wear. The current version of the model can be used to predict the spatial distribution and rates of tread wear across the shoe. Future versions of this wear model should advance this framework by using wear coefficients (*k*) which can be obtained *a priori* using shoe material wear testing [38]. Future versions should also aim to include whole-shoe geometry to simulate changes to the forefoot and subject-specific boundary conditions (i.e. linear and angular kinematics and kinetics) based on each person's gait parameters. This inclusion and individualization based on one's gait profile will allow predictions to quantify a shoe's duration of usage until the shoe becomes too worn and the risk of a slip and fall increases [28, 51]. Once these models become available, more reliable predictions on shoe wear and durable slip-resistant designs will become feasible. This result will promote the long-term goal of reducing slip and fall injuries.

F.5. Study #5: Predicting Hydrodynamic Conditions under Worn Shoes using the Tapered-Wedge Solution of Reynolds Equation [114] (Aim 3, Key Finding 7)

F.5.1. Methods

This study represents a post-hoc analysis of data that has been previously reported [61, 115]. Specifically, this study applies the tapered wedge solution of Reynolds equation (modeling) to relate the measured size of the worn region to the measured under-shoe fluid load support (experimental). An iterative experimental procedure was performed that alternated between: 1) abrading of shoe outsoles; and 2) testing coefficient of friction, under-shoe fluid pressures, and tread volume loss (Figure 1; adapted from [61]). Previously, we have reported changes in friction performance and under-shoe fluid hydrodynamics during wear progression [61]. Furthermore, we have reported a finite element model that predicted changes in tread geometry due to wear [115]. Given these previous reports, the methodological details are only briefly described.

F.5.1.1.Abrasion Protocol

Five shoes labeled as slip-resistant shoes were used in this study (Figure 20; adapted from [61]). The right shoe of each pair was mechanically abraded at three different shoe orientations (17°, 7°, 2°). The angles were chosen to reflect the orientation of the shoe during walking from heel strike to flat foot [41]. One of the five shoes was excluded from this analysis since two distinct worn regions were observed in the middle of the heel compared to a single worn region at the rear of the heel that was observed for the other shoes. To wear the shoes, abrasive paper (180µm diameter particles) was slid across each shoe at 9.65 m/s for 20 seconds at each of the three angles. The normal force was ~40 N. Abrasive grease was used to reduce heat buildup and was cleaned from the shoes before friction testing. The shoes were progressively worn using this protocol. The number of wear iterations ranged from 13 to 35.

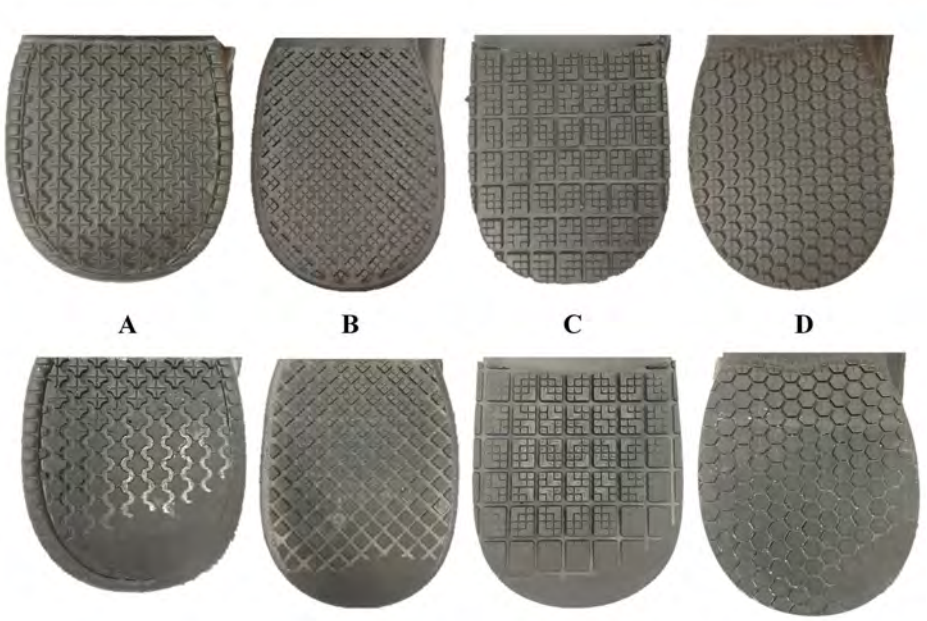

Figure 20. The heel of the four shoes mechanically abraded at baseline (top) and after the last wear cycle (bottom).

F.5.1.2.Mechanical Shoe Testing Protocol:

Prior to wear and after each wear cycle, the shoes were slid across a contaminated floor surface that simulated a slipping action using a robotic device as seen in a previous study [61]. The robotic slip tester measured ground reaction forces and under-shoe fluid pressures. The fluid pressure sensors each had an inlet diameter of 3.2 mm and were recessed beneath the floor surface.

The shoes, attached to a shoe last, were slid across a vinyl composite tile (Armstrong, 51804; R_q = 3.13±0.42 µm) covered with a diluted glycerol solution (90% glycerol, 10% water by volume; 219 cP). Sliding conditions that are valid predictors of slipping and consistent with the shoe at the onset of slipping were used (shoe angle of 17° [45, 47], sliding speed of 0.3 m/s [45, 47, 48], and normal force of 250 N [49, 50]). Twenty fluid pressure scans were collected at 5 mm intervals to estimate under-shoe fluid pressures.

At baseline and after each wear cycle, the heel tread geometry was recorded by creating a silicone rubber mold of the shoe heel as reported in a previous study [61]. Using this mold, the size of the worn region was measured for each shoe heel outsole at baseline and after each wear cycle. This metric was defined as the product of the longest and widest continuous area without tread channels. The length (*l*) was measured along the long axis of the foot (anterior to posterior) and the width (*b*) was measured perpendicular to the long axis (medial to lateral).

F.5.2. Theory & Calculations

F.5.2.1.Data Analysis:

The average friction coefficient across the five trials per wear cycle was calculated from the ground reaction forces. Fluid pressure sensor data that were five standard deviations above the baseline levels were included in the analysis [28, 61]. Numerical integration was performed to calculate the fluid force (i.e., load supported by the fluid) based on the fluid pressure at the ith frame (p_i), perpendicular distance between scans (Δx = 5 mm), the sliding velocity (u = 0.3 m/s), and the time between each frame (Δt = 2 ms), Eq. (7) [51]. Fluid force across the twenty scans (4 scans per trial * 5 trials) was summed, Eq. (7).

F.5.2.2.Fluid Film Calculations:

The tapered-wedge solution by Fuller, which was later applied to shoes by Proctor and Coleman, was used to apply hydrodynamic theory to a shoe-floor contaminant interface [116, 117]. In the solution, the minimum film thickness, h_0, occurs at the rear edge of the wedge [116]. As such, the predicted film thickness (PFT) applies to the rear edge of the worn heel. The predicted film thickness (PFT) was calculated as a function of dynamic viscosity ($\eta = 214\ cP$), the sliding speed ($v = 0.3\frac{m}{s}$), length of the wedge (*l*), width of the wedge (*b*), normal force applied to the wedge ($F = 250\ N$), and K_p, a factor calculated from the incline of the wedge [116], Eq. (8). An average K_p value of 0.025 was used to simplify the calculations [116].

$$h_0 = \sqrt{\frac{6\eta v l^2 b}{F} * K_p}$$ Eq. (8)

This equation was adapted to allow for side leakage since the shoes contained no border to prevent leakage. Thus, the factor, γ, was added as a correction factor related to the ratio of the width over the length of the wedge [116]. The factor, γ, is dependent on the geometry of the region of the shoe without tread and was calculated for each shoe and wear cycle. Therefore, γ, and thus PFT values were calculated separately for each wear cycle, *j*, Eq. (9).

$$PFT_j = h_{0_j} = \sqrt{\frac{6\eta v {l_j}^2 b_j \gamma_j K_p}{F}}$$ Eq. (9)

F.5.2.3.Statistical Analysis:

To quantify the relationship between the PFT and the fluid force, ANOVA methods were used. Specifically, the dependent variable was the experimentally-measured fluid force and the independent variables were shoe, PFT, and their interaction. To normalize residuals of the fluid force data and satisfy the assumptions of the statistical model, a square root transformation was used. When the size of the worn region did not change between wear cycles, only the first data point was used until the worn region increased.

F.5.3. Results

In the experiment, the fluid force values ranged from 0 to 97.4 N and the friction coefficient ranged from 0.057 to 0.41. Applying the size of the worn region to the tapered-wedge solution model, the PFT values ranged from 0.6 to 42 μm with an average film thickness of 18.7±11.6 μm. An increase in fluid force was associated with an increase in PFT (Figure 21; $F_{1,71}$ = 462.1, $p < .001$, R^2=.89). Fluid force was influenced by shoe type ($F_{3,71}$ = 45.7, $p < .001$). The fluid force was not affected by the interaction of the PFT and the shoe type ($F_{3,71}$ = 2.2, $p = .098$).

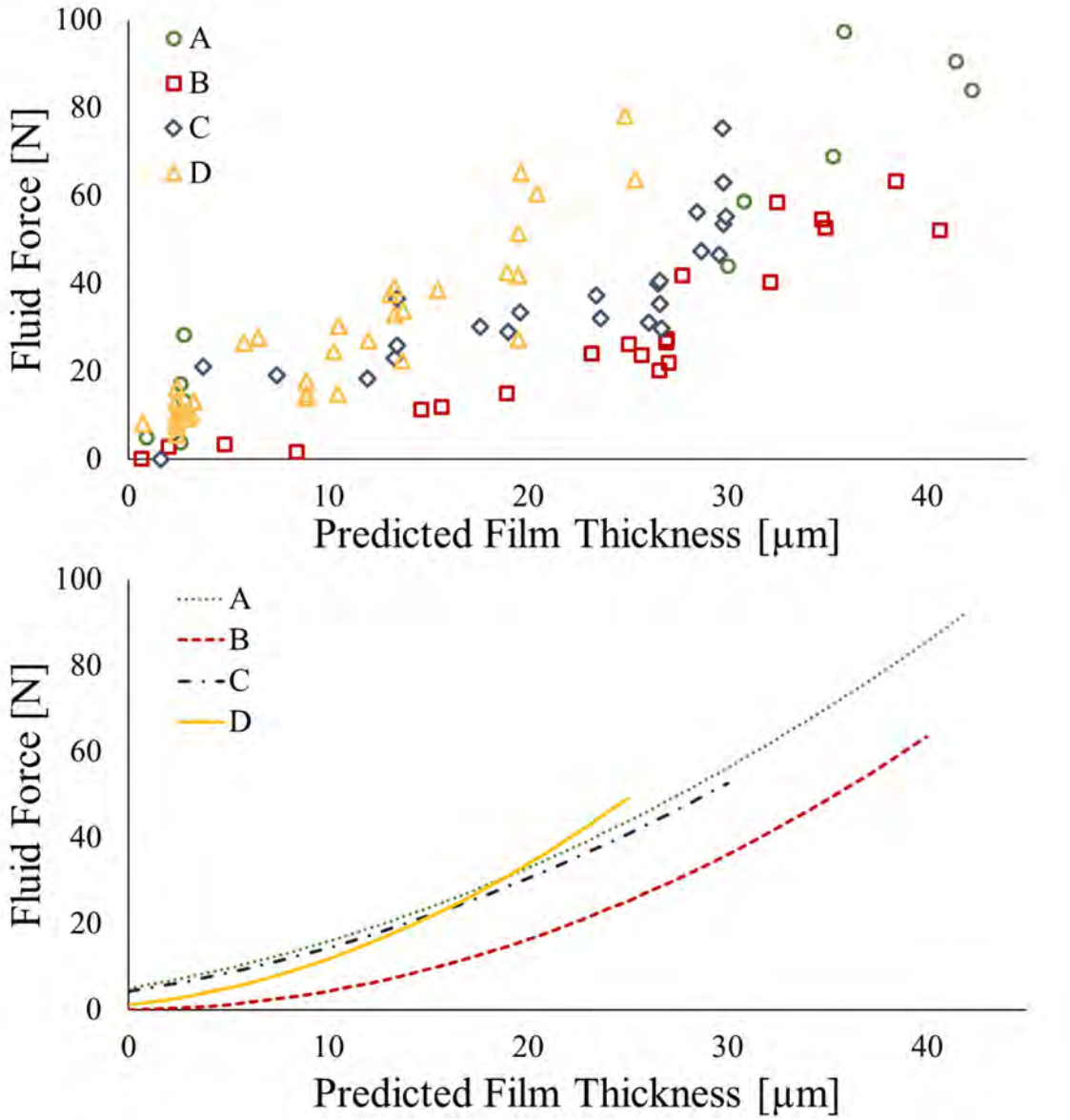

Figure 21. (Top) Experimentally-measured fluid force with respect to the PFT for the shoes A-D. (Bottom) Regression lines for fluid force and PFT relationship for each shoe based on statistical analysis.

F.5.4. Discussion

In this study, the tapered-wedge model of film thickness was predictive of the experimentally-measured fluid force. An increase in fluid force coincided with an increase in PFT, which was based on size of the worn region and testing parameters. This relationship was seen regardless of shoe tread type for all SR shoes. As such, calculating film thickness based on geometric measures and fluid viscosity may be feasible for predicting the fluid dispersion capabilities of shoe tread.

The PFT values reasonably predicted the lubrication regime of the shoe-floor-liquid system which has been shown to be sensitive to shoe wear [61]. The lubrication regime is often described using the lambda ratio (λ) which is the minimum film thickness normalized to the composite RMS surface roughness (R_q), Eq. (10) [118]. When $\lambda < 1$, the surfaces are acting in the boundary lubrication regime where the dominating asperities are in contact and friction is at a peak. As lambda increases, the interaction operates in the mixed lubrication regime ($1 < \lambda < 5$), and then moves into the hydrodynamic lubrication regime ($\lambda > 5$) or the elasto-hydrodynamic lubrication regime ($3 < \lambda < 10$). In this study, the fluid force started to increase when $\lambda \approx 1$ ($h_{\lambda=1}$=3.5±0.2). Thus, this simple model yields predictors in line with the experimentally observed transition from boundary to mixed lubrication. The friction coefficient decreased as the shoes became more worn. The increase in wear led to

an increase in the lambda ratio and PFT values, implying a shift from the boundary lubrication regime to the mixed lubrication. (Figure 22).

$$\lambda = \frac{h_0}{\sqrt{{Rq_{floor}}^2 + {Rq_{shoe}}^2}} \quad \text{Eq. (10)}$$

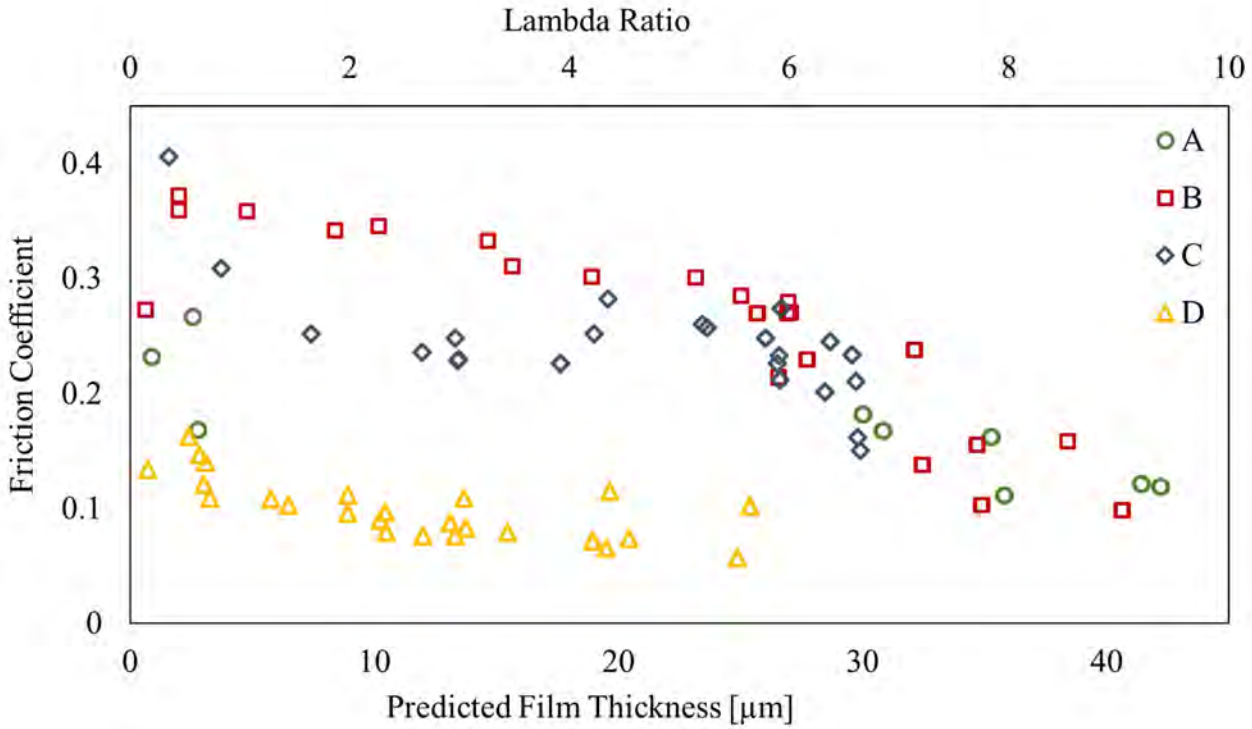

Figure 22. The friction coefficient with respect to the lambda ratio, λ (top axis) and PFT (bottom axis) for each shoe. The average roughness across shoe outsoles was used to determine the lambda ratio.

Simple modeling approaches may be useful for predicting under-shoe hydrodynamics even when more sophisticated approaches are available. Previous models have explored fluid dynamics and wear using sophisticated models. For example, Beschorner, et al. developed a mixed-lubrication model using a pin-on-disk apparatus based on Hertzian contact mechanics and Reynolds equation for understanding how shoe-floor friction changes with varying speed and shoe material changes [55]. Moghaddam et al., demonstrated the use of finite element analysis in modeling shoe wear progression [115]. These previous modeling efforts required iterative methods and complex solution techniques (finite difference method and finite element modeling, respectively) that might be inaccessible to non-engineering users. However, the method presented by Proctor and Coleman which is also utilized in the present study uses simpler methods to predict under-shoe hydrodynamic effects based on a reasonably simple equation (Eq. 8) and a few simple geometric measurements of the tread's worn region [117]. Importantly, this model was valid in its predictions despite its simplicity. The practicality and simplicity of the model presented in this study may enable it to be employed by a wide audience.

This solution can be used as a pragmatic tool for determining slip risk based on shoe geometry. Interestingly, the prediction of fluid force via film thickness (R^2=0.66) in this study was stronger compared to the prediction of fluid force based on wear sliding distance (R^2=0.38) as seen in Figure 23 and further explored in a previous study [61]. Thus, the actual shoe geometry acts as a better predictor of shoe wear and subsequent slip risk compared to the amount of usage. Practically, this is an important consideration for determining slip risk thresholds for shoe wear. Previous studies have focused primarily on time of wear as a metric for replacing shoe wear [54]. However, the shoe outsole geometry, specifically the size of the worn region, may be a better indicator of under-shoe hydrodynamics and thus, slip risk, as supported by this study and a previous study [61].

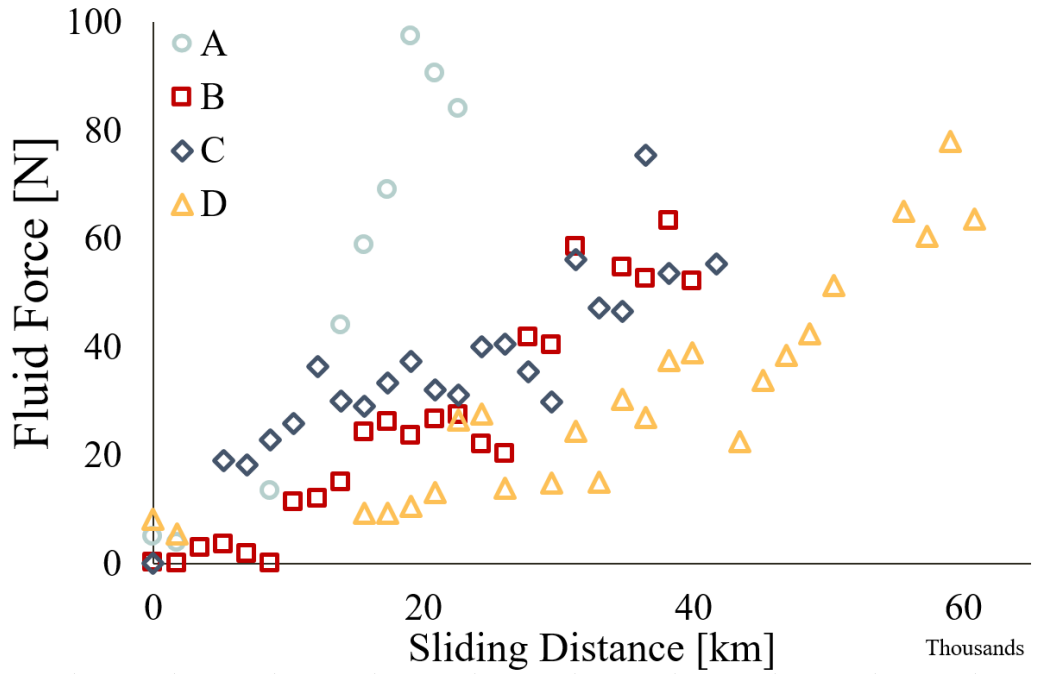

Figure 23. Fluid force with respect to the wear sliding distance of the simulated wear.

Certain study limitations and future directions should be noted. Only one flooring, and contaminant are utilized. Previous research has shown that under-shoe fluid pressures are sensitive to these metrics [71, 119, 120]. Thus, futures studies may consider expanding upon the work in this study to contaminants with varying material parameters (viscosity, shoe materials) that encompass an array of materials used in industrial settings. Validating this model with naturally-worn shoes and for human slips would increase confidence in its relevance to walking and slipping. Furthermore, comparing the model predictions to experimentally-measured film thickness values (e.g., using ultrasound methods [121]) may provide additional detail regarding the ability of this model to assess shoe-floor hydrodynamic conditions. Thus, important opportunities exist to further our understanding on how to apply the tapered wedge model to worn shoes.

F.5.5. Conclusion

Determining the influence of shoe tread wear on slip risk is a key factor in the design of safe and durable shoe tread for the workplace. The tapered wedge solution is a good start for understanding the relationship between wear and under-shoe hydrodynamics. Furthermore, this model may be useful for determining wear thresholds for particular shoe, floor, and liquid material properties to reduce slipping events.

F.6. Study #6: Traction performance across the life of slip-resistant footwear: preliminary results from a longitudinal study (Aim 4, Key Finding 8) [75]

F.6.1. Methods

In the longitudinal study, each participant received slip-resistant shoes which were worn in the workplace every other month to allow for traction performance and size of the worn region data collection on the months when the shoes were not worn. The distance the shoes were worn was recorded using a pedometer. At baseline and after each month of wear, ACOF and under-shoe fluid drainage measurements were collected. To record the geometry of the tread, negative molds of the heel tread were created. This paper presents initial findings for data collected so far from this study.

F.6.1.1.Subjects & Shoes

Seven participants (1 female participant – age: 26 years; height: 175 cm; mass: 76.8 kg; shoe size: 7.5 US Men's Sizing – and 6 males – mean age: 45.8±12.3 years; mean height: 185.3±10.0 cm; mean mass: 100.9±8.3 kg; mean shoe size: 12.4±1.7 US Men's Sizing) wearing one of the shoe brands from a larger study were included. The other requirement for inclusion was a cumulative walking distance of more than 200 km. The included participants were employed in diverse settings including transportation, utilities, education, health services, and the hospitality industry sectors. Inclusion criteria included: regularly wearing treaded shoes in the workplace; working on their feet for at least four hours in a typical day; having a BMI less than 35; and having no history of musculoskeletal injury in the previous 2 years. The study was approved by the University of Pittsburgh Institutional Review Board and the participants provided informed consent prior to participation in the study.

Participants were provided with either boots (safeTstep ®, Dawson 160004) or shoes (safeTstep ®, Blast Bouffee 159961) depending on their occupational requirements. Both the boots and shoes had the same tread design (Figure 24). The shoe outsole material was rubber with a Shore A Hardness of 62. Each shoe was outfitted with a pedometer (MilestonePod, Milestone Sports, Columbia, MD), [122] to track the distance traveled in each shoe. Shoes were retired from the study when the under-shoe fluid force for either the left or right shoe was greater than 50 N (see Section E.6.1.4.), or when the outsole or upper (i.e., part of the shoe or boot above the sole) became too worn at the discretion of the participant.

Figure 24. Shoe tread pattern at the heel for all shoes in this study.

F.6.1.2.Mechanical Testing of Shoes

A robotic slip tester (Figure 25) was used to assess the traction performance of the shoes (see Hemler, Charbonneau, et al., 2019 for details). The device consisted of a force plate measuring shear and normal forces (BP400600-1K-Q2046, AMTI, Watertown, MA, 02472), an adjustable platform instrumented with fluid pressure sensors (Gems ® 3100R10PG08F002) aligned in the X-direction, and three electromagnetic motors. One motor controlled the vertical displacement (Z-direction), and the two horizontal motors controlled the horizontal displacement (Y-direction) and the foot angle (YZ plane). Four fluid pressure sensors were aligned in the X-direction, embedded beneath the floor, spaced 25 mm apart and had an inlet diameter of 3.2 mm. The device is similar to the Portable Slip Simulator device [44-46]. Additionally this device has the ability to independently control the foot angle and has been used in previous research for traction performance testing [61].

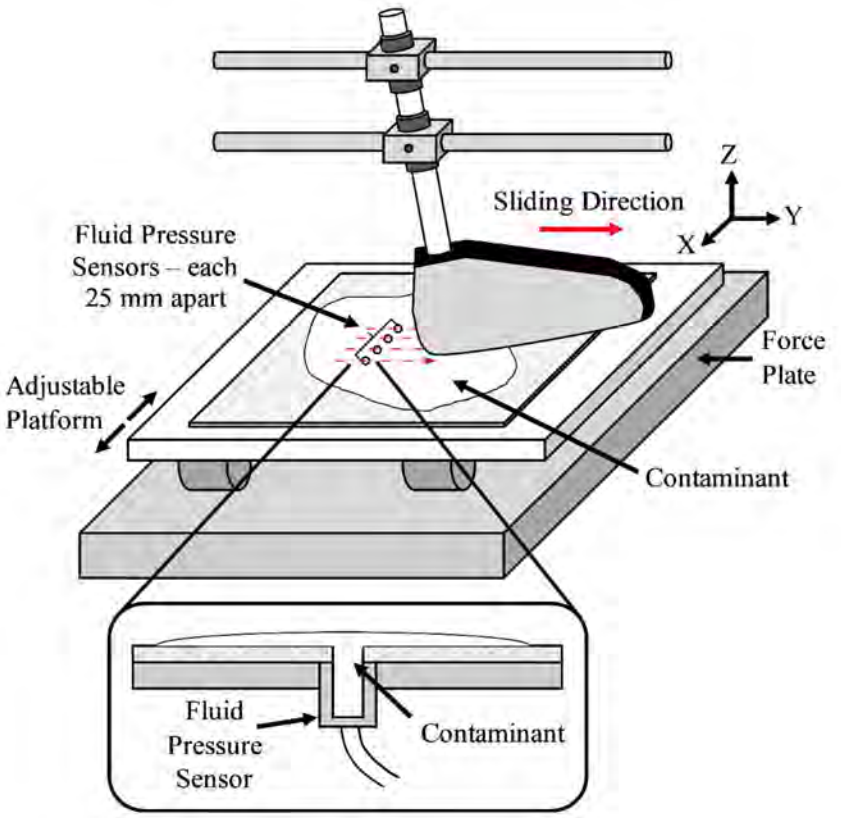

Figure 25. The robotic slip tester was used to slide the shoe across the contaminated surface along multiple parallel paths (adapted from Hemler, Charbonneau, et al., 2019).

Using the robotic slip tester, the right and left shoes of each pair were tested using a contaminated surface at baseline and after each month of wear. A vinyl composite tile flooring (Armstrong, 51804; with surface roughness characteristics: R_a = 2.19±0.29 µm, R_z = 16.13±2.74 µm, R_q = 3.13±0.42 µm; where R_a is the average asperity deviation from the mean line, R_z is the maximum asperity peak to valley distance, and R_q is the root mean square height of the profile) and a diluted glycerol contaminant solution (90% glycerol, 10% water by volume; 219 cP) were used. A sufficient amount of fluid was applied to the flooring to fully cover the floor asperities across the region that the shoe contacted. The contaminant was spread to cover the entire slipping area prior to each trial. To approximate the same conditions as a slipping incident, each shoe was slid at an angle of 17±1° [45, 47], speed of 0.3 m/s [45, 47, 48], and average normal force of 250 N ± 10 N [49, 50]. The platform was moved 5 mm in the positive X-direction between each trial for a total of 5 trials and 20 fluid pressure scans.

F.6.1.3.Worn region measurement

A mold of the heel tread was made at baseline and after each month of wear. The left and right heels were placed in a rectangular containment (92 mm x 76 mm x 28 mm) of silicone rubber compound (Smooth-On Inc.; Macungie, PA; Oomoo® 25) at an angle of 17° (Figure 26). The largest region of continuous wear was identified in each mold and the length along the long axis of the shoe and the width along the short axis of the shoe were measured. For baseline values and when no worn region had yet formed, the length and width of one tread block was recorded. The product of these two measurements comprised the size of the worn region on each shoe.

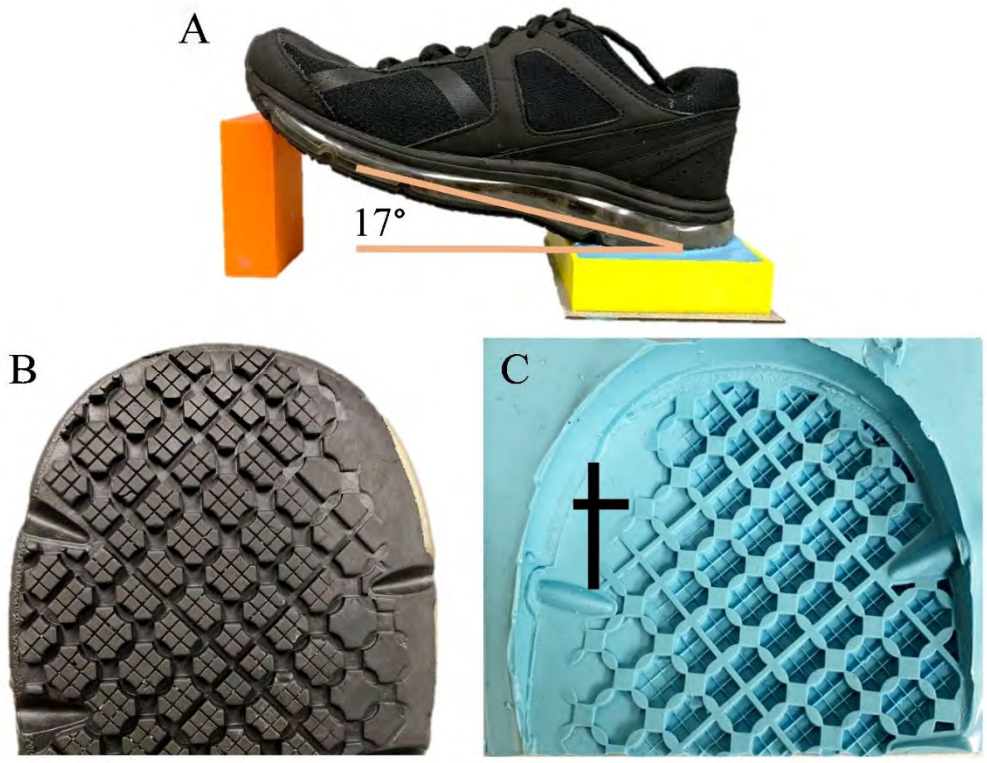

Figure 26. A) Molds of each shoe heel were created at a 17° angle to capture the B) shoe tread geometry. C) The length and the width of the largest continuous area without tread were measured at baseline and after each month of wear.

F.6.1.4.Data analysis

The ACOF was determined as the peak of the ratio of the resultant shear forces to the normal force, averaged across a 200 ms time period. This time period started when the normal force first reached 250 N. Fluid pressures that exceeded 10 kPa were included in the analysis. A numerical integration technique was used to determine the load supported by the fluid (hereafter, referred to as the fluid force) for each shoe [28, 61]. If either the right or left shoe reached a fluid force greater than 50 N, the pair of shoes was retired from the study as it was deemed unsafe for continued wear [61].

The aims of this study were to quantify traction performance in response to increased usage and growth of the size of the worn region. Thus, the ACOF and fluid force were the dependent variables. Predictor variables included the distance walked and size of the worn region. The analyses controlled for shoe side (left vs. right).

Repeated-measures ANOVA methods were used to analyze the effects of the predictor variables (size of worn region, distance walked) on the dependent variables (ACOF, fluid force). Specifically, two models were used to determine the response of ACOF and fluid force to the distance walked in the shoes (continuous). Two additional models were used to determine the response of ACOF and fluid force to the size of the worn region (continuous). Separate analyses were used for distance walked and the size of the worn region as predictor variables since these variables are correlated (Supplementary Materials). Participant was a random variable in these models. To normalize the residuals, a square transformation was applied to the ACOF data and a cube root transformation was applied to fluid force data prior to statistical analyses. To correct for a positive skew, a square root transformation was applied to the distance walked.

F.6.2. Results

A total of 35 subject-months of data are reported ranging from three to ten months per participant. The total distance walked ranged from 220 to 1255 km with an average ± standard deviation total distance of 231±262 km and a monthly average of 76±82 km. One pair of shoes was retired from the study due to the left shoe exceeding the 50 N fluid force safety threshold. Four pairs of shoes were retired due to significant wear to the footwear upper. Two participants are still enrolled in the study (S6 & S7). For all shoes, the worn region began on one shoe side (13 – lateral, 1 – medial) and a single wear patch grew with subsequent use.

The ACOF ranged from 0.081 to 0.212 (Figure 27) throughout the study and ACOF ranged from 0.134 to 0.207 at baseline. An increase in walking distance was associated with a decrease in ACOF ($F_{1,84}$=65.9, p < .001). There was an initial increase in ACOF for four left shoes and five right shoes (9 out of 14 shoes). Of these shoes, the ACOF fell below the baseline ACOF after 128±64 km of wear. After 210 km of wear, ACOF decreased from the baseline level for all shoes. The average ACOF decrease was 0.053±0.032 (28.1±13.6%) from baseline to present data collection. Across participants, the average (standard deviation) ACOF at baseline, from 0-200 km, and at each participant's last datum were 0.18 (0.023), 0.17 (0.030), and 0.13 (0.022), respectively.

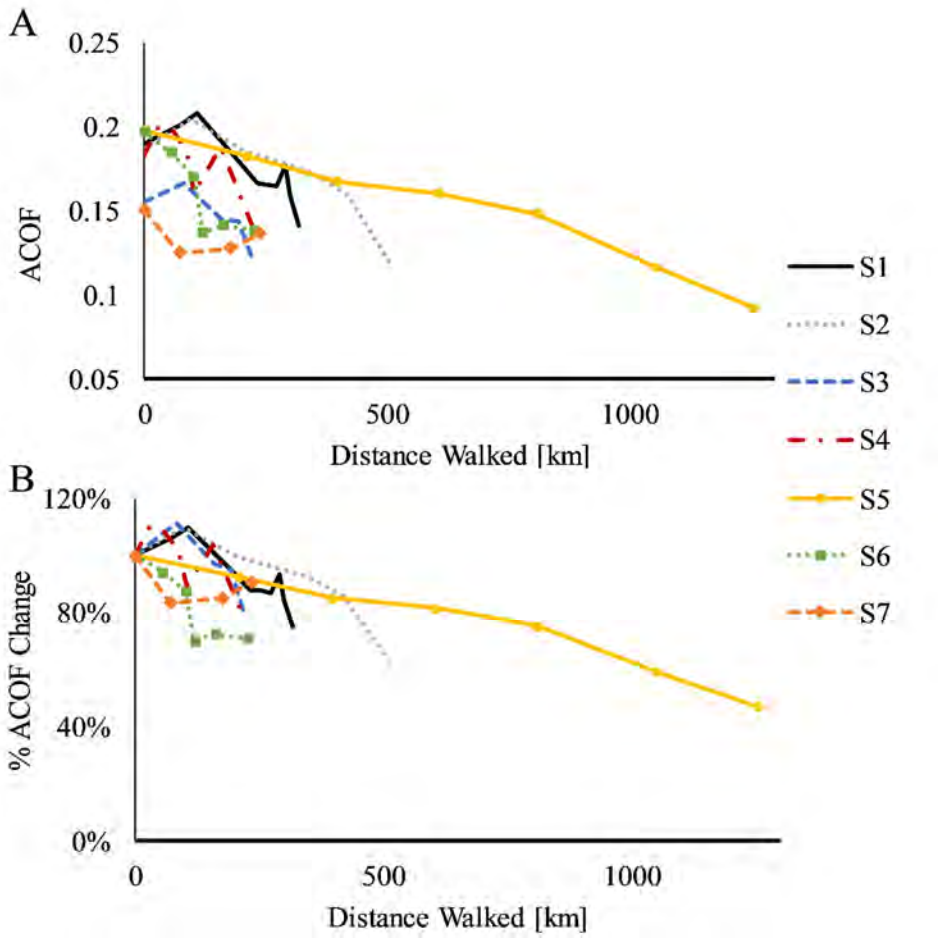

Figure 27. A) ACOF plotted against the distance walked for each participant. B) ACOF across the distance walked in the shoes as a percentage of the baseline ACOF. ACOF and percent of baseline ACOF are averaged across left and right shoe sides.

An increase in the distance walked was associated with increased fluid force ($F_{1,86}$=44.2, p < .001). The fluid force ranged from <0.1 to 63.8 N (Figure 28). Using the regression equation, Eq. (11), walking distances of 200 km and 1000 km were associated with an increase in fluid force of 6 N and 19 N, respectively.

$$F_{fluid}\ [N] = (1.16 + 0.05\sqrt{\text{Distance Walked [km]}})^3 \quad \text{Eq. (11)}$$

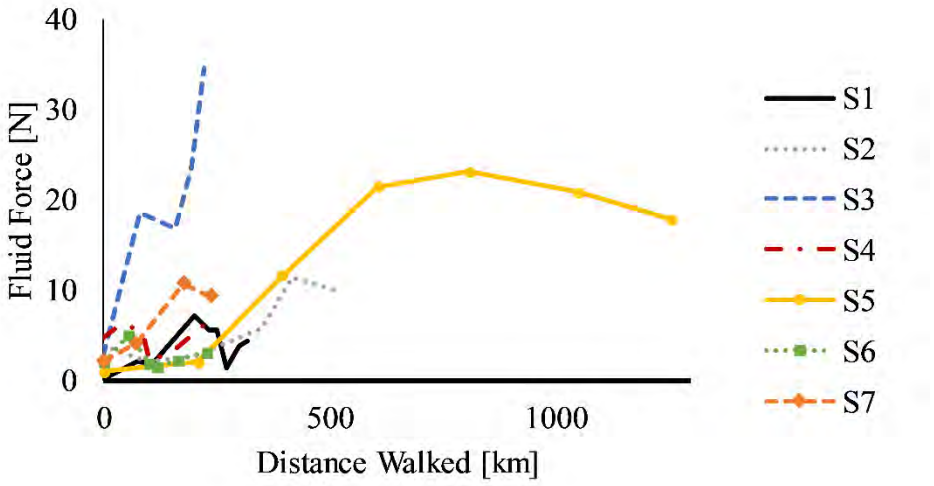

Figure 28. Fluid force (F_{fluid}) values are plotted against the distance walked which was averaged across the left and right shoes per subject.

The size of the worn region ranged from 12 to 2432 mm^2 and increased with respect to the distance walked (Figure 29). ACOF decreased as the size of the worn region increased ($F_{1,85}$=36.0, $p < .001$). When the size of the worn region grew to 1000 mm^2 and 2000 mm^2, the ACOF was predicted to decrease from baseline by 0.03 and 0.08, respectively, Eq. (12). The increase in fluid force was associated with increases in the size of the worn region ($F_{1,76}$=59.2, $p < .001$). Using the regression equation, Eq. (13), the fluid force was predicted as 11 N after the size of the worn region grew to 1000 mm^2 and as 29 N after the size of the worn region reached 2000 mm^2.

$$\text{ACOF} = \sqrt{0.03 - 1.08 * 10^{-5} * \text{SWR}\,[\text{mm}^2]} \quad \text{Eq. (12)}$$

$$\text{fluid force}\,[\text{N}] = (1.3 + 0.0009 * \text{SWR}[\text{mm}^2])^3 \quad \text{Eq. 13}$$

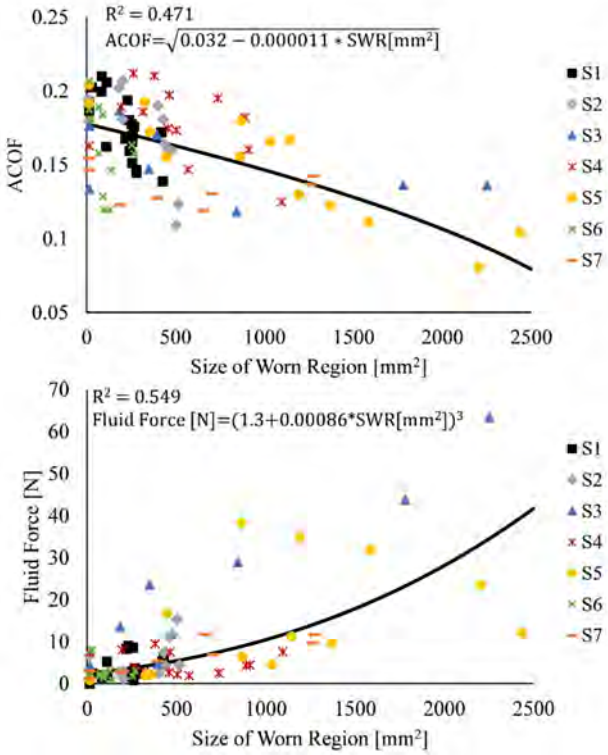

Figure 29. A) ACOF plotted against the size of the worn region. Different markers are used for each participant (legend). B) Fluid force plotted against the size of the worn region for all participants. Left and right shoe averages are shown for each participant. The regression functions for each model are

shown with the solid black line (SWR ≡ size of worn region [mm^2]). The regression equations and the R^2 values are shown in the top left of each plot.

F.6.3. Discussion

In this study, ACOF decreased and the fluid force generally increased as SR shoes became more worn. The increase in fluid pressure partially explains the decreased traction. There was an initial increase in ACOF from baseline for nine of the fourteen shoes, though the ACOF then decreased for all of the shoes after at most, 210 km of usage. The fluid force increase was associated with the increasing size of the worn region, presumably due to reduced fluid drainage.

The effects of usage and wear on ACOF and fluid force from this analysis are consistent with previous research. For progressively worn shoes using natural and simulated wear respectively, Grönqvist (1995) and Hemler, et al. (2019) reported an initial increase in ACOF followed by a decrease across the life of the shoes. In this study, similar trends are seen for the majority of the naturally worn shoes with an initial increase in ACOF for distances less than 210 km and subsequent decrease in ACOF. The increase in fluid force with increased wear is also consistent with previous studies [61]. The relationship between fluid force and size of the worn region is consistent with previous research that utilized an accelerated wear protocol to generate shoe wear [61]. Fluid force increased as the size of the worn region increased similar to Hemler, Charbonneau, et al., 2019, and consistent with hydrodynamic theory [85]. Therefore, this study adds to a growing body of evidence that traction performance degrades over usage and that this degradation can be assessed based on the size of the worn region.

The variation of ACOF observed in this study was within a critical range for determining slip likelihood. Human slipping studies have shown that the probability of a slip on level ground changes dramatically within the range of 0.12-0.21 [6, 45, 123]. Both the baseline ACOF values and the changes in ACOF due to wear vary within this range. This variability is not believed to be due to the device since repeatability is less than 0.01 for the portable slip tester [124], which is functionally similar to the slip testing device used in this study. The variation in ACOF at baseline for the shoes may be due to different heel tread block placements that arise from variations in shoe size-dependent molds. For example, on the heel, the general tread pattern is the same for all shoes. However, on the edges, some individual tread blocks are cut differently to fit the heel of the appropriate shoe size. These variations in tread on the edges may affect the ACOF.

This preliminary study has certain limitations. A single shoe tread pattern was used in order to limit variability across the participants. However, this limited the generalizability of the results to other types of shoes. The shoes were tested on the slip-testing device with a 0° medio-lateral tilt. Wear generally appeared first on the lateral side of the shoe outsoles, which may indicate that participants walked with a slight medio-lateral inversion. The slip testing device was unable to accommodate individual inversion angles, which may have led to the tread contact region being incongruent between traction performance testing and actual wearing.

F.6.4. Summary

The results found an association between the size of the worn tread region and traction performance loss for naturally worn, slip-resistant shoes. Consistent with accelerated wear experiments, an initial increase in traction was observed at low distances of usage followed by a steady decrease in traction with increasing distance. Fluid force measurements suggest that this steady decrease in traction is caused by an increase in hydrodynamic effects. The increase in hydrodynamic effects coincide with an increase in the size of the worn region, consistent with hydrodynamic theory. This study supports that usage and wear measures presented in this study are beneficial tools in mapping traction performance for slip-resistant shoes.

F.7. A hydrodynamics model to predict under-shoe fluid pressures based on the dimensions of a worn region [125] (Aim 4, Key finding 9)

F.7.1. Methods

This study analyzes data from three previous experiments (E1-simulated shoe wear [37], E2-progressive shoe wear [75], and E3-human slipping trials [76]). In each experiment, under-shoe fluid pressures are predicted by a solution of Reynolds equation based on shoe wear geometry measurements.

E1: Four right shoes were systematically abraded to simulate wear during gait. At baseline and after each wear cycle, under-shoe peak fluid pressures were measured as shoes were slid across a contamined surface.

E2: 13 participants wore two pairs of shoes in the workplace for one month at a time (n_{shoes}=22). At baseline and after each month of wear, fluid pressures were measured for both sides (L/R).

E3: 57 participants experienced a slippery condition, while wearing their own worn shoes. The liquid contaminant was spread across an array of pressure sensors. Under-shoe fluid pressures were measured during the unexpected slipping condition.

For all shoes, the size of the worn region (length, *l*, and width *b*) was measured based on the largest region without tread on the heel of the shoe. Measurements were repeated for each wear cycle and month of wear for E1 and E2. The tapered-wedge bearing solution of the Reynold's equation was used to predict the minimum film thickness (PFT) based on the size of the worn region along with the dynamic viscosity of the 90% glycerol used in all experiments ($\eta = 214\ cP$), the sliding speed ($v_{E1,E2} = 0.3\frac{m}{s}, v_{E3} = 0.1\frac{m}{s}$ [6]), normal force ($F_{E1,E2} = 250\ N, F_{E3} = 179\ N$ [50]), a wedge incline factor ($K_p = 0.025$) [116], and a wedge-fluid, side leakage factor (γ) which was dependent on the worn region size, Eq. (14).

$$PFT = \sqrt{\frac{6\eta v l^2 b \gamma K_p}{F}} \quad \text{Eq. (14)}$$

Three statistical models were used to test the effect of PFT on the peak fluid pressures. Specifically, two repeated-measures regression models (E1 and E2) and one linear regression model (E3) were used where the independent variables were PFT (E1-3), shoe type (E2), and side (E2), and the dependent variable was the peak fluid pressure (E1-3). Random variables of shoe type (E1) and participant (E2) were included in the models.

F.7.2. Results and Discussion

PFT predicted peak fluid pressure for all three models: E1 - $F_{1,75}$=95.7, p<.001, E2 - $F_{1,180}$=47.9, p<.001, and E3 - $F_{1,55}$=16.5, p<.001 (Figure 30).

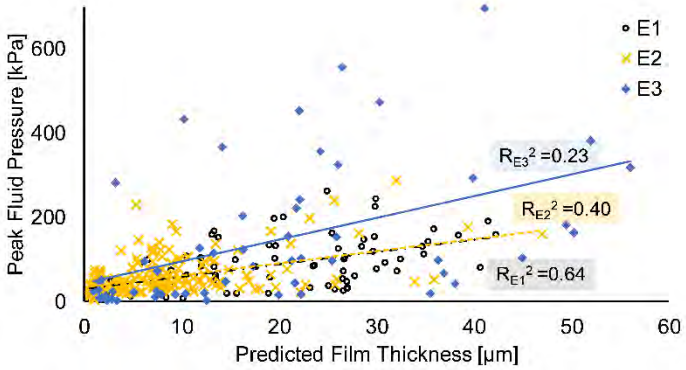

Figure *30*: Peak fluid pressure with respect to the PFT across E1, E2, & E3. Trend lines per experiment and respective R^2 values are shown.

This research validates the use of PFT based on the tapered-wedge solution of Reynolds equation to predict under-shoe fluid pressure in multiple experimental contexts. Consequently, the size of the worn region of the shoe outsole wear is a good indicator of under-shoe hydrodynamics.

F.7.3. Significance

Shoe traction performance is dependent on effective drainage that minimizes under-shoe fluid pressures. By applying fluid mechanics to a simple metric of shoe wear, this research supplies a clearer understanding of how shoe outsole wear geometry influences under-shoe fluid pressures. This research provides a foundation for developing a measurement tool to assess the worn region of shoe outsoles and supply replacement recommendations. Such a tool would guide appropriate shoe replacement, enhance the performance of workplace footwear [76], and thus reduce slip and fall accidents [50, 76].

F.8. Traction performance across the life of slip-resistant shoes: a prospective study [confidential] (Aim 4, Key finding 9)

F.8.1. Methods

This section describes the full data set from the study described in Section E.6.1. The only methodological difference in this section is the number of subjects and the number of months that the participants were tracked. In addition, the predicted film thickness (PFT) was calculated for each shoe (see Section E.5.2.2.).

In this study, 23 participants were enrolled to wear two pairs of shoes in their workplace (n_{shoes} = 46. Eight participants and 22 pairs of shoes were excluded from the analysis for three primary reason: 3 participants (n_{shoes} = 4) discontinued wearing the shoe due to experiencing shoe discomfort in the workplace, six participants withdrew from the study prior to completing one month of walking in the shoes (n_{shoes} = 7), and five participants walked fewer than 100 km prior to completion of enrollment due to low activity levels (n_{shoes} = 11). Therefore, 15 participants (M: 12, F: 3; age: 41.7 ± 12 yrs; mass: 89.8 ± 12.5 kg; height: 176.7 ± 10.3 cm; BMI: 28.8 ± 3.4) and 24 pairs of shoes are included in this analysis (US Men's Shoe Size: 10.1 ±2.3). The experiment consisted of two components: 1) a gait assessment and 2) a wear-at-work component described in Section E.6.1. Participants were provided with two pairs of footwear – shoe A and: shoe B or shoe C. Within each shoe type, boots or shoes with the same tread pattern were provided depending on their occupational requirements. As shoe B was discontinued from manufacturing during the study, four participants received shoe C rather than shoe B.

Statistical analyses were performed to test the effects of wear on traction performance changes. Six repeated-measures ANOVA models (3 models where the independent variable was different x 2 dependent variables) with subject as a random variable were used to assess the impact of the distance, month, and worn region size (each of these were an independent variable in separate regression models) on the ACOF and fluid force (dependent variables). Separate models were used to determine whether time, use (walking distance), or actual shoe condition (worn region size) best predicted loss in performance. In each model, shoe type (A, B, C) and side (left, right) were additional covariates along with all first-order interaction effects. Therefore, the first model included ACOF as the dependent variable and distance, shoe type, distance*shoe type, side, distance*side, and shoe type*side as the independent variables. Predicted film thickness (PFT) was calculated consistent with previous methods (Eq. 9). A mixed linear regression was used to assess the relationship between PFT and fluid force. Specifically, the dependent variable was fluid force and the independent variables were PFT, shoe type, and their interaction. For all models, a square root transformation was applied to the distance walked to correct for a positive skew, and the ACOF and fluid force were natural log-transformed to normalize residuals.

F.8.2. Results

Participants walked 103-2053 km in the shoes across 1-11 months for a total of 199 subject-months of data. Across the shoes, participants walked an average (standard deviation) of 474.1 (454.0) km across 5.0 (3.1) months with 82.6 (84.9) km per month (Table 8). The ACOF and fluid force were the highest for shoe A and smallest for shoe B at baseline and overall. The range in ACOF was largest for shoe A and smallest for shoe B. The range in fluid force was the largest for shoe C and the smallest for shoe B. Shoe A experienced the largest and shoe C experienced the smallest changes in ACOF

from baseline (%ACOF from baseline). ACOF increased from baseline for 54 of the 286 shoes with the most shoes experiencing an increase for shoe B.

Table 8. Data organized by shoe type and then across all shoes. Data is the average (standard deviation) unless otherwise stated in the column description.

	A	B	C	All Shoes
Number of months worn	3.8 (2.9)	6.8 (2.0)	5.0 (4.2)	5.0 (3.1)
Total distance walked [km]	443 (541)	464 (359)	588 (431)	474 (454)
Distance walked per month [km]	98 (104)	65 (71)	98 (64)	83 (85)
Baseline ACOF	0.301 (0.075)	0.172 (0.024)	0.205 (0.047)	0.237 (0.082)
Overall ACOF	0.207 (0.073)	0.159 (0.027)	0.160 (0.041)	0.177 (0.055)
Range ACOF (min, max)	(0.097, 0.414)	(0.080, 0.212)	(0.088, 0.285)	(0.080, 0.414)
Overall %ACOF from Baseline	70% (28%)	94% (17%)	75% (27%)	82% (26%)
Number of shoe months (increased, decreased) from baseline	(4, 100)	(45, 89)	(5, 43)	(54, 232)
Range %ACOF from Baseline (min, max)	(32%, 202%)	(40%, 139%)	(31%, 152%)	(31%, 202%)
Baseline Peak Fluid Pressure [kPa]	45 (35)	31 (20)	25 (10)	36 (28)
Overall Peak Fluid Pressure [kPa]	56 (38)	51 (44)	44 (24)	52 (39)
Range Peak Fluid Pressure [kPa] (min, max)	(12, 230)	(4, 286)	(15, 127)	(4, 286)
Baseline Fluid Force [N]	5.4 (5.0)	(2.1, 2.1)	2.2 (0.7)	3.6 (4.0)
Overall Fluid Force [N]	12.1 (11.7)	6.7 (9.0)	8.8 (6.4)	9.0 (10.0)
Range Fluid Force [N] (min, max)	(0.2, 70.1)	(0.0, 63.4)	(1.5, 25.7)	(0.0, 70.1)
Baseline Worn Region Size [mm^2]	50.1 (54.4)	1.0 (0.6)	8.4 (0.0)	29.3 (41.2)
Average Worn Region Size [mm^2]	239 (287)	296 (299)	(272, 339)	(272, 302)
Range Worn Region Size [mm^2] (min, max)	(25, 1357)	(10, 1413)	(8, 1385)	(8, 1413)
Baseline Predicted Film Thickness [um]	2.5 (2.0)	0.9 (0.1)	(0.68, 0.0)	(1.6, 1.6)
Average Predicted Film Thickness [um]	6.4 (5.5)	8.1 (6.5)	(8.0, 7.7)	(7.5, 6.4)
Range Predicted Film Thickness [um] (min, max)	(1.5, 26.7)	(0.79, 26.6)	(0.7, 31.6)	(0.7, 31.6)

As distance walked, months worn, and the worn region size increased, the ACOF decreased and the fluid force increased (Figures 31-32, Table 9). In all the models, shoe type had a main and an interaction effect with the wear parameter (walking distance, month, or worn region size). This suggests that the wear response was dependent on the shoe. Shoe A started with the highest ACOF but also experienced the biggest effects of wear. The rate of fluid force change varied across shoe types. The fluid force increased slower for Shoe A than the other shoes. The fluid force was positively associated with the predicted film thickness and varied across shoes (Figure 33), but the rate of fluid force change was not affected by shoe type. The R^2 values were similar across models (ranged from 0.466 to 0.584). Interestingly, the predicted film thickness model achieved similar R^2 values to the other models with fewer inputs.

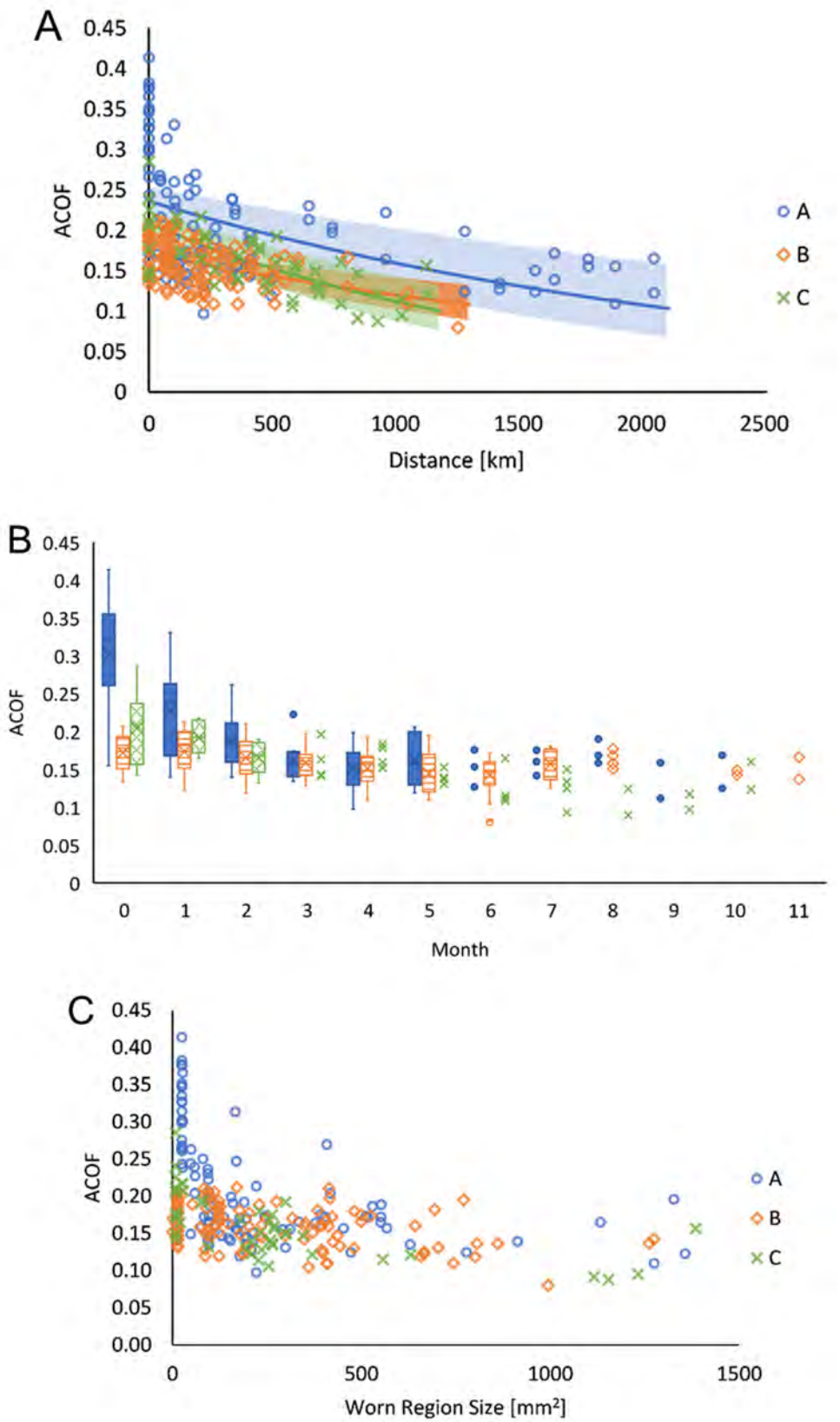

Figure 31. ACOF with respect to A) distance walked in the shoes; B) month of shoe wear; and C) size of the worn region. Exponential fit regression lines with a 95% confidence interval are shown for in graph A. Box plots are shown for months in which there were more than 4 data points per shoe.

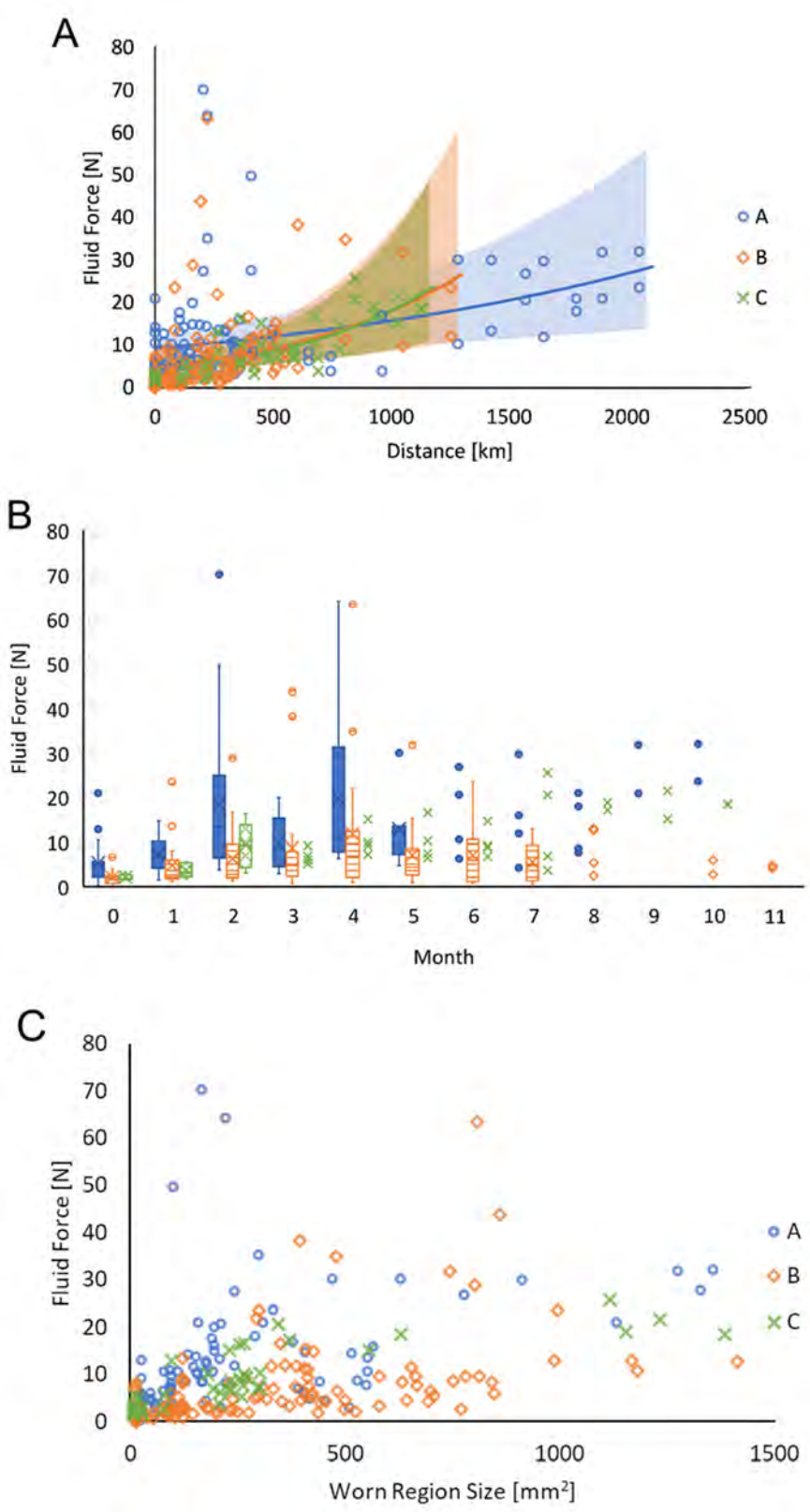

Figure 32. Fluid Force with respect to A) distance walked in the shoes; B) month of shoe wear; and C) size of the worn region. Exponential fit regression lines with a 95% confidence interval are shown for in graph A. Box plots are shown for months in which there were more than 4 data points per shoe.

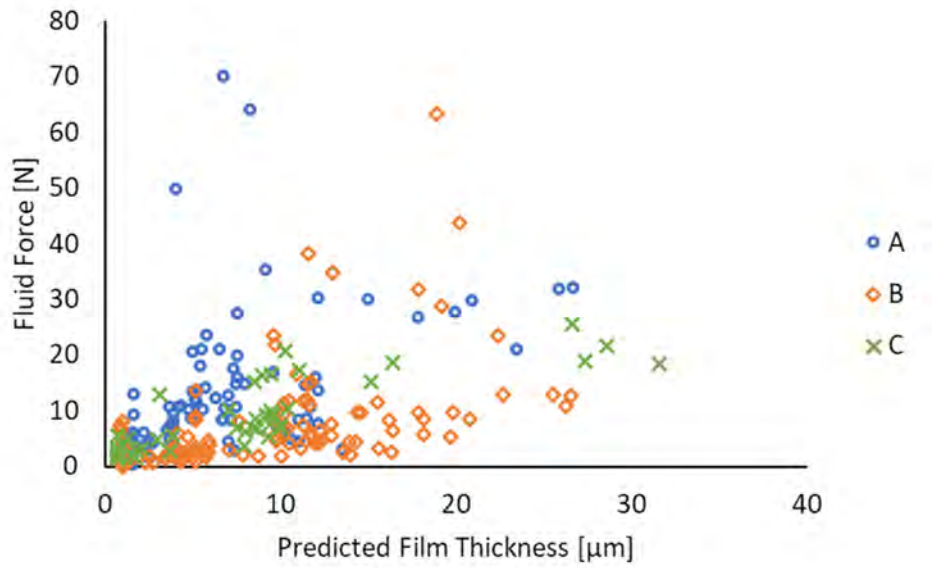

Figure 33. Fluid force with respect to the predicted film thickness for each shoe type.

Table 9. Statistical Analyses for the effects of wear and usage on traction performance in addition to the fluid model analysis. Significant p-values are bolded.

Dependent Variable	R^2	Independent Variable(s)	F-ratio	p-value
ln(ACOF)	0.588	sqrt(Distance)	$F_{(1,276)}$=135.4	**<.001**
		Shoe	$F_{(2,234)}$=29.6	**<.001**
		Side	$F_{(1,258)}$=0.4	0.503
		sqrt(Distance)*shoe	$F_{(2,274)}$=5.9	**0.044**
		sqrt(Distance)*side	$F_{(1,258)}$=4.8	**0.030**
		Shoe*side	$F_{(2,258)}$=0.6	0.57
ln(Fluid Force)	0.587	sqrt(Distance)	$F_{(1,276)}$=140	**<.001**
		Shoe	$F_{(2,239)}$=29.2	**<.001**
		Side	$F_{(1,259)}$=0.6	0.429
		sqrt(Distance)*shoe	$F_{(2,273)}$=7.5	**<.001**
		sqrt(Distance)*side	$F_{(1,259)}$=3.7	0.055
		Shoe*side	$F_{(2,259)}$=0.7	0.506
ln(ACOF)	0.522	Month	$F_{(1,258)}$=114.6	**<.001**
		Shoe	$F_{(2,116)}$=19.5	**<.001**
		Side	$F_{(1,258)}$=0.6	0.445
		Month*shoe	$F_{(2,274)}$=15.5	**<.001**
		Month*side	$F_{(1,258)}$=1.1	0.286
		Shoe*side	$F_{(2,258)}$=1.0	0.375
ln(Fluid Force)	0.464	Month	$F_{(1,275)}$=61.3	**<.001**
		Shoe	$F_{(2,245)}$=25.9	**<.001**
		Side	$F_{(1,261)}$=0.6	0.423
		Month*shoe	$F_{(2,270)}$=0.2	0.829
		Month*side	$F_{(1,261)}$=2.0	0.164
		Shoe*side	$F_{(2,261)}$=0.9	0.407
ln(ACOF)	0.446	Worn Region Size	$F_{(1,253)}$=60.8	**<.001**
		Shoe	$F_{(2,154)}$=22.2	**<.001**

		Side	$F_{(1,250)}$=1.1	0.298
		Worn Region Size*shoe	$F_{(2,261)}$=5.1	**0.007**
		Worn Region Size*side	$F_{(1,259)}$=0.1	0.794
		Shoe*side	$F_{(2,248)}$=1.1	0.874
ln(Fluid Force)	0.491	Worn Region Size	$F_{(1,237)}$=76.7	**<.001**
		Shoe	$F_{(2,120)}$=22.6	**<.001**
		Side	$F_{(1,250)}$=0.0.5	0.472
		Worn Region Size*shoe	$F_{(2,259)}$=1.8	0.163
		Worn Region Size*side	$F_{(1,260)}$=1.7	0.197
		Shoe*side	$F_{(2,248)}$=0.5	0.592
ln(Fluid Force)	0.478	Predicted Film Thickness	$F_{(1,269)}$=149.5	**<.001**
		Shoe	$F_{(2,269)}$=39.8	**<.001**
		Predicted Film Thickness*shoe	$F_{(2,269)}$=2.3	0.105

F.8.3. Discussion

This study showed that increases in shoe usage and wear lead to decreases in ACOF and increases in fluid force. These decreases in traction performance (decreased friction and poorer under-shoe fluid drainage) varied across the three types of shoes. Furthermore, the fluid model introduced in Section E.7.1 applied to this study showed that PFT which employed the shoe outsole worn region size was associated with the under-shoe fluid force during sliding.

This study is consistent with previous research and expands upon those findings. The results of decreased traction performance with wear are consistent with previous research that examined mechanical wear or worn shoes in a cross-sectional study [37, 73, 114, 126, 127]. Research from Section E.7.1 used the PFT to predict peak fluid pressures. Fluid force is a more rigorous measure of under-shoe hydrodynamics as it assesses the load supported by the fluid across the entire shoe heel during sliding [82]. As such, this model's ability to predict fluid force in addition to peak fluid pressures is supported by hydrodynamic theory and is important for application of using the worn region size as an indicator for traction performance decline.

Multiple metrics of wear (time, walking distance, and worn condition) were found to predict loss in friction performance. This suggests that multiple methods may be effective for monitoring and implementing shoe maintenance program. We should acknowledge that shoes were removed from the study when they were deemed to have lost too much friction performance by the research team. This led to fewer data points for the individuals who had the greatest wear. This may have led to greater weighting to low wear individuals. Furthermore, individuals with the lowest wear rates would also have the greatest ranges with respect to time and distance, which would provide them more leverage. Therefore, the results that time and distance were similar predictors to worn condition should be interpreted cautiously.

From an applied perspective, a combination of monitoring methods may be preferred. For example, measuring physical wear may be best for high wear individuals with additional requirements that shoes be replaced after exceeding a certain amount of time or wear distance. Furthermore, the distance walked in the shoes and months of use may not always be reliable measurements depending on the tracking method and worker recollection, respectively. Worn region size, which does not depend on past measurements, may be a more feasible method for assessing traction performance in many work environments. However, this study suggests that any of these methods of monitoring offers at least some value and that workplaces with different needs can adopt their preferred monitoring method.

F.9. Study 9: Gait Kinetics Impact Shoe Tread Wear Rate [confidential] (Aim 4, Key finding 10)

F.9.1. Methods:

This research consisted of a longitudinal study comprised of a gait assessment and wearing shoes in the workplace (Figure 34). Two pairs of SR shoes were fitted to each participant. Gait kinetics and kinematics were collected during dry, over-ground walking in each pair of shoes. Participants then wore the shoes in the workplace alternating between pairs each month. At baseline and during the off-month of wear, tread geometry was captured using negative molds of the heel of the shoes to determine the volumetric tread loss and subsequent wear rate based on the distance walked by the participants. The change in ACOF and under-shoe fluid pressures was also tracked and reported [73, 128].

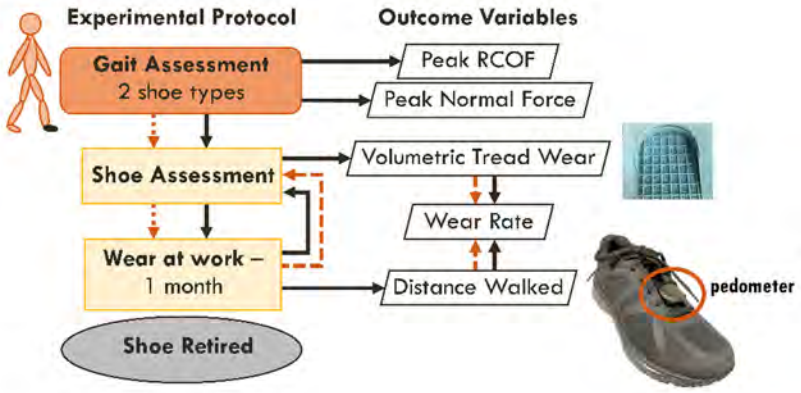

Figure 34. Flowchart of experimental protocol.

F.9.1.1.Participants

Fourteen healthy participants (11 male and 3 female; age: 42 ± 13 yr; height: 177 ± 11 cm; mass: 91 ± 13 kg; shoe size 9.6 ± 2.3 US Men's Sizing) from a recruited cohort of 23 recruited participants were analyzed. Inclusion criteria included participants who regularly wore treaded shoes, spent more than 75% of walking time on manmade surfaces, and were on their feet for at least 4 hours in a typical day. Exclusion criteria included any neurological problems, musculoskeletal history in the previous 2 years, musculoskeletal disorders, neurological problems, osteoporosis, or arthritis. Included participants worked in the following industries: trade, transportation & utilities, manufacturing, leisure and hospitality, and education and health services. Only right shoes that were worn for 100 km were included in this analysis (excluding 23 pairs of shoes leading to 23 pairs of shoes included in the study) since preliminary observations revealed that this was the minimum amount of use where a reliably measurable amount of wear could be observed. Reasons that shoes did not reach 100 km included low participant activity levels (n_{shoes} = 8), participant discontinued the shoe because they reported discomfort while wearing the shoes at work (n_{shoes} = 4), the participant withdrew from the study prior to completing one month of walking in the shoes (n_{shoes} = 11). Written informed consent was obtained at the start of the study according to the University of Pittsburgh Institutional Review Board and the research has been conducted in accordance with the principles of the Declaration of Helsinki.

F.9.1.2.Experiment Protocol

Participants were provided with two pairs of either boots or shoes depending on their occupational requirements. They were asked to complete a series of dry, over-ground walking trials at a pace resembling their gait while in their workplace. While wearing each pair of the given shoes (Table 10) and reflective markers to track motion, participants walked over two force plates (Bertec 4060A, Columbus, OH) which collected normal and shear forces at 1080 Hz. The gait assessment concluded when ten good force plate hits were recorded for the right foot for each shoe type. The right shoe of each pair was fitted with a pedometer to track the distance walked (MilestonePod, Milestone Sports,

Columbia, MD), [122]. Shoes were then shipped to participants to wear in their workplace for one month at a time.

Table 10: List of footwear code, brand, model, and short-term hardness for each men's and women's footwear option. Two footwear options were used for Shoe A – Boot as the first model was discontinued during the recruitment phase.

Footwear Code	Shoe/Boot Option	Footwear Brand	Men's Model	Women's Model	Short Term Hardness (Shore A)
A	Shoe	SRMax	SRB1977	SRB972	48.3
	Boot	SRMax	[1]SRM4750/[2]SRM225	SRM2550	[1]50.5/[2]48.5
B	Shoe	safeTstep	Blast Bouffee 159961	Blast Bouffee 159961	65.4
	Boot	safeTstep	Dawson 160004	–	74.1
C	Boot	ShoesFor Crews	Rowan 77280	August 77319	49.9

At baseline and after each month of wear, the tread wear of the shoes was measured. A rectangular mold (92 mm x 76 mm x 28 mm) of each shoe heel was made using a silicone rubber compound (Smooth-On Inc.; Macungie, PA; Oomoo® 25) at an angle of 17° as in previous experiments [61, 128]. The right foot molds for the baseline level and the first month of wear that surpassed the 100 km threshold were used to determine the volumetric tread loss during wear in the workplace. Each mold was placed on a scale (MicroMall™ 300g/0.001g B3003T) and the inverse tread blocks were filled with water using a pipette. The mass of the water required to fill the molds was measured three times. The molds were allowed to dry between measurements. The change in the water mass between the baseline level and threshold-passing mold was calculated, converted to volume, and normalized to the cumulative distance the shoes were worn to that point of wear. This metric was termed the wear rate [mm^3/km].

F.9.1.3.Statistical Analysis

Three, mixed linear regression models were used in this study. Specifically, the first model consisted of testing the effect of peak normal force (between subject) and shoe type (within subject) on wear rate (dependent variable). The second model assessed the effect of peak shear force (between subject) and shoe type (within subject) on wear rate (dependent variable). Lastly, the third model tested the effect of peak RCOF (between group) and shoe type (within group) on wear rate (dependent variable). For all models, wear rate was logarithmic-transformed to normalize residuals and satisfy the linearity assumption.

F.9.2. Results

Participants walked a cumulative distance of 167 ± 69 km (range: 101-351 km) until the time when wear volume was determined (i.e., end of the first month when shoe usage exceeded the 100 km threshold) which occurred after 1.9 ± 1.4 months (range: 1-7 months). Within those months, participants walked 100 ± 80 km per month. The standard deviation between the three volume measurements of each mold was 54 mm^3, on average (the standard deviation ranged from 6-125 mm^3). The cumulative volumetric tread wear ranged from 324-3450 mm^3 (baseline to the 100 km threshold month) across the shoes.

Peak normal force ranged from 816 to 1270 N, peak shear force ranged from 87 to 235 N, and peak RCOF ranged from 0.090 to 0.23. The geometric mean of the wear rate was 6.7 mm^3/km with a range from 1.7 to 20.0 mm^3/km, and a mean 95% confidence interval of 5.1-8.9 mm^3/km. Overall, Shoe A had the largest range for the wear rate, peak normal force, peak shear force, and peak RCOF. Shoe C had the smallest range for the wear rate, peak normal force, and peak shear force, and lowest average values across all four variables while Shoe B had the highest average values across the four variables.

In the first model (AICc = 63.2), peak normal force ($F_{1,12}$=.01, p=0.924) and shoe type ($F_{2,9}$=3.8, p=0.063) were not associated with wear rate (Figure 35). In the second model, (AICc = 56.4), the peak

shear force was positively associated with wear rate ($F_{1,14}$=5.4, p=0.037), but there was no association between wear rate and the shoe type ($F_{2,9}$=2.7, p=0.118). In the third model (AICc = 42.6), peak RCOF ($F_{1,14}$=6.6, p=0.023) was positively associated with wear rate, and shoe type ($F_{2,11}$=2.9 p=0.100) was not. Furthermore, in the third model, increases in RCOF of 0.01 and 0.1 were associated with increases in wear rate of 6.8% and 93.0%, respectively.

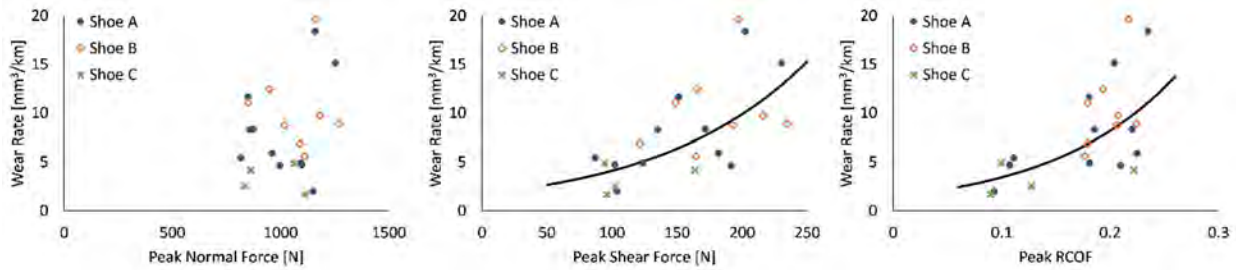

Figure 35. Wear rate with respect to A) peak normal force, B) peak shear force, and C) peak RCOF for the three shoe types. The regression line is shown in black according to the natural logarithmic transformation for the peak shear force and peak RCOF.

F.9.3. Discussion

In this study, the peak shear forces and peak RCOF, but not the peak normal force, were associated with the wear rate. The peak RCOF model showed increases of 0.1 in the RCOF were associated with nearly doubling of the predicted wear rate. As such, the service life of shoes (use before requiring replacement) is highly dependent on that individual's gait kinetics, specifically the shear force and its ratio to the normal force (RCOF).

This research builds off previous literature which has shown that gait parameters are related to slip risk [6, 50, 129]. Previous research has shown that RCOF during dry locomotion is predictive of slip risk [129], and thus a reasonable gait metric to study for assessing slip risk. This study identifies a second pathway in which RCOF could increase slip risk. Increased wear rate (associated with higher RCOF) will lead to faster growth of a worn region. The amount of shoe outsole wear, measured by the size of the worn region, was associated with decreased ACOF, increased under-shoe fluid pressures, is associated with increased slip risk [61, 130, 131].

These results are consistent with the fatigue failure wear theory as a mechanism for shoe outsole elastomeric wear. Tearing energy, also known as the strain energy release rate, has been shown to contribute to elastomer fatigue and subsequent failure [132, 133]. Furthermore, an advantage of applying this fatigue failure wear theory lies in the geometry-independent determination of using fatigue life as a characteristic of elastomer [133]. These findings on fatigue failure are applicable for shoe outsole wear regardless of tread design. However, designs to reinforce material properties in the directions of principle shear for a given tread design could potentially influence wear rate. These principle shear directions are determined by the characteristics of locomotion.

Gait kinetics impact shoe wear rate. The results are consistent with an elastomer fatigue failure model of shoe wear. Although this work focused on slip-resistant shoes, the theoretical approach and conclusions are valid for both slip-resistant and non-slip-resistant shoes. Furthermore, this research suggests that a person's gait has an impact on wear, which has potential impact for informing individual shoe replacements recommendations.

F.9.4. Conclusion

Overall, this research identifies individual peak shear forces and peak RCOF as predictors of shoe wear rate, which may also provide insight into a fatigue failure as the mechanism dominating the wear of shoe outsoles. In this study, peak shear forces and peak RCOF, a measure of peak shear forces relative to normal forces during dry walking, were found to be associated with tread wear rate. This work supports fatigue failure as a mechanism of shoe tread wear for normal gait. As such, specific shoe recommendations and wear thresholds may be informed from understanding the gait kinetics and wear mechanism presented in this research.

F.10. Study 10: Worn Region Size of Shoe Outsole Impacts Human Slips: Testing a Mechanistic Model [76] (Aims 4 and 5, Key findings 9 and 11)

F.10.1. Methods

This observational, cross-sectional study measured under-shoe fluid pressure and slip risk during a single testing session, while participants wore their own, naturally worn shoes. The participants were full-time workers and donned their work shoes during the study. Participants completed a series of walking trials ending with an unexpected slip trial while wearing their shoes (Figure 36A). During the unexpected slip trial, participants were aligned to step over a contaminant-covered array of fluid pressure sensors (Figure 36B) and slip outcome was determined. The worn heel region size (Figure 37) was measured for each shoe, and each shoe was also tested on a portable slip tester to determine the ACOF.

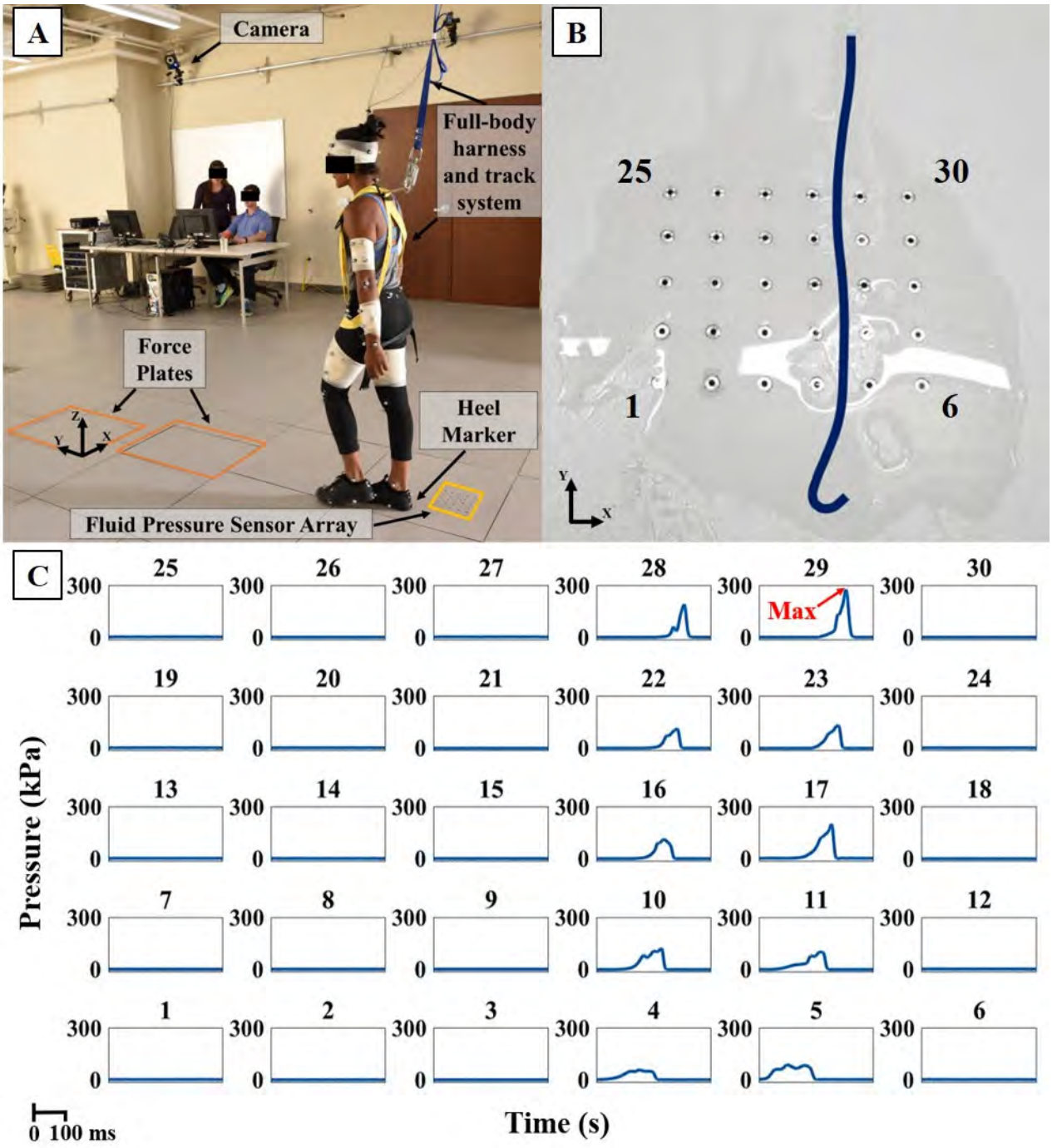

Figure 36. A: The experimental setup for exposing participants to slippery conditions. The cameras surrounding the gait testing area collected the position of the reflective markers. The force plates, fluid pressure sensor array, and harness are labeled. B: The heel marker was used to assess slipping, including the slip trajectory (blue line) as the foot crossed the fluid pressure sensor array covered in a liquid contaminant. Sensors are numbered by row then column. C: The fluid pressure data from the 30 sensors (numbered above each plot) were used to find the maximum pressure value ("Max").

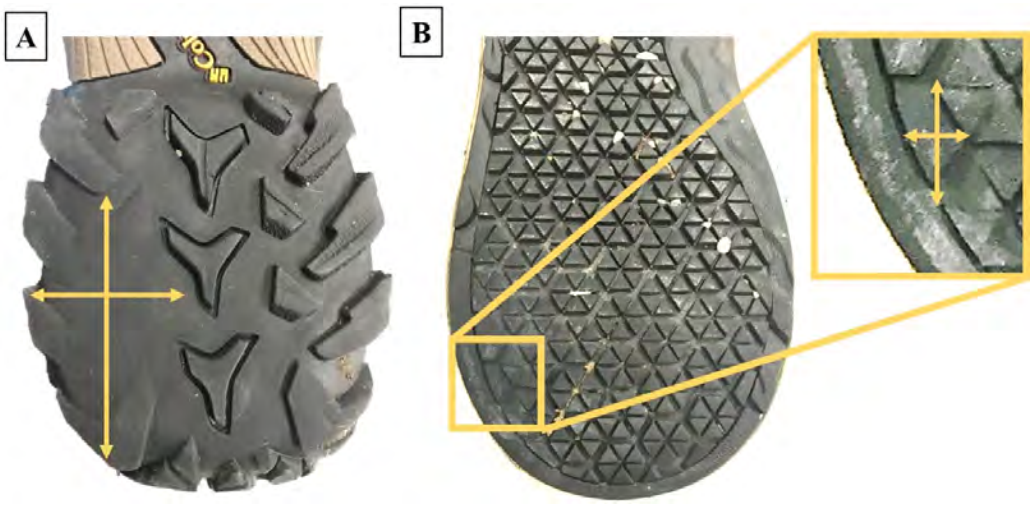

Figure 37. Examples of shoes and the worn region size included in the study. Shoe A is an NSR shoe with a moderate worn region size and Shoe B is a SR shoe with a smaller worn region size. The yellow arrows indicate the length and width of the worn region size that was measured.

F.10.1.1.Participants

Fifty-seven participants (mean age: 34±13 years, mean height: 169.7±9.5 cm, mean weight: 79.4±17.8 kg, 25: 28 female: male) were analyzed from a cohort of 90 recruited participants. Participants were excluded if they reported being aware of the contaminant prior to stepping on it (n = 9); they did not step on the fluid pressure sensors in the floor during the slip trial (n = 16); their shoe tread were clogged with substances such as food (n = 1); or their shoes had holes in the outsole (n = 5). Participants also agreed to forfeit their shoes. The eligibility criteria included an age between 18 and 65 years, a BMI less than 35 kg/m^2, wearing the same closed-toed, flat, and intact shoes at least 5 days a week, and no major musculoskeletal or neurological medical complications. Participants who worked at least 30 hours per week in any industry sector were recruited for the study. Of those included, 20 shoe pairs were reported to be worn less than 6 months, 23 worn between 6-12 months, and 10 shoes were worn greater than 12 months. Thirty-two shoes were designated by the manufacturer as slip resistant (SR) and twenty-one shoes were not slip resistant (NSR). The procedures were approved by the University of Pittsburgh Institutional Review Board (#PRO15030214) and all participants signed an informed consent form.

F.10.1.2.Experimental Setup and Procedure

Prior to data collection, participants donned tight-fitting clothes and their personal shoes. Seventy-nine reflective markers were placed on bony landmarks of interest to track the participant's motion during each trial using a motion capture system (Fig.2A) [134].

Participants completed a series of walking trials based on similar methods used by Beschorner et al. in a study that examined the influence of tread on fluid pressure and its correlation with slip severity (2014). During the baseline (without contaminant) walking trials preceding exposure to the contaminant, the participants were aligned to ensure foot strike on two force plates (Bertec 4060A, Columbus, OH) until 5 clean strikes per shoe were recorded. The forces were used to quantify required coefficient of friction (RCOF). The participants' starting point was then adjusted to align step position with the 30-fluid pressure sensor array (Fig. 2B), which was embedded in a floor tile. This tile was encountered by the participant about one step before the first force plate. The contaminant (100mL of a 90% glycerol-10% water by volume solution) was poured across the sensor array to completely cover all sensors; this process was completed while the participant was distracted. The participant was instructed to face away from the walking path, while listening to music and completing a puzzle for one minute before each walking trial. This distraction task along with dimmed lighting was intended to reduce participants' awareness of the liquid contaminant placed on the floor during the unexpected slip

trial. Marker data were collected at 120 Hz. Ground reaction forces and fluid pressures were collected at 1080 Hz.

F.10.1.3.Data Analysis for Human Testing

Ground reaction forces from the five baseline dry walking trials were used to calculate the RCOF, defined by the ratio of the shear force to the normal force. The shear force was defined as the resultant magnitude of the horizontal ground reaction forces and the normal force was defined as the vertical ground reaction force [45, 129, 135]. The peak of the RCOF time series was calculated during weight acceptance criteria based on normal force magnitude, shear force direction, time, and slope consistent with previous research methods [45, 129, 135, 136]. The average of the peak RCOF values from the five baseline dry trials was used for the analysis.

The coordinates of the heel marker (located at the most inferior position of the posterior section of the shoe), Figure 36A, were recorded to identify the initial heel contact location during the unexpected slip trial [46, 129, 137]. The peak fluid pressure value was determined as the maximum pressure across all 30 sensors (Fig. 2C). The location of the slip relative to the fluid pressure sensor array was assessed to determine if the foot slipped across the pressure sensor array; fluid pressure data was excluded if the foot did not contact the floor within this region.

The peak slip speed (PSS) was also quantified from the human gait data. The resultant speed of the heel marker was calculated using two-time step differentiation [138] based on both the anterior-posterior and medial-lateral components. PSS was calculated as the first local maximum heel speed that occurred at least 50 ms after heel contact [134]. A participant was considered to have slipped if the PSS exceeded 0.2 m/s. This cutoff was established *a priori* (prior to data collection) based on previous data showing a bimodal distribution of low-severity slips for treaded slip-resistant shoes below this value and high severity slips for fully worn shoes above this value [28]. All kinematic data were filtered with a 4th order, low-pass Butterworth filter using a 24 Hz cutoff frequency [45].

F.10.1.4.Footwear Characterization

The worn heel region size was determined by measuring the length and width of the worn heel region relative to the long axis of the shoe (Fig. 3). The length was defined as the longest anterior-posterior length of the largest continuous section on the shoe heel outsole [37]. The maximum allowable wear length was 50 mm for completely worn shoes since previous research has shown that fully worn shoes tend to only experience fluid pressures in the posterior 50 mm of the shoe [82]. The width was the maximum medial-lateral dimension of the worn region.

F.10.1.5.Shoe-Floor ACOF Testing Procedure

ACOF was recorded for the shoes using the portable slip simulator [45, 46, 139, 140]. The shoes that contacted the slippery contaminant (all right shoes except one left shoe) were tested. The shoes were tested against the same flooring (laminate) and contaminant (90% glycerol) as the unexpected slip trial. Test conditions included a normal force of 250 N, sliding speed of 0.5 m/s, and shoe-floor angle of 17° [45, 46, 69]. These test conditions have been determined to be relevant to slipping biomechanics [45, 137] and predictive of slip outcomes [45]. Shear and normal forces were recorded with a force plate (Bertec FP4060, Columbus, OH) at 500 Hz and ACOF was calculated as the ratio of shear to normal force over a 200 ms period. The ACOF was averaged across five repeated trials. Between each trail, the contaminant was redistributed to cover the surface.

F.10.1.6.Statistical Analysis

A series of regression analyses was performed to assess the impact of the size of the worn region on slip outcome and evaluate the proposed mechanistic model. To analyze Hypothesis 1, two logistic regression analyses were performed using slip outcome as the dependent variable with worn region size as the independent variable. A univariate model and a multivariate model were performed with the multivariate model including individual RCOF and the slip-resistant shoe category as covariates. The mechanistic model (described by Hypotheses 2-4) was tested via three regression models. To test Hypothesis 2, a regression model was performed to determine the effects of the worn

region size (independent variable) on fluid pressures (dependent variable) with slip-resistant shoe category and its interaction with worn region size as covariates. Hypothesis 3 was tested with a regression model to determine the influence of fluid pressure (independent variable) on ACOF (dependent variable), with slip-resistant shoe category and its interaction with fluid pressure as model covariates. Finally, to test Hypothesis 4, the effect of ACOF on slip outcome was tested with a logistic regression analysis, while controlling for RCOF. Inclusion of slip-resistant shoe category and RCOF as covariates was based on previous research that shows these variables are relevant to slip risk [54, 129]. Peak pressure values and shoe wear were square-root transformed to satisfy normality and linearity assumptions. All analyses used a significance level of 0.05 and were completed using statistical software (JMP, SAS Corp., NC). All statistical analyses (including the covariates but excluding the transformations) were designed prior to performing statistical analyses on this dataset.

F.10.2. Results

H1: Worn Region – Slip Outcome: The mean worn region size (mean ± standard deviation) varied across the shoes (all shoes: 1290 ± 1240 mm^2; SR shoes: 760 ± 910 mm^2; NSR shoes: 2200 ± 1220 mm^2). Slips were observed for 41 participants (71.9%). Slipping increased with the size of the worn region size for both the multivariate and univariate analyses (multivariate: $\chi^2_{(1)} = 4.2$, $p = 0.040$; univariate: $\chi^2_{(1)} = 20.6$, $p < 0.001$) (Figure 38). Specifically, for every 1 mm increase in the characteristic length of the worn region (i.e., square root of worn region size), the odds of slipping increased by 8.6% for the multivariate model and by 11.6% for the univariate model. Neither RCOF nor slip-resistant shoe category significantly influenced slip risk.

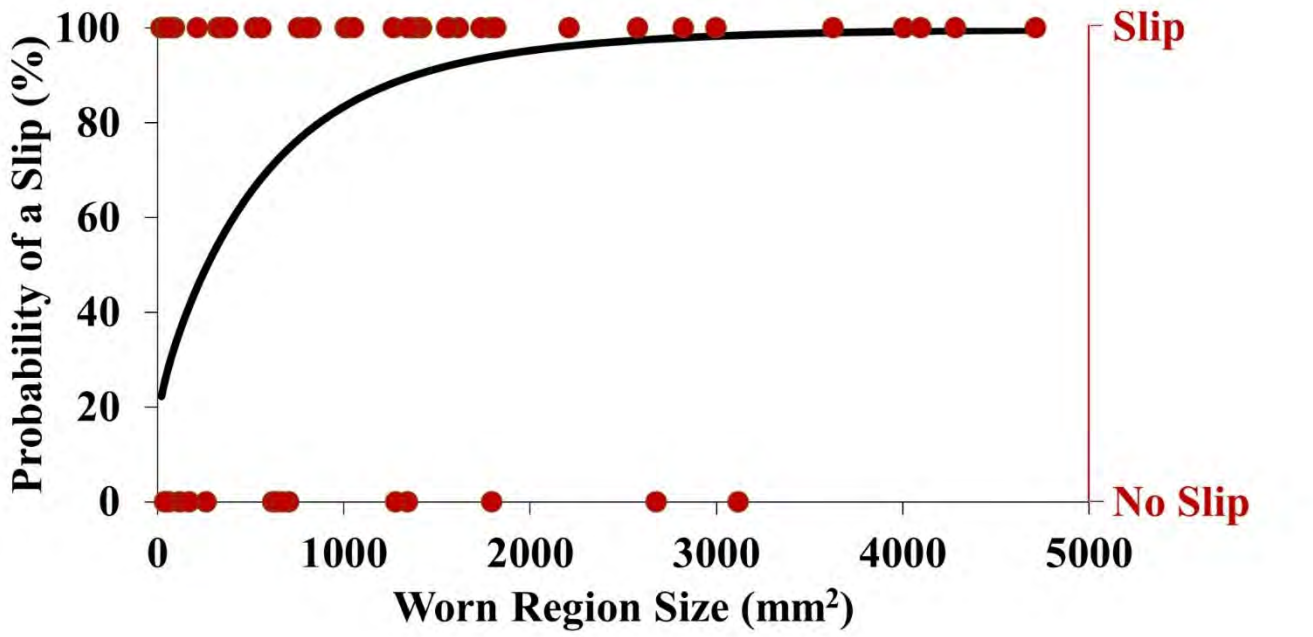

Figure 38. The predicted probability of a slip (solid black line) and the measured slip outcomes (circles) based on the worn region size for all included participants. The predicted line was computed using the model fit for the univariate model (H1B).

H2: Worn Region – Fluid Pressure: The peak hydrodynamic pressure for all shoes, SR shoes, and NSR shoes was 140.1 ± 161.8 kPa, 99.7 ± 148.1 kPa, and 209.3 ± 164.2 kPa, respectively. The size of the worn region was positively correlated to peak fluid pressure ($F_{1,53} = 10.1$, $p = 0.003$) (Figure 39). Slip resistance category (SR vs. NSR) and its interaction with worn region size did not influence fluid pressures.

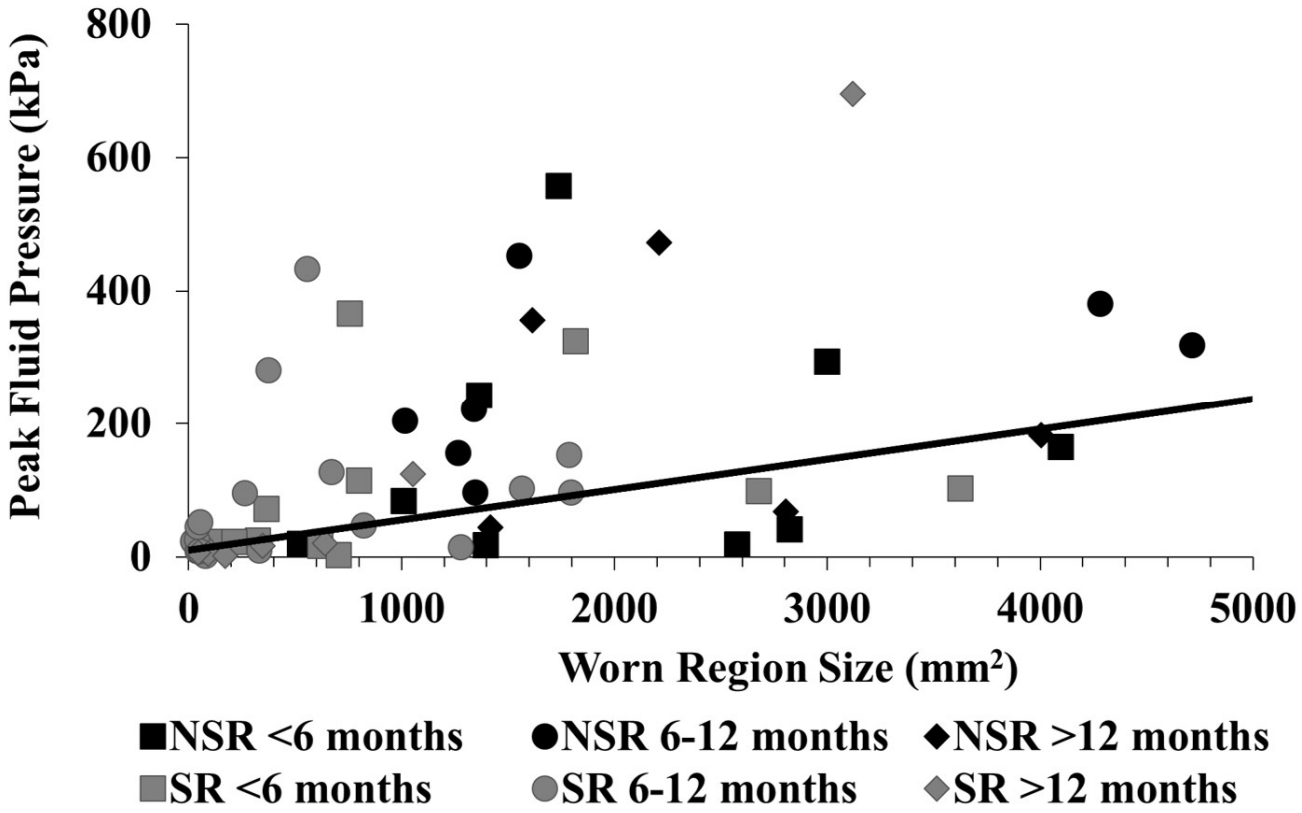

Figure 39. Results from Hypothesis 2: The effect of worn region size on peak fluid pressure. The black lines show the regression fit line. Different markers represent different slip-resistant categories and shoe age.

H3: Fluid Pressure – ACOF: The measured ACOF values for all shoes, SR shoes, and NSR shoes were 0.124±0.069, 0.153 ± 0.065, and 0.077 ± 0.044, respectively. Peak pressures were significantly associated with decreased ACOF ($F_{1,53} = 24.3$, $p < 0.001$) (Figure 40). In addition, SR shoes had a higher ACOF than NSR shoes. The relationship between fluid pressure and ACOF was not influenced by the slip resistance category of the shoe (i.e., no interaction effect was observed).

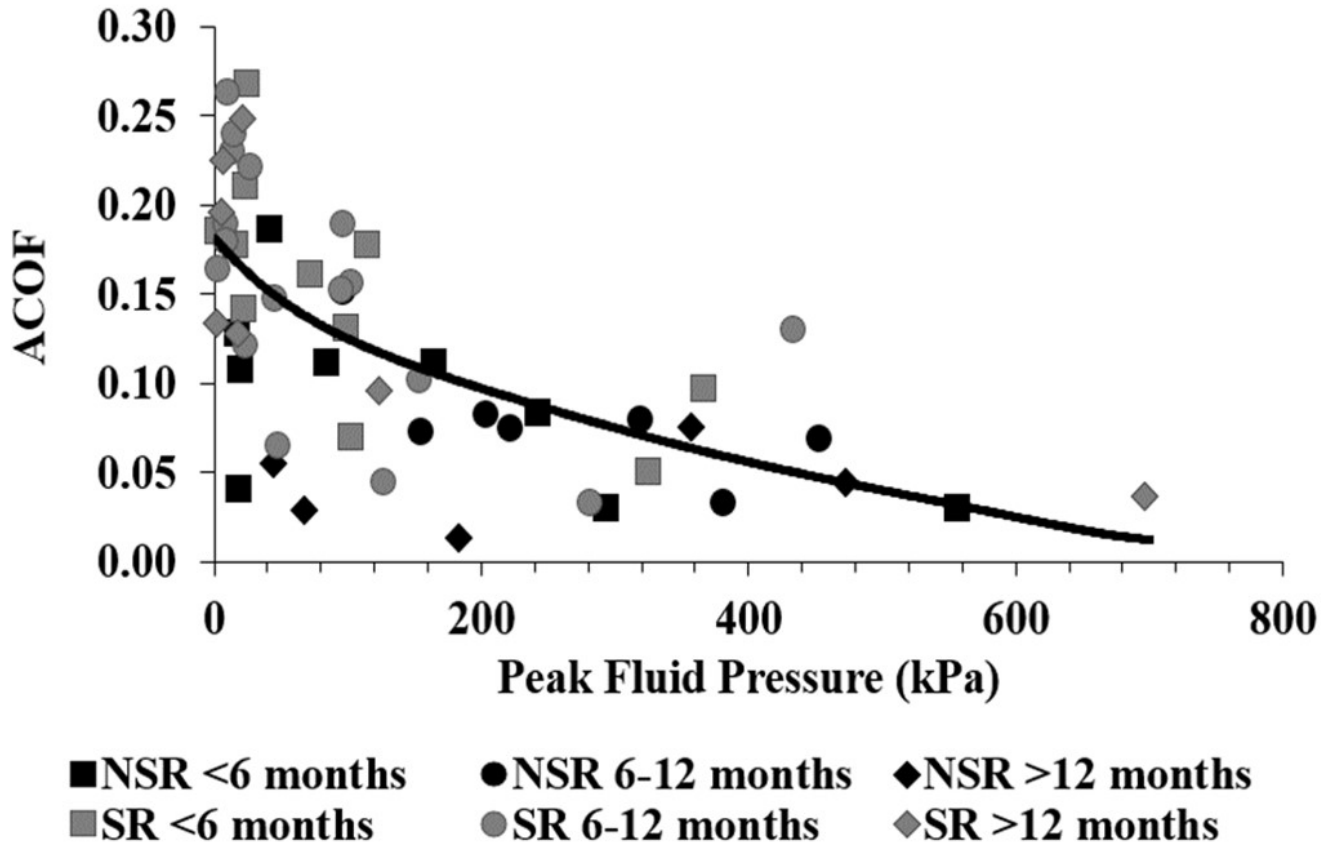

Figure 40. Results from Hypothesis 3: a negative correlation ($p < 0.001$) was observed between peak fluid pressure and ACOF. Different markers represent different slip-resistant categories and shoe age.

H4: ACOF – Slip Outcome: An increase in ACOF was associated with a reduction in slips ($\chi^2_{(1)} = 15.3$, $p < 0.001$). An increase in ACOF of 0.01 was associated with a 21% reduction in chance of slipping odds (Figure 41). Increased RCOF was associated with an increase in slipping.

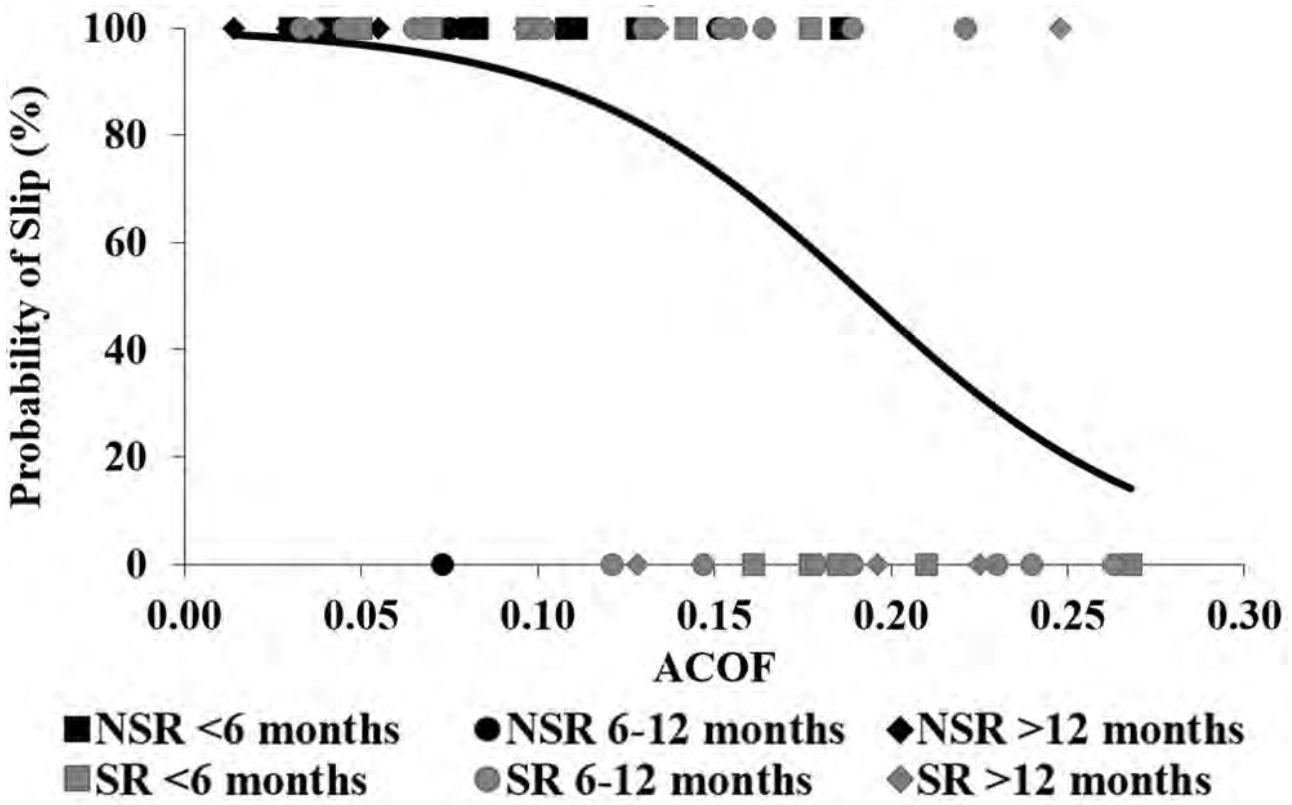

Figure 41. Results from hypothesis 4: slipping was negatively correlated with the ACOF. Different markers represent different slip-resistant categories and shoe age.

F.10.3. Discussion

The results show a positive correlation between the heel worn region size and slip outcome as well as support for the proposed mechanistic model. Specifically, a larger worn region size was associated with higher fluid pressures, which were associated with reduced ACOF. These lower ACOF values were associated with increased likelihood of a slip. Although SR shoes typically had smaller worn regions than NSR shoes, the trends for increased hydrodynamic pressure and slip outcome were observed even when controlling for the slip-resistant shoe category. Importantly, this study demonstrated these trends across a wide range of shoe ages and both slip resistant categories.

The finding that the hydrodynamic pressure increased with an increase in worn region size is consistent with expectations that shoe tread channels mitigate under-shoe fluid pressure and reduce slip risk [28]. The correlation between worn region size and fluid pressure is also consistent with tribology theory; a large worn region size leads to longer pathways for fluid to flow in order to reach the outside of the contact region [85, 116]. Additionally, the results of this study support previous studies that found a decrease in ACOF values with higher peak fluid pressures, resulting in an increased chance of slipping [10, 80]. This increase in fluid pressure causes an increased separation between the shoe and the surface to increase, leading to a decrease in ACOF (Fig.6) [85]. Lastly, the relationship between ACOF and slip risk is consistent with previous research that has consistently demonstrated this empirical relationship especially when RCOF is considered [45, 77, 123, 129].

This study has important occupational and public safety implications. The size of the worn region at the heel is an important parameter to monitor when considering whether worn shoes should be replaced. Worn shoes become less safe as this region becomes larger. Also, a large spread was observed in the size of the worn region and hydrodynamic pressures for each shoe age group (Fig.5). This may indicate that relying on workers' recollection of shoe age may not be as predictive as actual measurements of the worn shoe condition. This empirical relationship can guide a worker's decision to replace worn shoes by tracking the size of the worn region. For example, the size of the worn region

can be compared with a common object (e.g., a AAA or AA battery) to guide when shoes reach a wear level that justifies replacement.

Certain limitations should be acknowledged in this study. First, only a single flooring and lubricant were considered. Previous research has demonstrated a non-linear relationship between flooring topography and under-shoe fluid pressures [141]; however, the interaction between flooring and the worn region on under-shoe hydrodynamics remains largely unknown. While only a single lubricant was considered, hydrodynamic models predict that fluid pressures should scale linearly with viscosity [85]. Thus, higher viscosity contaminants would likely amplify the effects of worn region size on fluid pressures and reduction in ACOF. Lastly, the study utilized a single walking task in a laboratory environment. Confirming the relationship between worn region size and slip risk in authentic occupational environments would confirm the relevance of this parameter to occupational safety programs.

F.10.4. Conclusion

This study highlights the importance of monitoring worn heel region size to mitigate slip risk. The hypotheses (H2-H4) for the mechanistic pathway were supported, consistent with theoretical expectations [10, 28, 37, 45, 80, 123, 129]. A larger worn region in the heel increased peak fluid pressure leading to a decrease in ACOF, which correlated to increased slip risk. The correlation between a larger worn heel region and higher slip risk demonstrates the utility of using worn region for making shoe replacement decisions. As such, the results support the use of worn region size to identify shoes in need of replacement and thus reduce occupational injuries related to slipping.

F.11. Barriers and obstacles impeding progress

Consistent with most research projects, certain unexpected challenges were expected that impeded progress towards the originally planned aims and hypotheses. In addition, certain observations led us to alter our research approach in future experiments. Despite these barriers and obstacles, our research team believes that a substantial amount of progress was made for each aim consistent with the intent of our original proposal.

F.11.1. Accelerated (abrasive) wear methods used instead of adhesive wear methods

The methodology for Aims 1 and 2 were modified from a plan to use a robotic slip-tester in order to simulate wear to a new plan, which used abrasive wear to accelerate the wear process. We were successful in programming our robot to perform simulated steps (documented in previous progress reports) and utilized it to simulate tens of thousands of steps. During this process, however, we discovered that the wear process was too slow. This led us to the conclusion that continuing this approach for wear would not allow us to test enough shoes in order to accomplish the goals of the study. Thus, a separate accelerated wear protocol that relied on material abrasion was developed and utilized for Aims 1 and 2. This method allowed us to assess the impact of shoe design on wear and the impact of shoe wear on friction performance. Unfortunately, this method did not permit testing the impact of floor roughness on wear. Fortunately, other research has recently emerged that has answered the questions regarding how floor roughness influences shoe wear [142]. Thus, this deviation has not had a negative effect on the collective understanding of the mechanics of shoe wear.

F.11.2. Size of the worn region used instead of tread depth for inspecting shoes

We deviated from our plan to develop tread depth thresholds for when worn shoes should be replaced. During our initial experiments, we discovered that shoe tread wears unevenly with some portions of tread wearing away quickly and other portions of tread wearing away slowly. This led to the elimination of tread channels from part of the shoe early in the wear process (Figure 7). However, degradation of friction performance was not observed during this initial wear period. Instead degradation of friction performance and increase in under-shoe fluid pressures were observed as the size of the worn region became larger. Thus, we modified our methods of assessing worn condition from examining tread depth to examining the size of the worn region. This change is believed to be an important paradigm shift in assessing worn shoes.

F.11.3. Fluid model was developed instead of including multiple viscosity and floor roughness conditions

The paradigm shift (that the size of the worn region predicted change in shoe friction performance) described in F.11.2. enabled us to utilize tribology methods that relate lubrication theory to the size of the bearing. Instead of conducting a large number of experiments on different surfaces and different viscosity levels, we developed a model that could be generalized to a wide variety of conditions (See E.7. Study #7). Furthermore, we validated a new ergonomic test (the battery test, See E.3. Study #3). We believe that developing this theory for how worn regions influence friction will promote better generalizability than conducting more experiments since experimental data would have been limited to the conditions included in those experiments.

F.12. References for Scientific Report

1. U.S. Department of Labor- Bureau of Labor Statistics, *Nonfatal Occupational Injuries and Illnesses Requiring Days Away From Work: Table 5. Number, incidence rate, and median days away from work for nonfatal occupational injuries and illnesses involving days away from work by selected injury or illness characteristics and private industry, state government, and local government, 2012*. 2013: Washington, D.C.
2. U.S. Department of Labor- Bureau of Labor Statistics, *Census of Fatal Occupational Injuries Summary: Table 2. Fatal occupational injuries by industry and selected event or exposure, 2012*. 2013: Washington, D.C.
3. Liberty Mutual Research Institute, *Liberty Mutual Workplace Safety Index*. 2012.
4. Courtney, T.K., G.S. Sorock, D.P. Manning, J.W. Collins, and M.A. Holbein-Jenny, *Occupational slip, trip, and fall-related injuries--can the contribution of slipperiness be isolated?* Ergonomics, 2001. **44**(13): p. 1118-37.
5. Burnfield, J.M. and C.M. Powers, *Prediction of slip events during walking: An analysis of utilized coefficient of friction and available slip resistance.* Ergonomics, 2006. **49**(10): p. 982-985.
6. Hanson, J.P., M.S. Redfern, and M. Mazumdar, *Predicting slips and falls considering required and available friction.* Ergonomics, 1999. **42**(12): p. 1619-1633.
7. Chang, W.R., R. Gronqvist, S. Leclercq, R.J. Brungraber, U. Mattke, L. Strandberg, S.C. Thorpe, R. Myung, L. Makkonen, and T.K. Courtney, *The role of friction in the measurement of slipperiness, Part 2: survey of friction measurement devices.* Ergonomics, 2001. **44**(13): p. 1233-61.
8. Powers, C.M., J.R. Brault, M.A. Stefanou, Y.J. Tsai, J. Flynn, and G.P. Siegmund, *Assessment of Walkway Tribometer Readings in Evaluating Slip Resistance: A Gait-Based Approach.* Journal of forensic sciences, 2007. **52**(2): p. 400-405.
9. Ricotti, R., M. Delucchi, and G. Cerisola, *A comparison of results from portable and laboratory floor slipperiness testers.* International Journal of Industrial Ergonomics, 2009. **39**(2): p. 353-357.
10. Beschorner, K., M. Lovell, C.F. Higgs III, and M.S. Redfern, *Modeling Mixed-Lubrication of a Shoe-Floor Interface Applied to a Pin-on-Disk Apparatus.* Tribology Transactions, 2009. **52**(4): p. 560-568.
11. Mirhassani Moghaddam, S.R., *Finite Element Analysis of Contribution of Adhesion and Hysteresis to Shoe-floor Friction.* 2013.
12. Moore, C.T., P.L. Menezes, M. Lovell, and K. Beschorner, *Analysis of Shoe Friction During Sliding Against Floor Material: Role of Fluid Contaminant.* Journal of Tribology, 2012. **134**: p. 041104.
13. Strobel, C.M., P.L. Menezes, M. Lovell, and K. Beschorner, *Analysis of the Contribution of Adhesion and Hysteresis to Shoe-Floor Lubricated Friction in the Boundary Lubrication Regime.* Tribology Letters, 2012. **46**(3): p. 341-7.
14. Anderson, D., C. Franck, and M. Madigan, *Age differences in the required coefficient of friction during level walking do not exist when experimentally-controlling speed and step length.* Journal of Applied Biomechanics, 2014. **30**(4): p. 542-546.

15. Chambers, A.J. and R. Cham, *Slip-related muscle activation patterns in the stance leg during walking.* Gait & Posture, 2007. **25**(4): p. 565-572.
16. Lancaster, J.K., *Chapter 14: Friction and Wear*, in *Polymer Science, A Materials Science Handbook*, A.D. Jenkins, Editor. 1972, North Holland Publishing.
17. Moyer, B., M. Redfern, and R. Cham, *Biomechanics of trailing leg response to slipping-Evidence of interlimb and intralimb coordination.* Gait & posture, 2009. **29**(4): p. 565-570.
18. Tang, P.-F. and M.H. Woollacott, *Inefficient postural responses to unexpected slips during walking in older adults.* The Journals of Gerontology Series A: Biological Sciences and Medical Sciences, 1998. **53**(6): p. M471-M480.
19. Bell, J.L., J.W. Collins, L. Wolf, R. Grönqvist, S. Chiou, W.R. Chang, G.S. Sorock, T.K. Courtney, D.A. Lombardi, and B. Evanoff, *Evaluation of a comprehensive slip, trip and fall prevention programme for hospital employees∗∗.* Ergonomics, 2008. **51**(12): p. 1906-1925.
20. Lewis, R., *Pier 1's slip-and-fall success.* Occupational Health & Safety, 1997. **66**(8): p. 34-38.
21. Verma, S.K., W.R. Chang, T.K. Courtney, D.A. Lombardi, Y.H. Huang, M.J. Brennan, M.A. Mittleman, J.H. Ware, and M.J. Perry, *A prospective study of floor surface, shoes, floor cleaning and slipping in US limited-service restaurant workers.* Occupational and environmental medicine, 2011. **68**(4): p. 279.
22. Beschorner, K.E. and G. Singh. *A novel method for evaluating the effectiveness of shoe-tread designs relevant to slip and fall accidents*. in *Proceedings of the Human Factors and Ergonomics Society Annual Meeting*. 2012. SAGE Publications.
23. Gronqvist, R., *Mechanisms of friction and assessment of slip resistance of new and used footwear soles on contaminated floors.* Ergonomics, 1995. **38**(2): p. 224-241.
24. Chiou, S.-y., A. Bhattacharya, and P.A. Succop, *Effect of workers' shoe wear on objective and subjective assessment of slipperiness.* American Industrial Hygiene Association Journal, 1996. **57**(9): p. 825-831.
25. Bentley, T. and R. Haslam, *Identification of risk factors and countermeasures for slip, trip and fall accidents during the delivery of mail.* Applied Ergonomics, 2001. **32**(2): p. 127-134.
26. Bentley, T., D. Tappin, D. Moore, S. Legg, L. Ashby, and R. Parker, *Investigating slips, trips and falls in the New Zealand dairy farming sector.* Ergonomics, 2005. **48**(8): p. 1008-1019.
27. Verma, S.K., Z. Zhao, T.K. Courtney, W.-R. Chang, D.A. Lombardi, Y.-H. Huang, M.J. Brennan, and M.J. Perry, *Duration of slip-resistant shoe usage and the rate of slipping in limited-service restaurants: results from a prospective and crossover study.* Ergonomics, 2014(ahead-of-print): p. 1-8.
28. Beschorner, K.E., D.L. Albert, A.J. Chambers, and M.S. Redfern, *Fluid pressures at the shoe–floor–contaminant interface during slips: Effects of tread & implications on slip severity.* Journal of Biomechanics, 2014. **47**(2): p. 458-463.
29. Singh, G. and K.E. Beschorner, *A Method for Measuring Hydrodynamic Lubrication in the Shoe-Floor-Fluid Interface: Application to Shoe Tread Evaluation.* IIE Transactions on Occupational Ergonomics and Human Factors, 2014. **2**: p. 53-59.
30. Kim, I.-J., *Development of a new analyzing model for quantifying pedestrian slip resistance characteristics: part II—Experiments and validations.* International Journal of Industrial Ergonomics, 2004. **33**(5): p. 403-414.
31. Kim, I.J. *Wear Progression of Shoe Heels during Slip Resistance Measurements*. in *Proceedings of the Human Factors and Ergonomics Society Annual Meeting*. 2000. SAGE Publications.
32. Tudor-Locke, C. and D.R. Bassett Jr, *How many steps/day are enough?* Sports Medicine, 2004. **34**(1): p. 1-8.
33. Archard, J., *Contact and rubbing of flat surfaces.* Journal of applied physics, 1953. **24**(8): p. 981-988.
34. Békési, N. and K. Váradi, *Wear simulation of a reciprocating seal by global remeshing.* Periodica Polytechnica, Mechanical Engineering, 2010. **54**(2): p. 71-75.
35. Lupker, H., F. Cheli, F. Braghin, E. Gelosa, and A. Keckman, *Numerical prediction of car tire wear.* Tire Science and Technology, 2004. **32**(3): p. 164-186.

36. Maxian, T.A., T.D. Brown, D.R. Pedersen, and J.J. Callaghan, *3-Dimensional sliding/contact computational simulation of total hip wear.* Clinical orthopaedics and related research, 1996. **333**: p. 41-50.
37. Hemler, S., D. Charbonneau, A. Iraqi, M.S. Redfern, J.M. Haight, B.E. Moyer, and K.E. Beschorner, *Changes in Under-Shoe Traction and Fluid Drainage for Progressively Worn Shoe Tread.* Applied ergonomics, 2019. **80**(October 2019): p. 35-42.
38. Hemler, S.L., D.N. Charbonneau, and K.E. Beschorner. *Effects of Shoe Wear on Slipping–Implications for Shoe Replacement Threshold*. in *Proceedings of the Human Factors and Ergonomics Society Annual Meeting*. 2017. SAGE Publications Sage CA: Los Angeles, CA.
39. ISO/IEC, *ISO 20871:2001 Footwear - Test methods for outsoles - Abrasion resistance*. 2001, ISO/IEC: Geneva, Switzerland.
40. Manning, D., C. Jones, and M. Bruce, *Proof of shoe slip-resistance by a walking traction test.* Journal of Occupational Accidents, 1990. **12**(4): p. 255-270.
41. Kadaba, M.P., H. Ramakrishnan, and M. Wootten, *Measurement of lower extremity kinematics during level walking.* Journal of orthopaedic research, 1990. **8**(3): p. 383-392.
42. ASTM, American Society for Testing and Materials, *ASTM D2240-15: Standard Test Method for Rubber Property-Durometer Hardness*. 2015, ASTM International.
43. Moghaddam, S.R.M., S.L. Hemler, M.S. Redfern, T.D. Jacobs, and K.E. Beschorner, *Computational model of shoe wear progression: Comparison with experimental results.* Wear, 2019. **422**: p. 235-241.
44. Aschan, C., M. Hirvonen, T. Mannelin, and E. Rajamäki, *Development and validation of a novel portable slip simulator.* Applied ergonomics, 2005. **36**(5): p. 585-593.
45. Iraqi, A., R. Cham, M.S. Redfern, and K.E. Beschorner, *Coefficient of friction testing parameters influence the prediction of human slips.* Applied ergonomics, 2018. **70**: p. 118-126.
46. Jones, T.G., A. Iraqi, and K.E. Beschorner, *Performance testing of work shoes labeled as slip resistant.* Applied ergonomics, 2018. **68**: p. 304-312.
47. Albert, D.L., B. Moyer, and K.E. Beschorner, *Three-Dimensional Shoe Kinematics During Unexpected Slips: Implications for Shoe–Floor Friction Testing.* IISE Transactions on Occupational Ergonomics and Human Factors, 2017. **5**(1): p. 1-11.
48. ASTM, American Society for Testing and Materials, *ASTM F2913-11: Standard Test method for Measuring the Coefficient of Friction for Evaluation of Slip performance of Footwear and Test Surfaces/Flooring Using a Whole Shoe Tester*. 2011, ASTM International: West Conshohocken, PA.
49. Iraqi, A. and K.E. Beschorner. *Vertical Ground Reaction Forces During Unexpected Human Slips*. in *Proceedings of the Human Factors and Ergonomics Society Annual Meeting*. 2017. SAGE Publications Sage CA: Los Angeles, CA.
50. Iraqi, A., R. Cham, M.S. Redfern, N.S. Vidic, and K.E. Beschorner, *Kinematics and Kinetics of the Shoe during Human Slips.* Journal of Biomechanics, 2018. **74**: p. 57-63.
51. Singh, G. and K.E. Beschorner, *A Method for Measuring Fluid Pressures in the Shoe–Floor–Fluid Interface: Application to Shoe Tread Evaluation.* IIE Transactions on Occupational Ergonomics and Human Factors, 2014. **2**(2): p. 53-59.
52. Moghaddam, S.R.M., A. Iraqi, and K.E. Beschorner, *Finite Element Model of Wear Progression in Shoe Soles*, in *STLE Tribology Frontiers Conference*. 2014: Chicago.
53. Moghaddam, S.R.M., *Computational Models for Predicting Shoe Friction and Wear*, in *Swanson School of Engineering*. 2018, University of Pittsburgh. p. 147.
54. Verma, S.K., Z. Zhao, T.K. Courtney, W.-R. Chang, D.A. Lombardi, Y.-H. Huang, M.J. Brennan, and M.J. Perry, *Duration of slip-resistant shoe usage and the rate of slipping in limited-service restaurants: results from a prospective and crossover study.* Ergonomics, 2014. **57**(12): p. 1919-1926.
55. Beschorner, K.E., M. Lovell, C.F. Higgs III, and M.S. Redfern, *Modeling mixed-lubrication of a shoe-floor interface applied to a pin-on-disk apparatus.* Tribology Transactions, 2009. **52**(4): p. 560-568.
56. Imbimbo, M. and A. De Luca, *FE stress analysis of rubber bearings under axial loads.* Computers & structures, 1998. **68**(1): p. 31-39.

57. Sridharan, K. and R. Sivaramakrishnan, *Dynamic behavior of tyre tread block.* American Journal of Engineering and Applied Sciences, 2012. **5**(2).
58. Yamaguchi, T., Y. Katsurashima, and K. Hokkirigawa, *Effect of rubber block height and orientation on the coefficients of friction against smooth steel surface lubricated with glycerol solution.* Tribology International, 2017. **110**: p. 96-102.
59. Maegawa, S., F. Itoigawa, and T. Nakamura, *A role of friction-induced torque in sliding friction of rubber materials.* Tribology International, 2016. **93**: p. 182-189.
60. ShoesForCrews. *Shoe Care and Cleaning Tips. Accessed 18 January 2019.* 2019 [cited 2019 18 January]; Available from: https://www.shoesforcrews.com/sfc3/index.cfm?changeWebsite=US_en&route=inserts.QA/cleaning_caring.
61. Hemler, S.L., D.N. Charbonneau, A. Iraqi, M.S. Redfern, J.M. Haight, B.E. Moyer, and K.E. Beschorner, *Changes in under-shoe traction and fluid drainage for progressively worn shoe tread.* Applied Ergonomics, 2019. **80**: p. 35-42.
62. ASTM, *D2240, Standard test method for rubber property-Durometer hardness.* 2000. **18**.
63. Jones, T., A. Iraqi, and K. Beschorner, *Performance testing of work shoes labeled as slip resistant.* Applied ergonomics, 2018. **68**: p. 304-312.
64. Hemler, S.L., D.N. Charbonneau, and K.E. Beschorner, *Predicting hydrodynamic conditions under worn shoes using the tapered-wedge solution of Reynolds equation.* Tribology International, 2020. **145**: p. 106161.
65. Sundaram, V.H., S.L. Hemler, A. Chanda, J.M. Haight, M.S. Redfern, and K.E. Beschorner, *Worn Region Size of Shoe Outsole Impacts Human Slips: Testing a Mechanistic Model.* Journal of Biomechanics, 2020: p. 109797.
66. Hemler, S.L., M.S. Redfern, J.M. Haight, and K.E. Beschorner. *Influence of Natural Wear Progression on Shoe Floor Traction–A Pilot Study*. in *Proceedings of the Human Factors and Ergonomics Society Annual Meeting*. 2018. SAGE Publications Sage CA: Los Angeles, CA.
67. Tsai, Y.J. and C.M. Powers, *The Influence of Footwear Sole Hardness on Slip Initiation in Young Adults*.* Journal of forensic sciences, 2008. **53**(4): p. 884-888.
68. Moghaddam, S.R.M., A. Acharya, M.S. Redfern, and K.E. Beschorner, *Predictive multiscale computational model of shoe-floor coefficient of friction.* Journal of biomechanics, 2018. **66**: p. 145-152.
69. Iraqi, A., N.S. Vidic, M.S. Redfern, and K.E. Beschorner, *Prediction of coefficient of friction based on footwear outsole features.* Applied ergonomics, 2020. **82**: p. 102963.
70. Hakami, F., A. Pramanik, A. Basak, and N. Ridgway, *Elastomers' wear: Comparison of theory with experiment.* Tribology International, 2019. **135**: p. 46-54.
71. Beschorner, K.E., M.S. Redfern, W.L. Porter, and R.E. Debski, *Effects of slip testing parameters on measured coefficient of friction.* Applied ergonomics, 2007. **38**(6): p. 773-780.
72. Beschorner, K.E., T.G. Jones, and A. Iraqi. *The Combined Benefits of Slip-Resistant Shoes and High Traction Flooring on Coefficient of Friction Exceeds Their Individual Contributions*. in *Proceedings of the Human Factors and Ergonomics Society Annual Meeting*. 2017. SAGE Publications Sage CA: Los Angeles, CA.
73. Beschorner, K.E., J.L. Siegel, S.L. Hemler, V.H. Sundaram, A. Chanda, A. Iraqi, J.M. Haight, and M.S. Redfern, *An observational ergonomic tool for assessing the worn condition of slip-resistant shoes.* Applied Ergonomics, 2020. **88**: p. 103140.
74. National Electrical Manufacturers Association/American National Standards Institute, *ANSI C18.1M, Part 1: American National Standard for Portable Primary Cells and Batteries with Aqueous Electrolyte—General and Specifications*. 2015: Arlington, VA.
75. Hemler, S.L., E.M. Pliner, M.S. Redfern, J.M. Haight, and K.E. Beschorner, *Traction performance across the life of slip-resistant footwear: preliminary results from a longitudinal study.* Journal of Safety Research, 2020. **74**: p. 219-225.
76. Sundaram, V.H., S.L. Hemler, A. Chanda, J.M. Haight, M.S. Redfern, and K.E. Beschorner, *Worn Region Size of Shoe Soles Impacts Human Slips: Testing a Mechanistic Model.* Journal of Biomechanics, 2020: p. 109797.

77. Hemler, S. and K.E. Beschorner. *Effects of Shoe Wear on Slipping – Implications for Shoe Replacement Threshold*. in *Human Factors and Ergonomics Society*. 2017. Austin, TX.
78. Marras, W.S. and W. Karwowski, *Fundamentals and assessment tools for occupational ergonomics*. 2006: CRC Press.
79. Hemler, S.L., J. Sider, and K.E. Beschorner. *Influence of required coefficient of friction on rate of shoe wear*. in *International Society of Posture and Gait Research*. 2019. Edinburgh, Scotland.
80. Beschorner, K.E. and G. Singh. *A Novel Method for Evaluating the Effectiveness of Shoe-Tread Designs Relevant to Slip and Fall Accidents*. in *Human Factors and Ergonomics Society*. 2012. Boston, MA.
81. Hemler, S.L., M.S. Redfern, J.M. Haight, and K.E. Beschorner. *Influence of Natural Wear Progression on Shoe Floor Traction – A Pilot Study*. in *Proceedings of the Human Factors and Ergonomics Society Annual Meeting*. 2018. Philadelphia, PA: Sage Publications.
82. Singh, G. and K.E. Beschorner, *A Method for Measuring Fluid Pressures in the Shoe-Floor-Fluid Interface: Application to Shoe Tread Evaluation.* IIE Transactions on Occupational Ergonomics and Human Factors, 2014. **2**(2): p. 53-59.
83. Beschorner, K.E., V. Sundaram, and S.L. Hemler. *Size of worn region predicts fluid pressures during human slips*. in *Society of Tribologists and Lubrication Engineers Annual Meeting*. 2019. Nashville, TN.
84. Redfern, M.S., R. Cham, K. Gielo-Perczak, R. Grönqvist, M. Hirvonen, H. Lanshammar, M. Marpet, C.Y.-C. Pai IV, and C. Powers, *Biomechanics of slips.* Ergonomics, 2001. **44**(13): p. 1138-1166.
85. Hamrock, B.J., S.R. Schmid, and B.O. Jacobson, *Fundamentals of fluid film lubrication*. 2004: CRC press.
86. Moghaddam, S.R.M., A. Acharya, M.S. Redfern, and K.E. Beschorner, *Predictive multiscale computational model of shoe-floor coefficient of friction original article.* Journal of biomechanics, 2017.
87. Békési, N. and K. Váradi, *Wear simulation of a reciprocating seal by global remeshing.* Periodica Polytechnica. Engineering. Mechanical Engineering, 2010. **54**(2): p. 71.
88. Mukras, S., N.H. Kim, W.G. Sawyer, D.B. Jackson, and L.W. Bergquist, *Numerical integration schemes and parallel computation for wear prediction using finite element method.* Wear, 2009. **266**(7-8): p. 822-831.
89. Gent, A.N., *On the relation between indentation hardness and Young's modulus.* Rubber Chemistry and Technology, 1958. **31**(4): p. 896-906.
90. Giacomin, A. and A. Mix, *Standardized polymer durometry.* Journal of Testing and evaluation, 2011. **39**(4): p. 1-10.
91. Centeno Gil, O.J., *Finite Element Modeling of Rubber Bushing for Crash Simulation-Experimental Tests and Validation.* 2009.
92. Suh, J.B., *Stress analysis of rubber blocks under vertical loading and shear loading*. 2007, University of Akron.
93. Erhart, T., *Review of solid element formulations in LS-DYNA.* LS-DYNA Entwicklerforum, 2011.
94. Bonet, J. and A. Burton, *A simple average nodal pressure tetrahedral element for incompressible and nearly incompressible dynamic explicit applications.* Communications in Numerical Methods in Engineering, 1998. **14**(5): p. 437-449.
95. Guide, A.M.U.s., *Rel. 14.5.* ANSYS Inc, 2012.
96. Cham, R. and M.S. Redfern, *Changes in gait when anticipating slippery floors.* Gait & posture, 2002. **15**(2): p. 159-171.
97. ISO/IEC, *ISO 20871:2001 Footwear - Test methods for outsoles - Abrasion resistance*. 2001, ISO/IEC: Geneva, Switzerland.
98. ASTM, *D2240, Test Method for Rubber Property–Durometer Hardness*. 2010, ASTM International.
99. Facey, O., I. Hannah, and D. Rosen, *Shoe wear patterns and pressure distribution under feet and shoes, determined by image analysis.* Journal of the Forensic Science Society, 1992. **32**(1): p. 15-25.

100. Söderberg, A. and S. Andersson, *Simulation of wear and contact pressure distribution at the pad-to-rotor interface in a disc brake using general purpose finite element analysis software.* Wear, 2009. **267**(12): p. 2243-2251.
101. Békési, N., K. Váradi, and D. Felhős, *Wear simulation of a reciprocating seal.* Journal of Tribology, 2011. **133**(3): p. 031601.
102. Podra, P. and S. Andersson, *Simulating sliding wear with finite element method.* Tribology international, 1999. **32**(2): p. 71-81.
103. Békési, N., *Modelling Friction and Abrasive Wear of Elastomers*, in *Advanced Elastomers-Technology, Properties and Applications*. 2012, InTech.
104. Békési, N., *Friction and wear of elastomers and sliding seals.* Budapest University of Technology and Economics, Budapest, 2011.
105. Lhymn, C. and Y. Lhymn, *Friction and wear of rubber/epoxy composites.* Journal of materials science, 1989. **24**(4): p. 1252-1256.
106. Padenko, E., P. Berki, B. Wetzel, and J. Karger-Kocsis, *Mechanical and abrasion wear properties of hydrogenated nitrile butadiene rubber of identical hardness filled with carbon black and silica.* Journal of Reinforced Plastics and Composites, 2016. **35**(1): p. 81-91.
107. Ludema, K., *Mechanism-based modeling of friction and wear.* Wear, 1996. **200**(1-2): p. 1-7.
108. Meng, H. and K. Ludema, *Wear models and predictive equations: their form and content.* Wear, 1995. **181**: p. 443-457.
109. Albert, D., B. Moyer, and K.E. Beschorner, *Three-Dimensional Shoe Kinematics During Unexpected Slips: Implications for Shoe–Floor Friction Testing.* IISE Transactions on Occupational Ergonomics and Human Factors, 2017. **5**(1): p. 1-11.
110. Trkov, M., J. Yi, T. Liu, and K. Li. *Shoe-floor interactions during human slip and fall: Modeling and experiments*. in *ASME 2014 Dynamic Systems and Control Conference*. 2014. American Society of Mechanical Engineers.
111. Moghaddam, S.R.M., A. Acharya, and K.E. Beschorner. *Multi-Scale Finite Element Model for Predicting Hysteresis Coefficient of Friction of Slip-Resistant Shoes*. in *2016 STLE Annual Meeting & Exhibition*. 2016.
112. Moghaddam, S.R.M. and K.E. Beschorner, *Multiscale Computational Modeling of Shoe-Floor Friction.* American Society of Biomechanics. Columbus, OH, 2015.
113. Moghaddam, S., A. Iraqi, and K. Beschorner. *Finite Element Model of Wear Progression in Shoe Soles*. in *STLE Tribology Frontiers Conference*. 2014.
114. Hemler, S., D. Charbonneau, and K. Beschorner, *Predicting hydrodynamic conditions under worn shoes using the tapered-wedge solution of Reynolds equation.* Tribology International, 2020. **145**: p. 106161.
115. Moghaddam, S.R.M., S.L. Hemler, M.S. Redfern, T.D. Jacobs, and K.E. Beschorner, *Computational Model of Shoe Wear Progression: Comparison with Experimental Results.* Wear, 2019.
116. Fuller, D.D., *Theory and practice of lubrication for engineers*. 1956: Wiley New York.
117. Proctor, T.D. and V. Coleman, *Slipping, tripping and falling accidents in Great Britain—present and future.* Journal of Occupational Accidents, 1988. **9**(4): p. 269-285.
118. Stachowiak, G. and A.W. Batchelor, *Engineering Tribology*. 2013, Oxford, UNITED STATES: Elsevier Science & Technology.
119. Chanda, A., T.G. Jones, and K.E. Beschorner, *Generalizability of Footwear Traction Performance across Flooring and Contaminant Conditions.* IISE Transactions on Occupational Ergonomics and Human Factors, 2018(just-accepted): p. 1-23.
120. Chanda, A., A. Reuter, and K.E. Beschorner, *Vinyl Composite Tile Surrogate for Mechanical Slip Testing.* IISE Transactions on Occupational Ergonomics and Human Factors, 2019. **7**(2): p. 132-141.
121. Dwyer-Joyce, R., B. Drinkwater, and C. Donohoe, *The measurement of lubricant–film thickness using ultrasound.* Proceedings of the Royal Society of London. Series A: Mathematical, Physical and Engineering Sciences, 2003. **459**(2032): p. 957-976.
122. Hunter, J.G., R.H. Miller, and S. Suydam. *Accuracy of a shoe-worn device to measure running mechanics*. 2017.

123. Burnfield, J.M. and C.M. Powers, *Prediction of slips: an evaluation of utilized coefficient of friction and available slip resistance.* Ergonomics, 2006. **49**(10): p. 982-995.
124. Beschorner, K.E., A. Iraqi, M.S. Redfern, B.E. Moyer, and R. Cham, *Influence of Averaging Time Interval on Shoe-Floor-Contaminant Coefficient of Friction Measurements.* Applied Ergonomics, In review, 2019.
125. Hemler, S.L., V.H. Sundaram, and K.E. Beschorner. *A hydrodynamics model to predict under-shoe fluid pressures based on the dimensions of a worn region*. in *American Society of Biomechanics*. 2020. Virtual online.
126. Grönqvist, R., *Mechanisms of friction and assessment of slip resistance of new and used footwear soles on contaminated floors.* Ergonomics, 1995. **28**: p. 224-241.
127. Sundaram, V., S.L. Hemler, A. Chanda, J.M. Haight, M.S. Redfern, and K.E. Beschorner, *Worn Region Size of Shoe Soles Impacts Human Slips: Testing a Mechanistic Model.* Journal of biomechanics, 2020: p. 109797.
128. Hemler, S.L., E.M. Pliner, M.S. Redfern, J.M. Haight, and K.E. Beschorner, *Traction performance across the life of slip-resistant footwear: preliminary results from a longitudinal study.* Journal of Safety Research., 2020.
129. Beschorner, K.E., D.L. Albert, and M.S. Redfern, *Required coefficient of friction during level walking is predictive of slipping.* Gait & posture, 2016. **48**: p. 256-260.
130. Sundaram, V.H., S.L. Hemler, A. Chanda, J.M. Haight, M.S. Redfern, and K.E. Beschorner, *Worn Region Size of Shoe Outsole Impacts Human Slips: Testing a Mechanistic Model.* Journal of Biomechanics, 2020. **105**(109797).
131. Hemler, S.L., V.H. Sundaram, and K.E. Beschorner. *Influence of slip-resistant shoe classification and shoe age on under-shoe hydrodynamics during human slips*. in *International Society of Biomechanics & American Society of Biomechanics*. 2019. Calgary, Alberta, Canada.
132. Mars, W.V. and A. Fatemi, *A literature survey on fatigue analysis approaches for rubber.* International Journal of fatigue, 2002. **24**(9): p. 949-961.
133. De, S.K. and J.R. White, *Rubber technologist's handbook*. Vol. 1. 2001: iSmithers Rapra Publishing.
134. Moyer, B., *Slip and Fall Risks: Pre-Slip Gait Contributions and Post-Slip Response Effects*. 2006, University of Pittsburgh: Pittsburgh.
135. Beschorner, K.E., A. Iraqi, M.S. Redfern, R. Cham, and Y. Li, *Predicting slips based on the STM 603 whole-footwear tribometer under different coefficient of friction testing conditions.* Ergonomics, 2019. **62**(5): p. 668-681.
136. Chang, W.-R., C.-C. Chang, and S. Matz, *The effect of transverse shear force on the required coefficient of friction for level walking.* Human Factors: The Journal of the Human Factors and Ergonomics Society, 2011. **53**(5): p. 461-473.
137. Albert, D.L., B. Moyer, and K.E. Beschorner, *Three-dimensional shoe kinematics during unexpected slips: Implications for shoe-floor friction testing.* IIE: Transactions on Occupational Ergonomics and Human Factors, 2017. **5**(1): p. 1-11.
138. Cham, R. and M.S. Redfern, *Heel contact dynamics during slip events on level and inclined surfaces.* Safety Science, 2002. **40**(7-8): p. 559-576.
139. Aschan, C., M. Hirvonen, T. Mannelin, and R. E., *Development and validation of a novel portable slip simulator.* Applied Ergonomics, 2005. **36**: p. 585-593.
140. Chanda, A., T.G. Jones, and K.E. Beschorner, *Generalizability of Footwear Traction Performance across Flooring and Contaminant Conditions.* IISE Transactions on Occupational Ergonomics and Human Factors, 2018. **6**(2): p. 98-108.
141. Iraqi, A., *Comparison of Interfacial Fluid Pressures Generated across Common Shoe-Floor Friction Testing Apparatuses*, in *Department of Mechanical Engineering*. 2013, Blekinge Institute of Technology: Karlskrona, Sweden.
142. Sato, S., T. Yamaguchi, K. Shibata, T. Nishi, K. Moriyasu, K. Harano, and K. Hokkirigawa, *Dry sliding friction and Wear behavior of thermoplastic polyurethane against abrasive paper.* Biotribology, 2020: p. 100130.

G.Publications

G.1. Journal Article:

1. Hemler, SL, Pliner, EM, Redfern, MS, Haight, JM, Beschorner, KE: [2020] Traction performance across the life of slip-resistant footwear: preliminary results from a longitudinal study. Journal of Safety Research, 74, 219-225. NIHMS ID: 1610100.
2. Iraqi, A, Vidic, N, Redfern, MS, Beschorner, KE: [2020] Prediction of coefficient of friction based on footwear outsole features. Applied Ergonomics, 80, 102963, Pubmed ID: PMC7365588.
3. Beschorner, KE, Siegel, JL, Hemler, SL, Sundaram, VH, Chanda, A, Iraqi, A, Haight, JM, Redfern, MS: [2020] An observational ergonomic tool for assessing the worn condition of slip-resistant shoes. Applied Ergonomics, 88, 103140. NIHMS ID: 1595192.
4. Sundaram, VH, Hemler, SL, Chanda, A, Haight, JM, Redfern, MS, Beschorner, KE: [2020] Worn Region Size of Shoe Soles Impacts Human Slips: Testing a Mechanistic Model. Journal of Biomechanics 105, 109797. NIHMS ID: 1588580
5. Hemler, SL, Charbonneau, D, Beschorner, KE: [2020] Predicting Hydrodynamic Conditions under Worn Shoes using the Tapered-Wedge Solution of Reynolds Equation. Tribology International, 145, 106161. NIHMS ID: 1549719
6. Beschorner, KE, Iraqi, A, Redfern, MS, Moyer, BE, Cham, R: [2020] Influence of Averaging Time Interval on Shoe-Floor-Contaminant Coefficient of Friction Measurements. Applied Ergonomics, 80, 102959. Pubmed ID: PMC6922306.
7. Hemler, SL, Charbonneau, DN, Iraqi, A, Redfern, MS, Haight, JM, Moyer, BE, Beschorner, KE: [2019] Changes in Under-Shoe Traction and Fluid Drainage for Progressively Worn Shoe Tread – Implications for Replacement Threshold. Applied Ergonomics, 80, 35-42. Pubmed ID: PMC6659727.
8. Chanda, A., Reuter, A., Beschorner, KE: [2019] Vinyl Composite Tile (VCT) Surrogate for Mechanical Slip Testing. IISE: Occupational Ergonomics and Human Factors, 7 (2), 132-141. NIHMS ID: 1549719.
9. Hemler, SL, Charbonneau, DN, Iraqi, A, Redfern, MS, Haight, JM, Moyer, BE, Beschorner, KE, 2019, Changes in Under-Shoe Traction and Fluid Drainage for Progressively Worn Shoe Tread – Implications for Replacement Threshold, Applied Ergonomics, 80, 35-42. Pubmed ID: PMC6659727.
10. Beschorner, KE, Iraqi, A, Redfern, MS, Cham, R, Li, Y: [2019] Predicting slips for the SATRA STM 603 whole-shoe tribometer under different coefficient of friction testing conditions. Ergonomics, 62 (5), 668-681, Pubmed ID: PMC7365591.
11. Chanda, A, Jones, TG, Beschorner, KE: [2018] Generalizability of Footwear Traction Performance across Flooring and Contaminant Conditions. IISE: Occupational Ergonomics and Human Factors 6, 98-108. Pubmed ID: PMC6860024.

G.2. Proceedings:

1. Bharthi, R, Sukinik, J, Hemler, SL, Beschorner, KE: [2020] Correlation between the locations of shoe wear region and center of the contact region at peak friction, Proc of 2020 Biomedical Engineering Society, Online, October 14-17.
2. Sukinik, J, Bharthi, R, Hemler, SL, Beschorner, KE: [2020] Relationship between center of pressure and contact region during gait: implications for shoe wear and slipping risk, Proc of 2020Biomedical Engineering Society, Online, October 14-17.
3. Beschorner, KE, Hemler, SL, Moghaddam, SRM, Iraqi, A, Redfern, MS, [2020] Footwear for the prevention of human slips: from friction mechanics to ergonomic solutions. Madrid, Spain, February 13-14, 2020. Editor: Fundación Gómez Pardo. Proceedings available at: https://af1f3fa0-867a-4e5a-a60a-e2070984b638.filesusr.com/ugd/022861_9a8a73fd23d94502add40687d8833301.pdf.

4. Hemler, SL, Beschorner, KE: [2020] Influence of individual gait and shoe design factors on tread wear. Slips, Trips, and Falls, Madrid, Spain. February 13-14, 2020. Editor: Fundación Gómez Pardo. Proceedings available at: https://af1f3fa0-867a-4e5a-a60a-e2070984b638.filesusr.com/ugd/022861_9a8a73fd23d94502add40687d8833301.pdf.
5. Hemler, SL, Sundaram, VH, Beschorner, KE: [2019] Influence of slip-resistant shoe classification and shoe age on under-shoe hydrodynamics during human slips. Proc of the International Society of Biomechanics, Calgary, Canada, July 31-August 4.
6. Hemler, SL, Sider, J, Beschorner, KE: [2019] Influence of required coefficient of friction on rate of shoe wear, Proc of International Society of Posture and Gait Research, Edinburgh, Scotland, June 30-July 4.
7. Beschorner, KE, Sundaram, V, Hemler, SL: [2019] Size of Worn Region Predicts Fluid Pressures during Human Slips. Proc of Society of Tribologists and Lubrication Engineers Annual Meeting, Nashville, TN, May 19-23.
8. Pliner, EM, Hemler, SL, Beschorner, KE: [2019] Gait parameters of shoe wear: A case study of the shoe wear rate by individual gait parameters. Proc of Society of Tribologists and Lubrication Engineers Annual Meeting, Nashville, TN, May 19-23.
9. Hemler, SL, Beschorner, KE: [2019] Effect of Progressive Shoe Wear and Heel Type on Traction Performance Changes. Proc of Society of Tribologists and Lubrication Engineers Annual Meeting, Nashville, TN, May 19-23.
10. Hemler, SL, Beschorner, KE: [2019] Predicting Slip Risk Based on Footwear, Society of Tribologists and Lubrication Engineers Annual Meeting, Nashville, TN, May 19-23.
11. Hemler, SL, Sider, JR, & Beschorner, KE: [2019] Effects of Walking Forces on Shoe Wear Rate. Proc of Northeast Bioengineering Conference, New Brunswick, NJ, March 20-22.
12. Beschorner, KE, Hemler, SL, Moghaddam, SR, Iraqi, A, Moyer, BE, Haight, JM, Redfern, MS: [2018] Preventing slip and fall accidents: Focus on footwear. Proc of National Occupational Injury Research Symposium, Morgantown, WV, October 19-21.
13. Hemler, SL, Redfern, MS, Haight, JL, Beschorner, KE: [2018] Mapping the traction performance of work shoes during natural progressive wear. Proc of National Occupational Injury Research Symposium, Morgantown, WV, October 19-21.
14. Hemler, SL, Redfern, MS, Haight, JM, Beschorner, KE: [2018] Influence of Natural Wear Progression on Shoe Floor Traction – A Pilot Study. In Proc of the Human Factors and Ergonomics Society Annual Meeting, vol. 62, no. 1, pp. 1358-1362. Sage CA: Los Angeles, CA: SAGE Publications, October 1-5.
15. Moghaddam, SR, Beschorner, KE: [2018] Frictional response of multiple slip-resistant flat and beveled shoes to normal loading. In Proc of American Society of Biomechanics, Rochester, MN, August 8-11.

G.3. Dissertation/Thesis

1. Moghaddam, SRM: [2018] Multiscale Finite Element Model for Shoe-Floor Friction and Wear, Ph.D. Thesis, University of Pittsburgh.
2. Iraqi, A: [2018] Predictive Statistical Models for Shoe-Floor-Contaminant Friction, Ph.D. Thesis, University of Pittsburgh.
3. Pliner, EM: [2020] Factors Contributing to Ladder Falls and Broader Impacts on Safety and Biomechanics, Ph.D. Thesis, University of Pittsburgh.

H.Inclusion Enrollment Table

View Burden Statement

PHS Inclusion Enrollment Report

This report format should NOT be used for collecting data from study participants.

OMB Number: 0925-0001 and 0925-0002
Expiration Date: 10/31/2018

*Study Title (must be unique): Impact of Worn Shoes on Slipping

* Delayed Onset Study? ☐ Yes ☒ No

If study is not delayed onset, the following selections are required:

Enrollment Type	☐ Planned	☒ Cumulative (Actual)
Using an Existing Dataset or Resource	☒ Yes	☐ No
Enrollment Location	☒ Domestic	☐ Foreign
Clinical Trial	☐ Yes	☒ No

NIH-Defined Phase III Clinical Trial ☐ Yes ☒ No

Comments:

Racial Categories	Ethnic Categories									
	Not Hispanic or Latino			Hispanic or Latino			Unknown/Not Reported Ethnicity			Total
	Female	Male	Unknown/ Not Reported	Female	Male	Unknown/ Not Reported	Female	Male	Unknown/ Not Reported	
American Indian/ Alaska Native	1	0	0	0	0	0	0	0	0	1
Asian	2	3	0	0	0	0	0	0	0	5
Native Hawaiian or Other Pacific Islander	0	0	0	0	0	0	0	0	0	0
Black or African American	20	25	0	0	1	0	0	0	0	46
White	27	31	0	1	2	0	0	0	0	61
More than One Race	0	0	0	0	0	0	0	0	0	0
Unknown or Not Reported	0	0	0	0	0	0	0	0	0	0
Total	50	59	0	1	3	0	0	0	0	113

Report 1 of 1

< Previous Report | Delete Report | Next Report >

To ensure proper performance, please save frequently.

I.Inclusion of Children

Children under 21 years of age were eligible and participated in this study. This study is similarly applicable to children of the ages 18 to 21 years since they participate in the workforce and are similarly at risk of slipping. We expect that the results of the study are similarly applicable to this segment of children and adults.

J.Materials Available for Other Investigators

We are currently in the process of making material available for other investigators. To this end, we have submitted a data use agreement request with the university for posting the data to Dryad, a repository that allows researchers to access data for free. Experiment #1 (Aims 1 and 2) will be posted publically since it is unique, of interest to other researchers and does not include any subject information (accelerated wear study). Partial data sets will be posted from Experiments #2 (Wear Progression) and #3 (Wear Slip study) in order to make as much data available without compromising the anonymity of the subjects. This data will be de-identified and subjects will be labeled with a code provided by the research team. Since the possibility of deductive disclosure exists, personal information such as age, height, weight, gender, biomechanics of walking and shoe size will not be shared. However, other data from Aim 4 (month, use, worn condition, predicted film thickness, fluid force, and ACOF) and from Aim 5 (wear condition of the shoe, fluid pressure from the slip event, ACOF, and slip outcomes) will be made available. Four data sets will be made available (two for Experiments #1 and

#2), one for Experiment #2, and one for Experiment #3. All data will be placed in a table. Spreadsheet file format will be used for wide accessibility of the data (.csv). Data files will be accompanied with a document that explains the data structure and provides descriptions for each column.